(41)

Simplified Theory for Contact Indentation of Sandwich Panels

by

Robin Olsson
Civilingenjör
(1987)

Submitted to the Department of
Aeronautics and Astronautics in Partial Fulfillment of
the Requirements for the Degree of

MASTER OF SCIENCE
in Aeronautics and Astronautics
at the

Massachusetts Institute of Technology
September 1994

Signature of Author_____
Department of Aeronautics and Astronautics,
August 1, 1994

Certified by_____
Professor Mårten T. Landahl
Thesis Supervisor

Certified by_____
Professor Hugh L. McManus
Thesis Supervisor

Accepted by_____
Professor Harold Y. Wachman
Chairman, Department Graduate Committee

Simplified Theory for Contact Indentation of Sandwich Panels

by
Robin Olsson

Submitted to the Department of Aeronautics and Astronautics
on August 18, 1994
in Partial Fulfillment of the Requirements for the Degree of
Master of Science in Aeronautics and Astronautics

Abstract

Previous attempts to analyze indentation of sandwich panels have been based on small deflection theory and an assumed elastic core behaviour. The agreement with experiments was poor. The present work includes core crushing and large deflections of the face sheets in a simplified model of sandwich contact indentation. The model assumes transverse isotropy with respect to the load axis and is based on an infinite, elastic face sheet on a core bonded to a rigid foundation. The core is assumed to be elastic in tension and elastic–ideally plastic in compression. After initiation of core yielding the problem is separated in two regions. In the inner, plastic region, the core has yielded and exert a constant reactive pressure on the face sheet. In the outer region the core acts as an elastic foundation. The plastic radius is found by matching boundary conditions for the two regions.

The outer region is modeled as a plate on an elastic foundation. The inner region is modeled using three different approaches. For small deflections classical plate theory with shear corrections is used. For intermediate deflections an upper limit of the contact force is given by first order large deflection plate theory and a lower limit by small deflection plate theory. The asymptotic behaviour at large deflections is given by an approximate solution based on membrane theory. The three solutions, which all require iteration, have been put in dimensionless form and tabulated. The approach due to Hertzian contact has been included in the plate solution. Bounds have been given for the residual indentation after unloading. Approximate expressions are given for analysis of orthotropic face sheets.

Good agreement with experiments was found for sandwich panels of different materials and thickness. The often observed, approximately linear, load–indentation relation is found to be the combined effect of softening due to core crushing and stiffening due to face sheet membrane effects. A limited parametric study indicates a strong influence of the core yield stress and the face sheet properties, and a relatively weak influence of the thickness and elastic properties of the core. The local indentation model may be used in a global impact model to predict impact response of sandwich panels, or as a starting point for more detailed stress analyses for prediction of damage due to impact and contact loads.

Thesis supervisors: Mårten T. Landahl
Professor of Aeronautics and Astronautics

Hugh L. McManus
Assistant Professor of Aeronautics and Astronautics

Contents

List of symbols

A	Orthotropy ratio
a	Plastic radius
$\bar{a}$	Dimensionless plastic radius
C	Membrane shape parameter
C_i	Integration constant
$\overline{C}_i$	Dimensionless integration constant
c	Contact radius
D, D_r	Radial plate stiffness
D^*	Effective plate stiffness
E, E_r	Radial plate modulus
E_c	Core modulus
F	Contact force
$\overline{F}$	Dimensionless contact force
$f(C)$	Polynomial dependent on C and ν.
f_n	Real part of $H_n^{(k)}$
G	Transverse shear modulus of the plate
G_c	Transverse shear modulus of the core
g_n	Imaginary part of $H_n^{(k)}$
$H_n^{(k)}$	Hankel function of n-th order, k-th kind
h	Face sheet thickness
h_c	Core thickness
h_c^*	Effective core thickness
i	$\sqrt{(-1)}$
J_n	Bessel function of n-th order

k Foundation stiffness

k_i Stiffness related to deformation of type i

L_0 Characteristic length

M Radial moment at $r = a$

$\overline{M}$ Dimensionless radial moment at $r = a$

M_i Dimensionless function related to M_r

M_r Radial moment

N Radial stress resultant at $r = a$

N_r Radial stress resultant

p Compressive stress on the core

p_0 Compressive yield stress of the core

Q Radial transverse shear force at $r = a$

Q_c Vertical stiffness of the core

Q_f Vertical stiffness of the face sheet

Q_b Stiffness of the face sheet

Q_i Dimensionless function related to Q_r

Q_r Radial transverse shear force

Q_α Contact modulus

q Applied pressure on the upper plate surface

R Tip radius of the indentor

r Radius

s Arbitrary integration variable

t_{ply} Ply thickness in laminate

U Total strain energy

u Radial displacement at $r = a$

u_n Real part of J_n

u_r Radial displacement

v_n Imaginary part of J_n

W Total work of external forces

w Total vertical displacement

$\overline{w}$ Dimensionless vertical displacement at $r = 0$

w_0 Vertical displacement at $r = 0$

w_a Vertical displacement at $r = a$

w_b Vertical displacement due to bending at $r = 0$

w_s Vertical displacement due to shear at $r = 0$

Z Vertical coordinate of the indentor surface

z Vertical coordinate

Greek letters

α Approach due to contact stresses

β Load parameter

δ Ratio of elastic constants

$\delta(\rho)$ Dirac's delta function

δw Difference in vertical displacements

ε_r Radial strain

η Effective elastic fraction of core after crushing

θ Slope angle at $r = a$

θ_i Dimensionless function associated with θ

λ Shear parameter

μ Exponent in dimensionless load-plastic radius relation

ν Poisson's ratio

Π Total potential energy

π 3.141593....

ρ Dimensionless radius

ρ_a Value of ρ at $r = a$

σ_i Membrane stress in direction i

σ Radial membrane stress at $r = a$

ψ Phase angle for complex number

ω_i Dimensionless function associated with ω_r

ω_r Rotation of plate mid plane normal

ω_p Work per unit area due to the uniform pressure

Superscripts

$\bar{}$ Standard dimensionless quantity

$\tilde{}$ Alternate dimensionless quantity

$\hat{}$ Peak value

$\breve{}$ Residual value

$*$ Effective property

$'$ Associated with rotated coordinate system

Subscripts

a	Value of quantity at $r = a$
b	Quantity related to bending
c	Core property
cl	Quantity for clamped plate
cr	Critical value (at initiation of core yielding)
F	Quantity related to the point load
f	Out-of-plane property of the face sheet
hi	Quantity for hinged plate
i	Free index
L	Quantity related to the linear solution
m	Quantity related to membrane behavior
max	Upper bound
min	Lower bound
NL	Quantity related to the nonlinear solution
n	Free cardinal number
p	Quantity related to the (uniform) pressure load
r	Quantity related to the radial direction
s	Quantity related to out-of-plane shear
z	Property in the out-of-plane direction
α	Quantity related to Hertzian contact deformation
ϕ	Quantity in the circumferential direction
ρ	Quantity in the radial direction
0	Value of quantity at the origin or certain constant value

List of figures

List of tables

1 Introduction

The growing use of fibrous composite materials in aircraft structures has lead to an increasing concern for impact damage, since laminated composite materials have been found to be particularly sensitive to impacts. An extensive review of theories and experiments dealing with impacts on laminated composites was given by Abrate (1991).

A sandwich panel may be considered as a composite structure where thin and stiff facesheets have been combined with a light and soft core to produce a highly weight effective structural element. The flexural stiffness per unit weight of a sandwich panel is considerably higher than for monolithic panels of the same flexural stiffness. The tradeoff is lower shear and through-the-thickness stiffnesses which will be of particular importance for concentrated loads such as impact loads. Common face sheet materials in aircraft applications are fibre composites and aluminium. Most core materials are cellular, either with randomly oriented cells (foams) or uniaxially oriented (honeycombs). Common core materials are either plastic foams, or honeycombs of aluminium or resin impregnated papers such as Nomex™.

Damage resulting from impact in monolithic laminates may result in significant reductions of their strength and stability. Damage typically consist of delaminations, matrix cracks and broken fibres. Similar damages have been observed in laminated face sheets of impacted sandwich panels. In addition, other damages, such as core cracking and face sheet-core

debonding, may occur. Reductions of panel compressive and tensile strength of over 50% have been observed even at low impact energies and with no visible face sheet damage.

Impact response of plates may be divided in two major categories; response governed by wave propagation (small mass impact) and response governed by fixed boundaries (large mass impact). Wave controlled responses may be further subdivided in responses governed by either dilatational/shear waves or by flexural waves. The distinction has been discussed in detail by Olsson (1993) who showed that the kind of response is governed primarily by the impactor/plate mass ratio. Fig. 1.1 schematically shows response controlled by: (a) shear and dilatational waves, (b) flexural waves, (c) fixed boundaries.

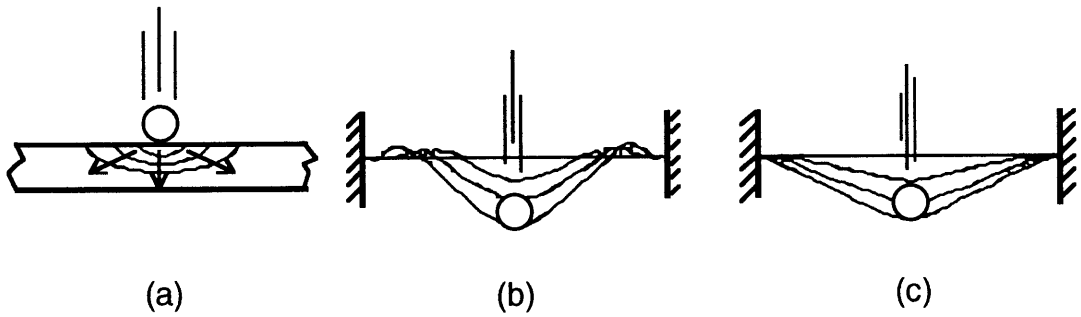

Figure 1.1 Classification of different plate impact responses.

Impact resistance, which is a measure of the structural damage caused by a given impact load, is most commonly determined experimentally. Analytical methods, however, are necessary both to predict damage initiation in a preliminary design stage and to design experiments more rationally. Numerical impact analyses are normally based on finite element models or mode summation methods like the Raleigh-Ritz method. Solutions

on closed form are often obtained using simplified models based on dashpots, springs and masses. A review of closed form analyses of impact on composite plates was given by Olsson(1993).

In an impact analysis the dynamic equations for the impactor and target motion are coupled through an equation describing the contact between the two bodies at the point of impact. To reduce computational effort both numerical and closed form analyses normally rely on a simplified load-indentation relation which may be determined either from experiments or derived from a more detailed local analysis of the contact problem.

The underlying assumption, often not stated, is that there is a negligible coupling between the global deflection and the local indentation problem. This assumption requires that the local problem affects only a very local region of the total structure and that the stresses due to the global deflection are negligible in comparison to the stresses in the local problem. An obvious geometrical condition is that the resulting plate curvature is small in comparison to the curvature of the indentor.

Each of the response forms shown in Fig. 1.1 may be associated with a simplified structural model describing the local and global response of the structure. As an example consider the boundary controlled response in Fig. 1.1c, which is typical for cases where the impactor mass is larger than the plate mass. A simplified model of this case consists of a series of two masses and two springs, Fig. 1.2. The effective plate mass can be obtained from the static stiffness and the fundamental vibration frequency of the plate. The global stiffness of the plate is generally nonlinear but may be

considered linear when large global deflections and shear need not be considered. A simplified spring system modeling shear and large deflection effects was proposed by Shivakumar, Elber and Illg (1985).

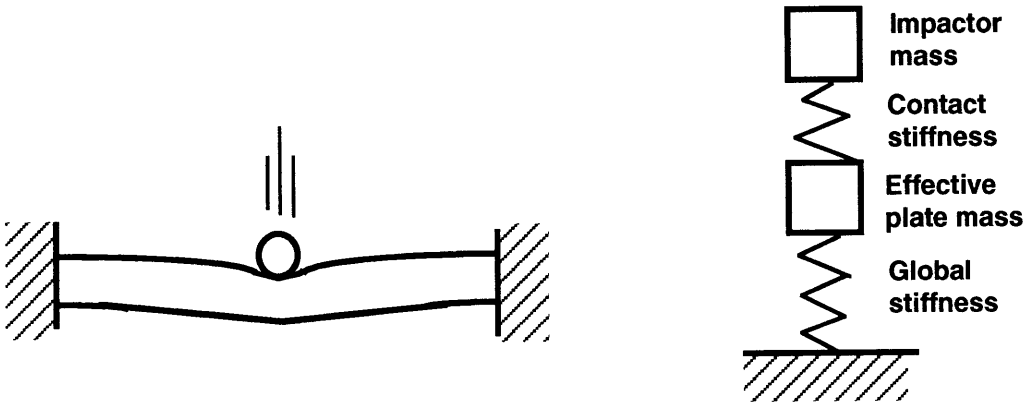

Figure 1.2 Simplified structural model for impact analysis

Completely different structural models apply for the global response to small mass impacts, which is governed by transient flexural waves or shear/dilatation waves. Generally, decreasing impactor masses give shorter impact times. Below a given impactor mass, the impacted plate is only deflected locally and smaller masses result in a response which is increasingly dominated by the local (contact) stiffness.

Irrespective of the global model, any impact analysis must also include a model of the local contact response. The local response model, which should describe the load-indentation relation, may be linear or nonlinear but is essentially independent of the global response as long as material rate effects and inertia effects can be neglected in the indentation problem.

Extensive experimental evidence shows that for practical use in impact analysis the load-indentation behaviour of monolithic laminates can be sufficiently accurately described by a closed form generalization of Hertz' contact theory for isotropic bodies, as discussed by Olsson(1993). For a sphere indenting a flat surface the force is proportional to the indentation raised to power 3/2, as shown schematically in Fig. 1.3.a.

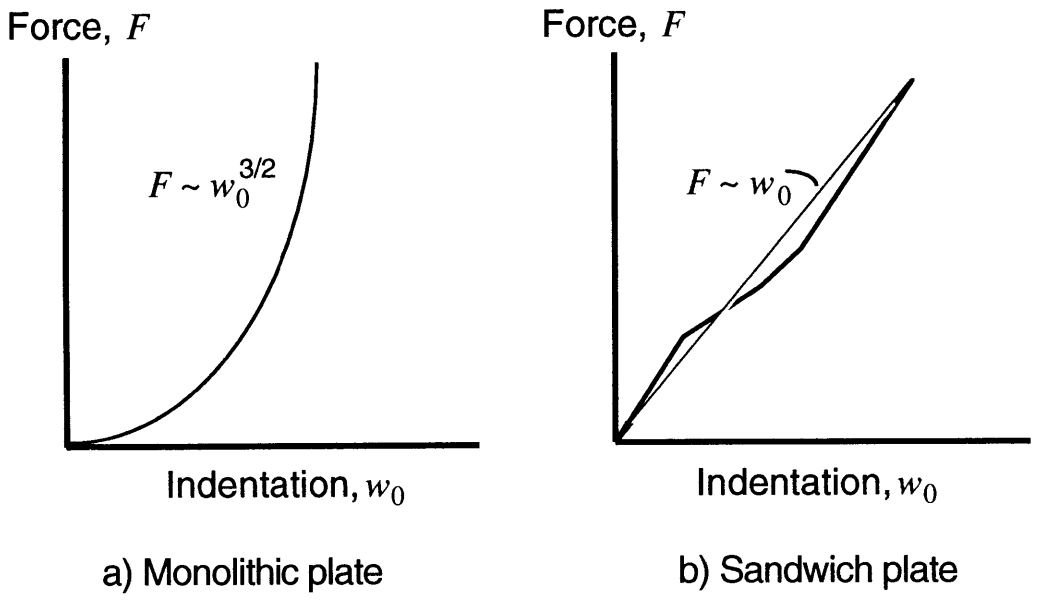

Figure 1.3 Load–indentation behaviour for plates indented by a sphere.

In many cases the contact compliance of monolithic plates is of minor importance in comparison to the flexural compliance. By contrast the contact compliance of a sandwich plate can be of the same order as the flexural compliance, as shown experimentally by Mines, Worrall and Gibson (1990) and Williamson and Lagace(1993).

Due to the facesheet-core interaction, indentation of sandwich plates is significantly more complex than indentation of monolithic plates. The soft core results in a local deflection of the face sheet in addition to the actual indentation of the face sheet, Fig. 1.2. It has been found that inelastic crushing of the core cells takes place even at small loads. Previous analytical solutions for indentation of sandwich panels show severe disagreement with experiments, except for a negligible initial phase. Empirically, the load-indentation relation has been found highly nonlinear, although from a gross perspective approximately linear for large values of indentation, as shown schematically in Fig. 1.3.b.

As shown by Jackson and Poe (1993) and Lagace et al. (1993), large mass impacts and static loading on monolithic laminates give virtually identical relations between damage size and peak load. Observations on the equivalence of damage resulting from static loads and quasi-static impact loads on sandwich panels have been reported by Williamson and Lagace(1993).

The peak impact force may be obtained from experiments or from an impact analysis. For impactors much heavier than the impacted plate, the system in Fig. 1.2 may be considered as a one-degree-of-freedom system. We note that the impact force will be related to the effective stiffness of the spring system and that this stiffness will be dominated by the most compliant spring. In the asymptotic small mass case, where no global deflections occur, the peak force is obtained by assuming an infinite global stiffness. Obviously, the local stiffness is even more important for the peak force during small mass impacts.

In monolithic laminates, impact loads slightly above the damage threshold usually result in delaminations having a size several times the plate thickness. In contrast, the initial damage in sandwich panels is highly localized, and normally confined to the permanent dent, which initially has a diameter much smaller than the panel thickness. For typical sandwich panels the local damage due to a given contact load appears to be independent of the global boundary conditions. For example, Williamson and Lagace (1993) observed identical damages in sandwich panels having a flat backface support and similar panels having an unsupported backface but two sides clamped. Thus, initiation and size of damage in sandwich panels with small to moderate span to thickness ratios is likely to depend on the peak contact force but not on the kind of global impact response.

In addition to providing a load-indentation relation which can be used to predict the peak impact force, a theory for sandwich indentation may also serve as a basis for further analysis of the local deformations that govern initiation and size of indentation damages caused by impact or other events resulting in concentrated loads.

The purpose of the present work is to develop a theory for the indentation of sandwich plates, based on the constitutive behaviour of the core and face sheet materials. Although the load-indentation relation will generally not be linear, it may be used as a basis for linear or other simplified approximations that can be used in a global impact model. In addition it is hoped that the present analysis can contribute to improved understanding and prediction of initiation and size of impact damages in sandwich panels.

The thesis is organized as follows:

In Chapter 2 we will review previous work on the present problem as well as other problems related to the present analysis.

In Chapter 3 the theory for indentation of transversely isotropic sandwich plates will be derived using three different approaches, all based on an elastic–ideally plastic compressive behaviour of the core. The first model is valid for small indentations and is based on small deflection plate theory. The second model, based on pure membrane theory, represents an asymptotic solution to the contact stiffness for large indentations. A third model based on first order large deflection corrections to the linear plate theory represents an intermediate solution. The solutions for deflection versus load are presented in dimensionless form.

In Chapter 4 we discuss additional considerations such as approximate methods to analyze anisotropic face sheets by the use of effective flexural and shear properties, unloading behaviour and methods to calculate the effective foundation stiffness of the core.

In Chapter 5 the theory is used for parametric studies and comparisons with published experimental data for several different material systems including cores of foam as well as Nomex and aluminium honeycomb.

In Chapter 6 recommendations for the use of the present theory will be given. We will also discuss the implications for impact analysis of sandwich

panels and give some preliminary conclusions on the formation of indentation damage together with recommendations for future work in this area.

In Chapter 7 the most important conclusions of the present work will be summarized.

2 Previous work

2.1 Topics of interest

Structural sandwich plates typically consist of stiff face sheets bonded to a compliant core. Under concentrated lateral loads, the deflection of the face sheet may be considerably larger than the face sheet thickness. Clearly, in addition to dealing with previous works on indentation and impact analysis of sandwich panels, a serious attempt to analyze sandwich indentation must touch on several additional topics such as constitutive behaviour of the core material, theories for face sheets on elastic foundations, and plate and membrane theories needed to analyze large deflections.

2.2 Impact and indentation of sandwich panels

The number of references dealing with impact on monolithic composite laminates is already extensive, as can be seen in the review by Abrate (1991). The number of works dealing with impact on sandwich panels is significantly smaller, but exceeds 60 references. A recent and relatively complete collection of references on sandwich impact was given by Tsang (1994).

A majority of the works cited by Tsang (1994) consist of experimental studies of how different parameters affect damage size and residual strength versus kinetic energy of the impactor. From the introduction it is clear that the results of such studies are limited to the particular test

configuration, since the peak contact force depends on the total structural stiffness. Furthermore they give no information on the load-deflection history and how it is related to damage. Experimental works use various impact metrics – energy, mass, velocity and impact force. The following discussion will use the impact metrics as they are used in each work cited.

The main contribution of these works is to show that impact on sandwich panels can result in significant (≥50%) reductions of the residual strength even at low impact energies and when no external damage is visible. Typical results have been given by Oplinger and Slepetz (1975). A general observation in all studies of impact on sandwich panels is that face sheet damage is preceded by core damage which occurs even at very low impact energies. Core damage usually consists of crushed core cells, while face sheet damage consists of delaminations and matrix cracks, followed by fibre breakage at higher impact energies (impact forces).

For a given load the local indentation in sandwich panels is significant and can easily be of the same order as the global deflection, even in relatively flexible panels. Experimental evidence can be found in the works by Mines, Worall and Gibson (1990) who studied large square panels and by Williamson (1991) who studied smaller beam-like specimens.

The static indentation behaviour of sandwich panels has been studied experimentally either by indenting a panel with a supported backface, or by measuring the difference in deflection of the upper and lower face in panels with supported edges. The two test methods were shown to give identical results for beam-like specimens tested by Williamson (1991). These results

are indirectly supported by the studies by Tsang and Dugundji (1992), Lie (1989) and Mines, Worall and Gibson (1990) who all based their predictions of impact response on indentation tests on panels with a supported backface.

A common result from all studies is an overall approximately linear force-indentation relation, which may be divided into an initial softening followed by a gradual stiffening. The behaviour has been observed in several different material systems. Graphite/epoxy skins on a Nomex honeycomb were studied by Slepetz et al. (1974), Lie (1989) and Williamson (1991), glass/epoxy skins on aluminium honeycomb by Mines, Worral and Gibson (1990) and graphite/epoxy skins on a Rohacell foam core by Tsang (1989). Selected results were later republished by Oplinger and Slepetz (1975) and Tsang and Dugundji (1992).

Possible dynamic material effects were revealed by Slepetz et al. (1974) who performed low- and high-speed non-impact indentation tests on graphite/epoxy skins on a Nomex honeycomb core. Signs of an increased softening were seen at the higher displacement rate.

The importance of including local indentation in sandwich panels was shown in a parametric study by Ericsson and Sankar (1992) who presented a serial solution to analyze concentrated static loads on simply supported sandwich panels with elastic orthotropic core and face sheets. The face sheets were modeled as laminated plates on a three-dimensional orthotropic solid.

Analytical models of sandwich indentation, as presented by Slepetz et al. (1974), Tsang (1989) and Lie (1989), have been based on assumptions of elastic core properties. Indentation experiments show an initial agreement with predictions, followed by a very significant softening at relatively small loads, obviously due to core crushing. These results clearly show the need to include core crushing in analytic indentation models.

Published impact analyses have almost exclusively dealt with large mass impacts, which result in a quasi-static response.

Mines, Worall and Gibson (1990) successfully predicted large mass impact response and damage initiation in sandwich panels using a serial spring model based on experimentally determined local and global panel stiffness.

Less simplified impact analyses have been based on either modal expansion techniques or on finite element analysis. Modal expansion was used by Lie (1989) and Tsang (1989), Tsang and Dugundji (1992). A three-dimensional analysis of an axisymmetric plate problem was performed by Nemes and Simmonds (1992), while Sun and Wu (1991) and Lee, Huang and Fann (1993) used plate elements to analyze two-dimensional beam problems. Comparisons between predicted and experimentally observed face sheet damage were given by Lie (1989) and Sun and Wu (1991). All analyses except two were based on experimentally determined force-indentation relations. Lie (1989) assumed an elastic core and used an assumed mode and energy minimization to model the local indentation behaviour while Nemes and Simmonds (1992) incorporated core yield by using a constitutive yield model for elastomeric foams.

The above analyses have been applied to large mass impact on a number of different systems of face sheets and cores. In all cases the agreement with experiments has been satisfactory. Analyses based on experimentally determined indentation behaviour have generally produced more accurate results.

A purely theoretical parametric study of small and large mass impacts on sandwich panels was performed by Riis (1992), who developed an efficient numerical analysis for simply supported panels. The total displacement was obtained by adding global panel deflection, face sheet compression and local face sheet deflection under the assumption of an elastic core.

All of the above analyses can be expected to be less accurate for small mass impacts, where the response is governed by transient flexural waves which are associated with higher modes and large strain gradients.

A theory for small mass impact on sandwich panels was developed by Koller (1986) who postulated that the contact stiffness was only governed by the face sheet properties. Experimental agreement was satisfactory for low velocity impacts where deflections were in the order of one percent of the face sheet thickness. However, the assumed independence of core properties must be questioned at larger face sheet deflections and impact forces, which will occur at higher velocities.

2.3 Face sheet-foundation models

Structural sandwich plates typically consist of stiff face sheets bonded to a compliant core. Most sandwich cores have been observed to yield at a low and relatively constant stress in compression while the behaviour in tension remains linearly elastic until final failure. These observations suggest that the deflection of sandwich face sheets may be modeled as a plate on an elastic-plastic foundation.

The deflection of plates on elastic foundations has been treated by several authors. Many references can be found in the review by Hétenyi (1966) and the monographs by Selvadurai (1979) and Gladwell (1980). The classical work by Schleicher (1926) assumed the foundation to be a continuum of independent springs normal to the plate surface, a so called Winkler–foundation. Later workers have included shear springs, resulting in a so called Pasternak–foundation. A unified treatment of foundation shear was given by Vlasov and Leont'ev (1966) who considered a non shearing plate on a three-dimensional foundation where the vertical displacements of the foundation were described by a shape function. Panc (1975) considered a shear deformable plate on a Winkler foundation and obtained a similar governing equation. Recently Chen and Gürdal (1990) presented an analytical method to analyze a point load on an infinite orthotropic plate on an elastic foundation. Deviations from the classical theory for plates on an elastic foundation for the case of a thin elastomeric foundation have been studied by Dillard (1989).

The only reference found dealing with plates on elastic-plastic foundations is a finite element analysis of a uniform load on a square patch of a square plate done by Lewandowski and Switka (1991).

Three dimensional solutions for rigid bodies indenting an elastic layer bonded to a substrate with different elastic properties have been presented by Yu, Sanday and Rath (1990) and Oda and Kubota (1992). However, these solutions are limited to linearly elastic isotropic materials and small strains, and are thus of limited value in the analysis of sandwich indentation.

2.4 Large deflection plate solutions

Impact and indentation on sandwich panels often result in local face sheet deflections considerably larger than the face sheet thickness. An extensive treatment of large deflection analysis of plates was given in the monograph by Chia (1980) which also covers anisotropic plates.

Equations for moderately large deflections of plates have been derived by von Karman, who assumed small strains and rotations while allowing for large deflections. The accuracy of von Karman's equations has been discussed by Hamada and Seguchi (1965) and Zhou and Zheng (1989) who compared them with the more general Reissner plate equations. Exact solutions to the coupled von Karman's equations have only been found for a few cases. Approximate solutions are usually found using Fourier series, perturbation methods or variational methods such as Ritz', Galerkin's or the principle of minimum of potential energy. Discussion and numerous examples are given by Chia (1980).

Large deflections due to a point load on a clamped finite circular plate on an elastic foundation were studied analytically and experimentally by Datta (1975). This solution is of limited practical value for the analysis of sandwich indentation, since the core will not behave elastically after crushing of core cells, which has been observed even at small face sheet deflections.

A large deflection analysis of the face sheet will generally involve the combined loading of a point load and a non uniform reactive normal pressure from the core, acting on a region with complex boundary conditions. Closed form solutions are only available for simple cases of combined loads and boundary conditions. Saibel and Tadjbaksh (1960) considered von Karman's equations for an immovably clamped plate under uniform pressure combined with a point load and obtained a perturbation solution based on the plate deflection. Schmidt and DaDeppo (1976) used nonlinear Kirchhoff plate theory to obtain a similar perturbation solution for the same combination of loads on a plate with edges in sliding clamps. Nowinski and Ismail (1964) presented a perturbation solution for a simply supported plate under combined point load and uniform pressure by using the two loads as perturbation parameters. Unfortunately this solution is of limited practical value since negative deflections are obtained even at relatively small loads.

Single load solutions (point load or uniform pressure) are not directly applicable to the present problem but are useful as benchmark tests for the combined load solutions. Volmir (1962) presented approximate solutions

based on the Galerkin method for both concentrated and uniform loads on plates with movable and immovable clamped and hinged edges. Similar solutions were given by Ferriss (1991) for the immovably clamped and simply supported (moving hinge) cases. Banerjee (1983) considered a point load on a plate with different boundary conditions by using a modified expression for the elastic energy including large deflections.

An exact power series solution for an immovably clamped plate under uniform load was given by Way (1934). Due to the complicated calculations involved the presentation is graphical rather than in closed form and results were given for deflections only slightly larger than the plate thickness. A recent Raleigh-Ritz solution to this problem was given by Schmidt (1987) who also provided an extensive discussion on previous results. The influence of inplane and rotational constraints on large deflections of uniformly loaded circular plates was studied by Cheng (1989).

An inherent weakness in all the approximate solutions above is the assumption that the deflection shape remains unchanged from the shape given by linear theory even when deflections are large. In addition the solutions are limited by the basic von Karman assumptions of small strains and rotations. A theory for axisymmetric deformation under arbitrarily large strains and rotations was developed by Brodland (1988) who considered uniform pressure on clamped and hinged circular plates. Later Dolovich, Brodland and Thornton-Trump (1988) applied Brodland's theory to a concentrated load on a rigidly clamped plate and obtained approximate polynomial expressions for load versus deflection.

A change in the deflection shape was also included in the analysis by Bert and Martindale (1988) who considered both uniform pressure and a point load on rigidly clamped plates. Numerical results based on nonlinear finite element analysis and an efficient differential curvature method were given by Striz, Jang and Bert (1988) who considered both uniform pressure and point loads on rigidly clamped and simply supported plates.

An interesting approach to the problem of a point load on a simply supported plate was provided by Frakes and Simmonds (1985) who used perturbation methods to derive overlapping asymptotic solutions for small and large ratios of bending stiffness versus membrane stiffness.

2.5 Membrane solutions

The literature on membrane theory is extensive, but only a few works deal with concentrated loads on membranes. The problem of a point load on an initially flat membrane was originally studied by Schwerin (1929), who solved the problem of a circular membrane with fixed edges and a Poisson's ratio not exceeding one third. A general solution for a point load on an initially flat membrane with prescribed edge displacement or edge stress was given by Jahsman, Field and Holmes (1962) who also performed an experimental verification. Schwerin's limitation to a Poisson's ratio not exceeding one third was removed by allowing for complex quantities in the equations. Flügge (1966) considered the related problem of a point load on an inflated balloon. Simplified membrane solutions for a point load on prestressed membranes have also been given by Leonard (1988). Another work of some interest is the one by Frakes and Simmonds (1985) who

obtained asymptotic solutions for a point load on a simply supported plate by using a perturbed membrane solution with non-zero bending stiffness.

2.6 Core behaviour

Sandwich cores typically consist of cellular materials, either in a two-dimensional structure of parallel cylinders (honeycombs), or a random three-dimensional cell structure (foams). An excellent and thorough presentation of cellular materials and their properties can be found in the book by Gibson and Ashby (1988), where an exhaustive review of previous works is given. The book includes both theories and experimental results for the constitutive behaviour of cellular material. Typical stress-strain curves for out-of-plane compression of cellular materials are given by Gibson and Ashby (1988) and have been shown schematically in Fig. 2.1.

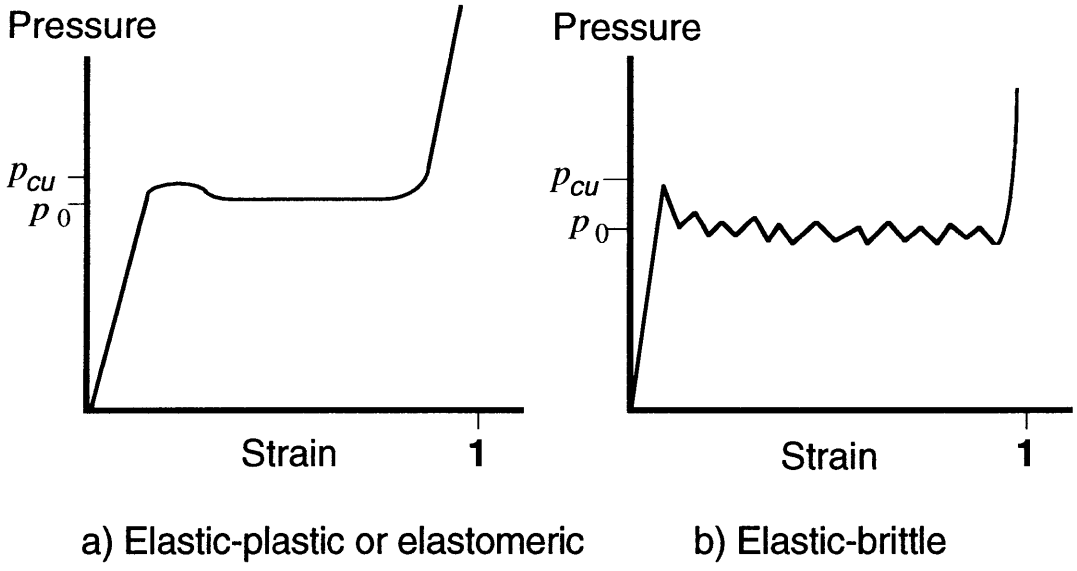

Figure 2.1 Typical behaviour of cellular materials during out-of-plane compression.

Under out-of-plane compression of cellular materials the initial elastic region is followed by elastic buckling of the cell walls, a plateau region and a final densification region where the modulus approaches that of the solid material. The plateau level in plastic materials is governed by plastic buckling of the cell walls, while the magnitude of the initial stress peak depends on the cell wall buckling load. For elastomeric materials the plateau stress is determined by the cell wall buckling and no initial peak is observed. Very brittle core materials fail through a sequence of cell fractures giving oscillations around an average plateau stress level. Constitutive models of cellular materials do of course depend on the failure mechanisms in the particular material. Published closed form models for the constitutive behaviour can be found in the book by Gibson and Ashby (1988).

More recent papers include a theoretical and experimental study of the out-of-plane properties of Nomex honeycombs by Zhang and Ashby (1992) and a similar study of several non-metallic honeycombs by Huang and Hahn (1990). A very general (and very theoretical) paper on the elastic properties of materials with randomly distributed cells was presented by Hall (1991). Goldsmith and Sackman (1992) studied dynamic crushing of honeycombs experimentally and made comparisons with published static crush theories.

3 Theory

3.1 Problem definition

The problem under consideration is to determine the relation between load and indentation for an elastic hemispherical body indenting a sandwich panel. The apparent indentation may be separated into a local deflection of the face sheet and a very local actual indentation of the face sheet. In the vicinity of the contact load a complex three–dimensional stress state will be present. The constitutive behavior of structural sandwich panels is dependent on the constituents, which typically consist of stiff elastic face sheets bonded to a compliant core. The core yields at a low and relatively constant compressive stress while the tensile behavior remains linearly elastic until failure. Due to the compliant core and relatively thin face sheets, indentation of sandwich panels often results in face sheet deflections that are considerably larger than the face sheet thickness.

In the following analysis we will model the face sheet/core system as a linear elastic, infinite plate on a foundation which is elastic in tension and elastic–ideally plastic in compression. The foundation is assumed to be bonded to a rigid base, so that no global bending is allowed.

In addition we make the following simplifying assumptions:

- The face sheet and core are both transversally isotropic with respect to the load axis, allowing an axisymmetric treatment.
- The contact pressure can be modeled as a resulting point load when calculating the local face sheet bending deflection.

- The contact pressure can be modeled as a uniform pressure over the contact area when calculating shear deflections.
- Transverse shear and large deflection effects can be neglected at some distance from the contact load.
- The curvature of the upper face due to local face sheet deflection is negligible in comparison to the curvature caused by indentation, so that the indentation and deflection problems are uncoupled.
- The core obeys the assumptions of a Winkler foundation, so that the reactive pressure at any point is proportional to the face sheet deflection and independent of deflections at neighboring points.

The assumed model problem is shown schematically in Fig. 3.1, where a point load F is applied normal to the face sheet. The coordinate axes r and z are aligned with the face sheet and load directions respectively, with the origin under the contact point at the face sheet midplane. The corresponding displacements are labeled u and w. The face sheet plate with thickness h is characterized by the radial plate stiffness D_r, the inplane modulus E_r, Poisson's ratio ν_r and out–of–plane shear modulus G_{rz}. The core is characterized by the compressive "yield" stress p_0, and by the foundation modulus $k = -\sigma_z/w$, which relates surface pressure to displacements. The foundation stiffness k is related to the core thickness, h_C and the core elastic properties E_{ij} and ν_{ij}.

Under the assumption of ideally plastic core behaviour in compression the plate–foundation model of Fig. 3.1 may be divided in two regions; one outer region, modeled as a plate on an elastic foundation, and an inner region, modeled as a plate on an ideally plastic foundation, as shown in Fig. 3.2.

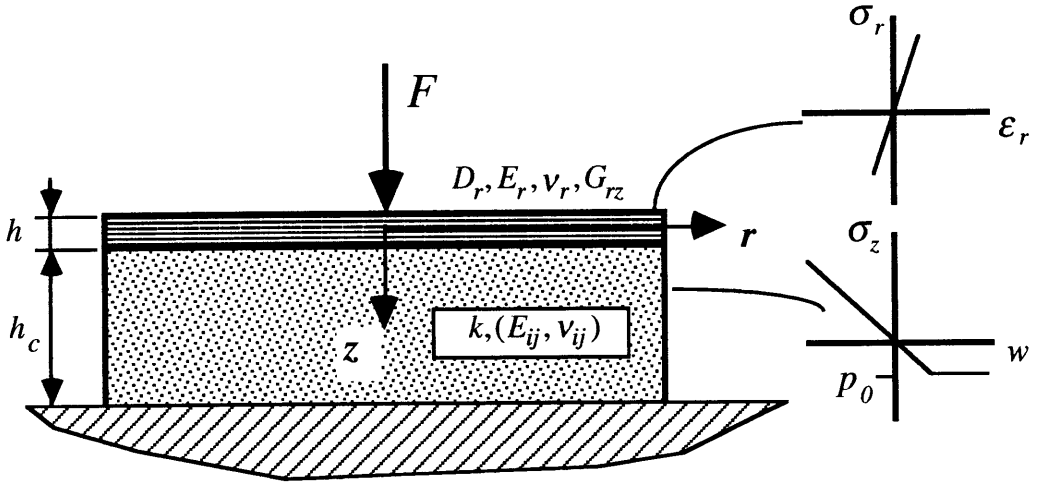

Figure 3.1 Assumed model problem.

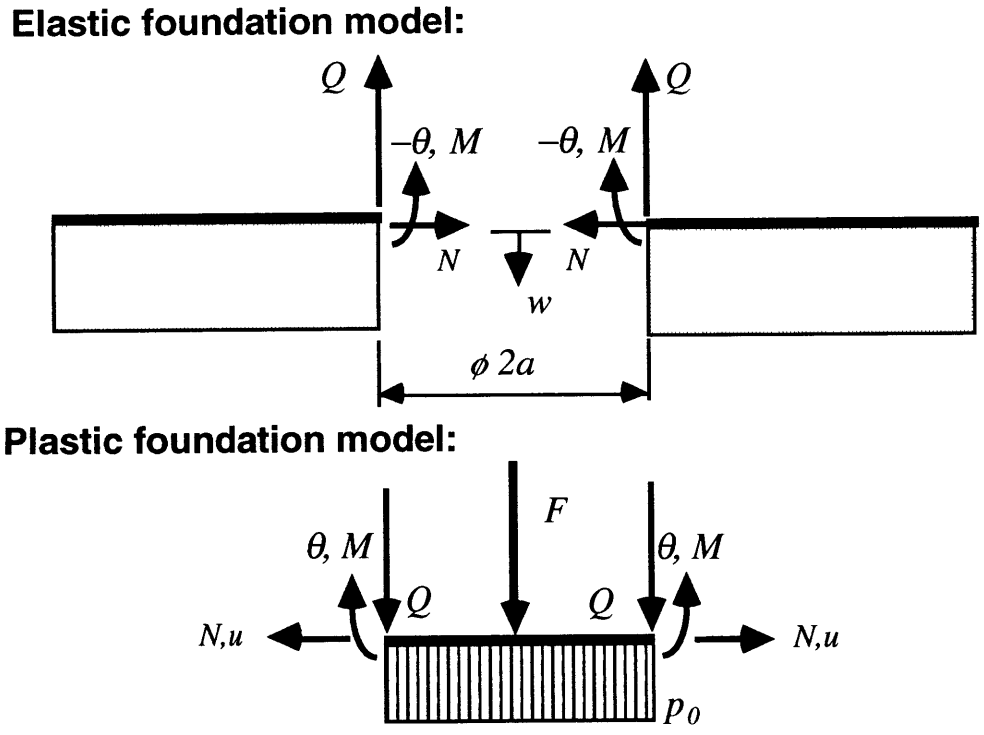

Figure 3.2 Substructuring of the model problem.

The loads acting on the face sheet are the contact load F, the reactive core pressure p_0, and radial stress resultants given by the moment M_r, the shear stress Q_r and the normal stress N_r. The resulting plate deflection is characterized by the deflection w and the slope angle $\theta=-dw/dr$. The transition from plastic to elastic core behaviour occurs at the plastic radius a.

For convenience we use the following simplified notation for face sheet elastic properties and stress resultants, deflection and slope angle at the plastic radius:

$$\begin{array}{llll} D_r \to D & E_r \to E & \nu_r \to \nu & w(a) \to w_a \\ Q_r(a) \to Q & M_r(a) \to M & N_r(a) \to N & dw(a)/dr \to -\theta \end{array} \tag{3.1}$$

Stress resultants and slope, which are only considered at the plastic radius, have been given no subscript. The deflection at $r = a$ has been given the subscript a, since we will also consider deflections at other locations. To simplify the analysis we also define the following characteristic length and dimensionless quantities:

$$L_0^4 = D/k \tag{3.2.a}$$

$$\bar{a} = \sqrt{p_0 \pi a^2 / F} \tag{3.2.b}$$

$$\bar{F} = F/\left(p_0 \pi L_0^2\right) \tag{3.2.c}$$

$$\bar{M} = M/\left(p_0 L_0^2\right) \tag{3.2.d}$$

$$\rho = r/L_0 \tag{3.2.e}$$

$$\rho_a = a/L_0 = \bar{a}\sqrt{\bar{F}} \tag{3.2.f}$$

Here ρ is a general dimensionless radius, $\overline{a}$ is the dimensionless plastic radius, $\overline{F}$ the dimensionless contact force, $\overline{M}$ the dimensionless edge moment at $r = a$ and L_0 a characteristic length dependent on the plate stiffness and foundation stiffness.

For a known edge moment and plastic radius, the deflections in the inner and outer regions are given by published elementary solutions. The major difficulty in the problem is that the edge moment and plastic radius are unknowns.

3.2 Overview of analysis

The unknown plastic radius and edge moment can be determined by matching the boundary conditions for the inner plastic region and the outer elastic region. Once the plastic radius and edge moment are known the deflections in the inner region can be calculated.

We will assume that the deflections in the outer region remain comparatively small, so that transverse shear and large deflections of the face sheet need not be considered. Thus the outer region will be analyzed using classical theory for plates on an elastic foundation. The deflection w_a at the plastic radius can then be obtained simply by dividing the elastic foundation modulus by the compressive yield stress of the core, i.e. $w_a=k/p_0$.

In the inner region we will consider both transverse shear and large deflections of the face sheet. The analysis of the inner region is illustrated by Fig. 3.3 which shows a simplified model for combined indentation and deflection of an elastic circular plate, proposed by Shivakumar, Elber and Illg (1985).

In this model the contact force is balanced by the force due to contact indentation of the face sheet upper surface. The latter force is balanced by forces due to bending, shear and membrane deformation of the face sheet, where bending and shear deformations are assumed to be uncoupled.

The stiffnesses associated with contact indentation, bending, shear and membrane deformation are symbolized by k_α, k_b, k_s and k_m respectively.

Note that all stiffnesses are functions of the plastic radius, and hence functions of the contact load. In addition, the shear stiffness is also a function of the contact radius, which is also a function of the contact load. The displacement of the upper face in the inner region is obtained by summing the displacement w_a at the edge of the plastic region, the relative approach α due to contact stresses, and the relative displacements w_b due to bending and w_s due to shearing.

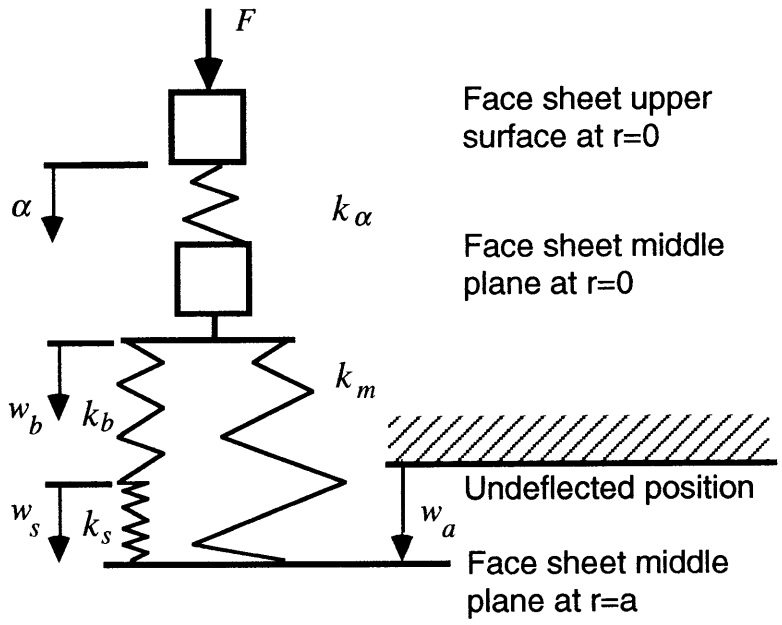

Figure 3.3 Simplified model of the face sheet in the inner region.

Generally, contact, shear, membrane and bending effects are coupled. The model with separate springs is based on the simplifying assumption that the load-deflection relations for the different effects are uncoupled.

The contact indentation is uncoupled from the face sheet deflections due to the assumption that the curvature caused by face sheet deflection is

negligible in comparison to the surface curvature due to indentation. The shear deflection is, however, coupled to the contact deformation through the dependence of the contact radius, which both are functions of the load.

For small deflections ($w/h<<1$) the membrane effects are negligible and shear and bending deflections uncoupled.

For larger deflections, membrane effects become increasingly important and couple with the shear and bending effects. For very large deflections ($w/h>>1$) the behaviour is dominated by membrane effects.

In order to cover the whole range of deflections three different approaches will be employed to model the inner plastically supported region: classical plate theory with shear corrections for small deflections, first order large deflection plate theory at intermediate deflections and membrane theory for large deflections.

For a given contact force and model of the inner region, the plastic radius and the edge moment can be obtained after iteration by satisfying the boundary conditions for the inner and outer region. In the present analysis the resulting equations have been put in dimensionless form and the solutions have been tabulated so that no further iterations are required to use the presented expressions.

For small deflections ($w/h<<1$) we will use classical plate theory with shear corrections and neglect membrane effects ($k_m=0$). The total center deflection

w_0 is then obtained by adding the displacements due to contact indentation α, bending deformation w_b, shear deformation w_s and edge displacement w_a:

$$w_0(F) = \alpha(F) + w_b(F) + w_s(F) + w_a \tag{3.3}$$

For large deflections ($w/h>>1$) we will use membrane theory ($k_b=k_s=0$) to model the inner region. In this case the contact indentation is not relevant since a membrane will have the same curvature as the indentor. The total displacement is obtained by summing the membrane deflection w_m and the edge displacement w_a :

$$w_0(F) = w_m(F) + w_a \tag{3.4}$$

For intermediate deflections ($w/h\sim1$) we will use the complete simplified model in Fig. 3.3 which corresponds to a first order large deflection plate theory:

$$w_0(F) = \alpha(F) + w_b(F_{bs}) + w_s(F_{bs}) + w_a$$

$$\text{where} \quad F = F_{bs} + F_m = k_b w_b + k_m(w_b + w_s)^3 \tag{3.5}$$

Here F_{bs} is the contact load required to obtain the deflection $w_b + w_s$ when small deflection theory is used and F is the contact force required to obtain the same deflection when large deflection membrane effects have been included.

A solution of Eq. (3.5) will generally require an iterative procedure since increments in the load F will result in increments in the plastic radius which affects the stiffness values. The iterative procedure is avoided by an approximate solution based on a first order approximation for the relation between load and plastic radius.

3.3 Equations for the elastic region

A theory for plates without shear on a solid elastic foundation with shear was given by Vlasov and Leont'ev (1966). A similar theory for a shear deformable plate on a Winkler foundation was presented by Panc (1975) who also showed how the analysis could be extended to a two parameter foundation. The complete equations for the two theories are presented in a unified notation in appendix A.

Since our main interest is core yielding and its effect on the face sheet deflection, a refined analysis in the elastically supported region will not be pursued. Thus, we will neglect core and face sheet shear effects in the elastically supported region. In this case, both theories result in the following equilibrium equation for axisymmetric deformation of a plate on an elastic foundation:

$$\Delta_\rho{}^2 w + w = q/k \qquad (3.6)$$

where $\Delta_\rho = d^2/d\rho^2 + \rho^{-1} d/d\rho$

Here k is the foundation stiffness (reactive pressure/unit displacement) and q the load applied on the upper surface of the plate. The dimensionless radius ρ has been defined in Eq. (3.2).

Prior to core yielding the elastic region includes a point load at the origin and the general equilibrium equation, Eq. (3.6), takes the following form:

$$\Delta_\rho^2 w + w = \delta(0)F/k \tag{3.7}$$

For the case of an infinite plate the solution to this equation is given by:

$$w(0) = \frac{FL_0^2}{8D} = \frac{F}{8\sqrt{kD}} \tag{3.8}$$

The reactive pressure in the elastic area is given by $p = kw$. Hence, after core yielding, the deflection w_a at the elastic–plastic transition radius will be given by

$$w_a = p_0 / k \tag{3.9}$$

where p_0 if compressive yield stress of the core. The critical load at initiation of core yielding is obtained by combining Eqs. (3.8) and (3.9):

$$F_{cr} = \frac{8p_0 D}{kL_0^2} = 8p_0 L_0^2 \tag{3.10}$$

After core yielding the point load at the origin is excluded from the elastic region and the general equilibrium equation, Eq. (3.6), takes the following form:

$$\Delta_\rho^2 w + w = 0 \tag{3.11}$$

The general solution to the homogenous differential equation, Eq. (3.11) is given by:

$$w(\rho) = C_1 u_0(\rho) + C_2 v_0(\rho) + C_3 f_0(\rho) + C_4 g_0(\rho) \qquad \text{where}$$

$$u_n(\rho) + i v_n(\rho) = J_n(\rho e^{i\psi}) \qquad f_n(\rho) + i g_n(\rho) = H_n^{(1)}(\rho e^{i\psi}) \qquad \psi = \pi/4 \tag{3.12}$$

Here the real functions u_n, v_n, f_n and g_n are the real and imaginary parts of the n-th order Bessel function J_n and the n-th order Hankel function of the first kind, $H_n^{(1)}$. Note that g_0 as given by Vlasov and Leont'ev(1966) involves a sign error since $g_n(\rho) = \mathrm{Im}\, H_n^{(1)}(\rho e^{i\psi}) = -\mathrm{Im}\, H_n^{(2)}(\rho e^{-i\psi})$.

The function f_0 is bounded everywhere. The function g_0 is unbounded at the origin while the functions u_0 and v_0 are unbounded at infinity. Consequently the constants C_1 and C_2 must be set to zero in order to obtain finite deflections in the present infinite plate problem. The constant C_4 need only be set to zero when the foundation is elastic at the origin which results in the solution given by Eq. (3.8).

Thus, for an infinite plate on an elastic foundation the general solution to the equilibrium equation, Eq. (3.11), is given by:

$$\begin{aligned} w(\rho) &= C_3 f_0(\rho) + C_4 g_0(\rho) \\ \frac{dw}{dr} &= -\frac{1}{L_0} \sum_{i=3}^{4} C_i \theta_i(\rho) \\ M_r &= \frac{D}{L_0^{\,2}} \sum_{i=3}^{4} C_i \left[M_i(\rho) - (1-\nu) \overline{M_i}(\rho) \right] \\ Q_r &= -\frac{D}{L_0^{\,3}} \sum_{i=3}^{4} C_i Q_i(\rho) \end{aligned} \tag{3.13}$$

Here M_r is the moment and Q_r the shear force on surfaces normal to the radius. The functions f_0, g_0,θ_i, M_i, $\overline{M}_i$ and Q_i are given by the following expressions:

$$
\begin{aligned}
f_n &= \operatorname{Re} H_n^{(1)}(\rho\sqrt{i}) = -\tfrac{2}{\pi}(-1)^n \operatorname{kei}_n \rho \\
g_n &= \operatorname{Im} H_n^{(1)}(\rho\sqrt{i}) = -\tfrac{2}{\pi}(-1)^n \operatorname{ker}_n \rho
\end{aligned}
$$

$$
\begin{aligned}
\theta_3 &= (f_1 - g_1)/\sqrt{2} \qquad \theta_4 = (f_1 + g_1)/\sqrt{2} \\
M_3 &= -g_0 \qquad\qquad M_4 = f_0 \\
\overline{M}_3 &= \theta_3/\rho \qquad\qquad \overline{M}_4 = \theta_4/\rho \\
Q_3 &= -\theta_4 \qquad\qquad Q_4 = \theta_3
\end{aligned}
\tag{3.14}
$$

In the latter expression f_n and g_n have been expressed in terms of Kelvin functions using Eq. (9.9.2) of Abramowitz and Stegun (1970) although f_n and g_n may be obtained directly from the tables by Panc (1975).

The unknown plastic radius and the constants C_3 and C_4 can be determined by matching three of the expressions given in Eq. (3.13) with corresponding expressions for the inner region.

When shear is included in Eq. (3.6) the argument ψ in Eq. (3.12) will vary from $\pi/4$ to $\pi/2$ and the functions in Eq. (3.14) are modified as shown in appendix A.

3.4 Linear plate analysis

3.4.1 Equations for the plastic region

The solution for small deflections in the plastic region is based on Kirchhoff's linear plate theory, and a superimposed transverse shear displacement. This solution neglects membrane stresses and shear-bending coupling, which are negligible for deflections significantly smaller than the plate thickness. As will be shown in section 3.6 the maximum ratio of deflection versus thickness where linear theory is still applicable ranges from one fourth to one, depending on the required accuracy, the type of load and the boundary conditions.

Using linear plate theory and neglecting shear we find the governing equations of the problem:

$$\Delta_r{}^2 w = \left[\delta(0)F - p_0\right]/D \qquad r \le a$$
$$\text{where} \qquad \Delta_r = d^2/dr^2 + r^{-1}\, d/dr \tag{3.15}$$

With the use of classical plate theory, as described for example by Timoshenko and Woinowsky-Krieger (1959), the general bending solution w_b of Eq. (3.15) is obtained by superposition of the deflections due to a central point load, a uniform pressure and a constant edge moment on a simply supported plate:

$$w_b = \frac{Fa^2(3+\nu)}{16\pi D(1+\nu)} - \frac{p_0 a^4(5+\nu)}{64D(1+\nu)} + \frac{Ma^2}{2D(1+\nu)}$$

$$\theta = \frac{Fa}{4\pi D(1+\nu)} - \frac{p_0 a^3}{8D(1+\nu)} + \frac{Ma}{D(1+\nu)}$$

With the use of the dimensionless quantities defined in Eq. (3.2) the above expressions may be rewritten as:

$$w_b = \frac{F^2\bar{a}^2}{16\pi^2 p_0 D(1+\nu)}\left[(3+\nu) - \bar{a}^2(5+\nu)/4 + 8\overline{M}/\overline{F}\right] \tag{3.16}$$

$$\theta = \frac{F\rho_a L_0}{8\pi D(1+\nu)}\left[2 - \bar{a}^2 + 8\overline{M}/\overline{F}\right] \tag{3.17}$$

The edge shear force Q is obtained from vertical equilibrium of the inner plate region:

$$Q = \left(p_0\pi a^2 - F\right)/(2\pi a) \;=\; \left(\bar{a}^2 - 1\right)F/(2\pi a) \tag{3.18}$$

3.4.2 Determination of the plastic radius

After core yielding the compatibility conditions at the plastic radius are:

$$\begin{aligned} w(a_+) &= w(a_-) = w_a = p_0/k \\ \theta(a_+) &= \theta(a_-) \\ Q(a_+) &= Q(a_-) \end{aligned} \tag{3.19}$$

The slope and shear force for the plastic region are given by Eqs. (3.17) and (3.18). The sectional quantities for the elastic region, given by Eq. (3.13), can be recast in the following form:

$$w_a = (p_0/k)\left[\overline{C}_3 f_0 + \overline{C}_4 g_0\right] \tag{3.20}$$

$$\theta = (p_0/k)\left[\overline{C}_3 \theta_3 + \overline{C}_4 \theta_4\right]/L_0 \tag{3.21}$$

$$M = (p_0/k)\left\{\overline{C}_3\left[M_3 - (1-\nu)\overline{M}_3\right] + \overline{C}_4\left[M_4 - (1-\nu)\overline{M}_4\right]\right\} D/L_0^2 \tag{3.22}$$

$$Q = -(p_0/k)\left[\overline{C}_3 Q_3 + \overline{C}_4 Q_4\right] D/L_0^3 = Q_r(\rho_a) \tag{3.23}$$

where we have introduced the dimensionless constants

$$\overline{C}_3 = C_3\, k/p_0 \quad \text{and} \quad \overline{C}_4 = C_4\, k/p_0 \tag{3.24}$$

The functions f_0, g_0, θ_i, M_i, $\overline{M}_i$ and Q_i have been defined in Eq. (3.14).

Now the three unknowns $\overline{C}_3$, $\overline{C}_4$ and ρ_a can be determined from the three compatibility equations (3.19). Eq (3.20) and the displacement condition in Eq. (3.19) immediately give:

$$\overline{C}_4 = \left[1 - \overline{C}_3 f_0\right]/g_0 \tag{3.25}$$

Matching shear loads, Eqs. (3.18) and (3.23), and using Eqs. (3.2) and (3.25) we find

$$\frac{\left(1-\overline{a}^2\right)F}{2\pi\rho_a L_0} = p_0 L_0\left[\overline{C}_3(Q_3 - Q_4 f_0/g_0) + Q_4/g_0\right]$$

Solving for $\overline{C}_3$ and using Eq. (3.2.a) we obtain:

$$\overline{C}_3 = \left[\left(\overline{F}/\rho_a - \rho_a\right)/2 - Q_4/g_0\right]/\left[Q_3 - Q_4 f_0/g_0\right] \tag{3.26}$$

Matching the slopes, Eqs. (3.17) and (3.21) gives

$$\frac{F\rho_a L_0}{8\pi D(1+\nu)}\left[2 - \overline{a}^2 + 8\overline{M}/\overline{F}\right] = \frac{p_0}{kL_0}\left[\overline{C}_3\theta_3 + \overline{C}_4\theta_4\right]$$

Using Eq. (3.2) and rearranging we find

$$\rho_a\overline{F}\left[\left(2-\overline{a}^2\right)/8 + \overline{M}/\overline{F}\right]/\left[\overline{C}_3\theta_3 + \overline{C}_4\theta_4\right] - (1+\nu) = 0$$

Using Eqs. (3.2) and (3.22) we finally get the following dimensionless equation relating ρ_a to $\overline{F}$:

$$\frac{\rho_a\left[\left(2\overline{F}-\rho_a{}^2\right)/8 + \left\{\overline{C}_3\left[M_3-(1-\nu)\overline{M}_3\right] + \overline{C}_4\left[M_4-(1-\nu)\overline{M}_4\right]\right\}\right]}{(1+\nu)\left[\overline{C}_3\theta_3+\overline{C}_4\theta_4\right]} - 1 = 0$$

where $\overline{F} \geq \overline{F}_{cr} = 8/\pi$

(3.27)

Here the functions θ_i, M_i and $\overline{M}_i$ which are functions of ρ_a have been defined in Eq. (3.14) , the dimensionless load $\overline{F}$ in Eq. (3.2.c) and the critical yield load F_{cr} in Eq. (3.10). The solution to Eq. (3.27) was obtained by numerical iteration to find $\overline{F}$ for different values of the argument ρ_a. The plastic radius was then obtained from the relation in Eq. (3.2.f) and has been plotted versus dimensionless force in Fig. 3.4. The solution has also been tabulated in appendix B for various values of ν. The resulting edge moment is dependent on Poisson's ratio, while no effect was seen on the plastic radius for Poisson's ratios between 0 and 1/2.

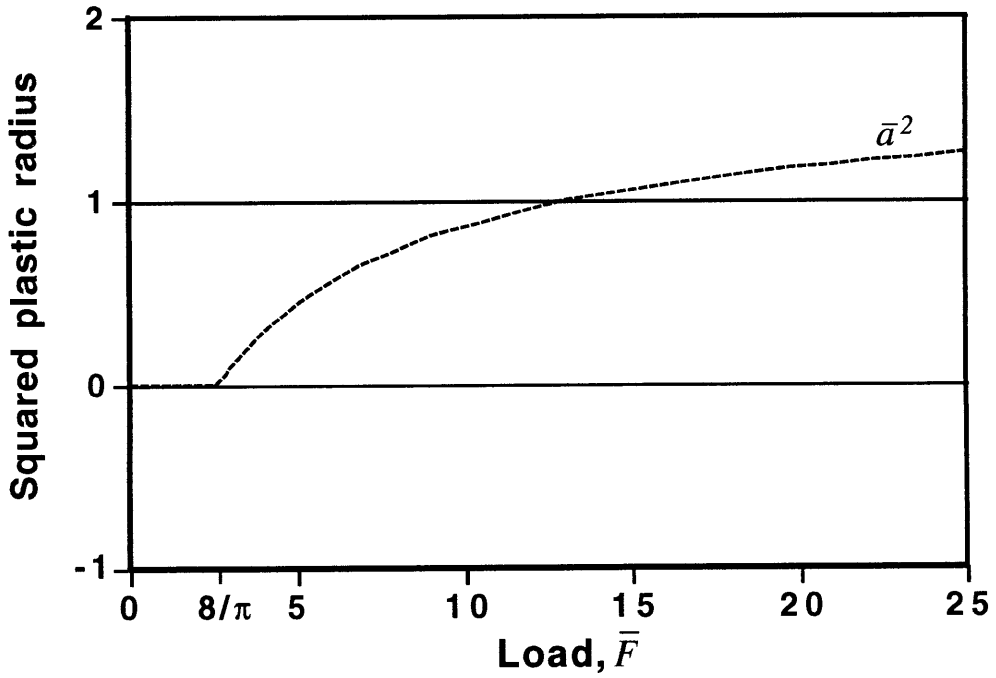

Figure 3.4 Dimensionless plastic radius versus load for the plate solution.

3.5 Membrane analysis

3.5.1 Determination of the plastic radius

For large deflections ($w/h>1$) the face sheet stress state will gradually be dominated by the membrane stress σ_r, Fig. 3.5. Obviously, since slopes in the outer region are small, the major membrane effect will come from the inner region. In this section we will model the face sheet in the inner region as a pure membrane, while the surrounding face sheet is still modeled as a plate.

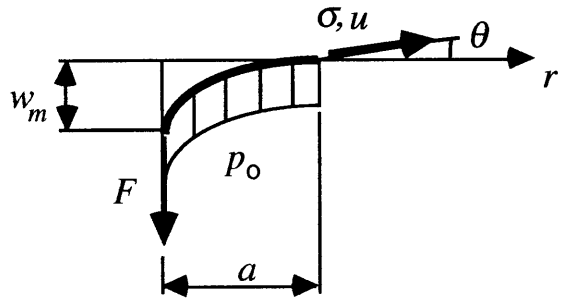

Figure 3.5 Membrane under combined loading

Vertical equilibrium for the inner region is given by:

$$F - p_0 \pi a^2 - 2\pi a \sigma h \theta = 0 \tag{3.28}$$

The last term on the left hand side is the vertical component of the membrane stress resultant at the membrane edge.

The boundary conditions at the plastic radius become:

$$\begin{aligned} &w(a_-) = w(a_+) = w_a = p_0/k \\ &M(a_-) = M(a_+) = 0 \\ &\sigma_r(a_-)h\theta = -Q(a_+) \end{aligned} \tag{3.29}$$

since membranes are unable to carry moments and shear. Equations (3.20) to (3.24) are still valid for the outer, elastically supported, region. Satisfaction of Eq. (3.20) together with the displacement boundary condition in Eq. (3.29) gives:

$$\overline{C}_4 = \left[1 - \overline{C}_3 f_0\right]/g_0 \tag{3.30}$$

Satisfaction of Eq. (3.22) together with Eq. (3.2) and the moment boundary condition in Eq. (3.29) gives

$$\overline{M} = \overline{C}_3\left\{\left[M_3 - (1-\nu)\overline{M}_3\right] - \left[M_4 - (1-\nu)\overline{M}_4\right]f_0/g_0\right\} + \left[M_4 - (1-\nu)\overline{M}_4\right]/g_0 = 0$$

Solving for the constant $\overline{C}_3$ we obtain

$$\overline{C}_3 = 1/\left\{f_0 - \left[M_3 - (1-\nu)\overline{M}_3\right]g_0/\left[M_4 - (1-\nu)\overline{M}_4\right]\right\} \tag{3.31}$$

Combination of Eqs. (3.23) and (3.28) and the boundary condition for vertical forces in Eq. (3.29) results in the following equation:

$$\frac{F - p_0\pi a^2}{2\pi a} = \frac{p_0 D}{kL_0^3}\left[\overline{C}_3(Q_3 - Q_4 f_0/g_0) + Q_4/g_0\right]$$

Rearranging terms and using Eqs. (3.2.a) and (3.2.f) finally gives the following equation for the dimensionless plastic radius versus dimensionless load:

$$\tfrac{1}{2}\left[\overline{F}/\rho_a - \rho_a\right]\Big/\left[\overline{C}_3\left(Q_3 - Q_4 f_0/g_0\right) + Q_4/g_0\right] - 1 = 0 \tag{3.32}$$

where $\overline{C}_3$ is given by Eq. (3.31). The solution has been plotted in Fig. 3.6.

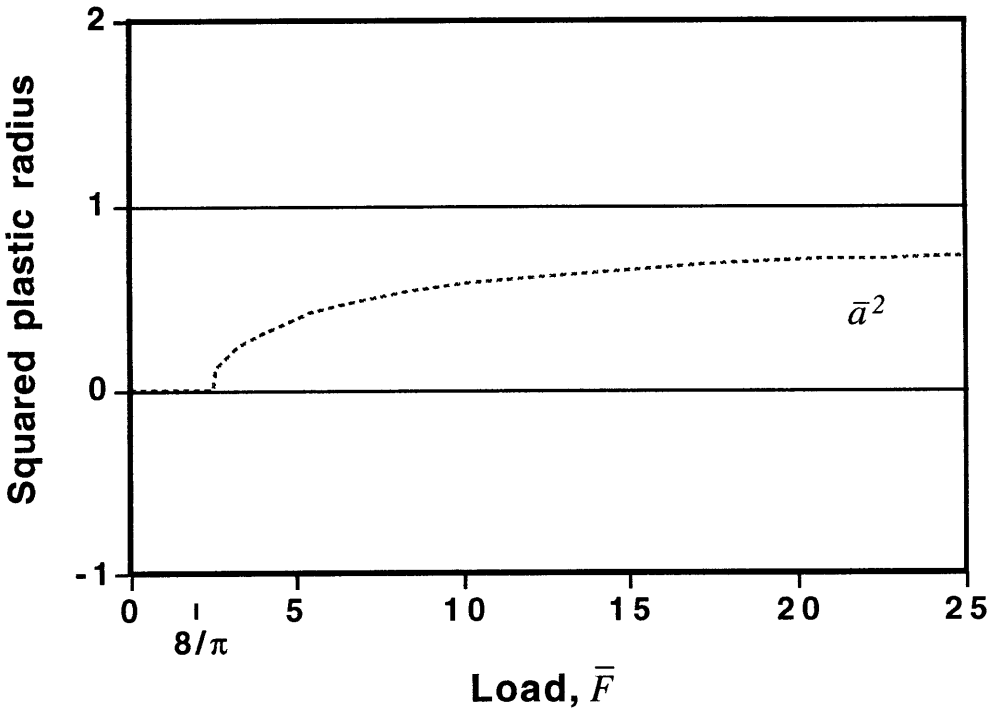

Figure 3.6 Dimensionless plastic radius versus load for the membrane solution.

3.5.2 Determination of edge constraints

In order to calculate the membrane deflections in the inner region we must determine the relation between the radial stresses and displacements at the boundary, i.e. the constraint imposed by the surrounding face sheet. The general solution for an axisymmetric membrane stress state, which can be found for example in Timoshenko(1951), is given by:

$$\begin{aligned} \sigma_r &= A_1/r^2 + A_2(1+2\ln r) + 2A_3 \\ \sigma_\varphi &= -A_1/r^2 + A_2(3+2\ln r) + 2A_3 \end{aligned} \tag{3.33}$$

If plane stress is assumed the radial strain is given by the following expression:

$$\varepsilon_r = du_r/dr = \left(\sigma_r - \nu\,\sigma_\varphi\right)/E \tag{3.34}$$

The boundary conditions for the outer region are:

$$\begin{aligned} &\sigma_r(a) = \sigma \\ &\sigma_r(r) \to 0 \quad \text{as } r \to \infty \\ &u_r(r) \to 0 \quad \text{as } r \to \infty \end{aligned} \tag{3.35}$$

Satisfying the stress condition in Eq. (3.35) at infinity forces the constants A_2 and A_3 to vanish. By solving for the constant A_1 we obtain the following expressions for the stresses:

$$-\sigma_\varphi = \sigma_r = \sigma(a/r)^2 \quad \text{for } r \geq a \tag{3.36}$$

By inserting Eq. (3.36) into (3.34), integrating, and satisfying the displacement condition in Eq. (3.35) we obtain the following expression for the radial displacement in the outer region:

$$u_r = -\frac{\sigma a^2}{Er}(1+\nu) \quad \text{for } r \geq a \tag{3.37}$$

At the plastic radius we obtain the following constitutive relation between the edge stress and edge displacement:

$$\frac{u/a}{\sigma/E} = -(1+\nu) \tag{3.38}$$

If a uniform stress state is assumed in the inner region we obtain:

$$\sigma_r(r) = \sigma_\varphi(r) = \sigma \quad \text{for } r < a \tag{3.39}$$

By inserting Eq. (3.39) into (3.34), integrating, and satisfying the symmetry condition of zero radial displacement at the origin we obtain the following expression for the displacement in the inner region under uniform stress:

$$u_r = r(1-\nu)\sigma_r/E \quad \text{for } r < a \tag{3.40}$$

If the stresses are caused by deflection of the inner region this is the necessary stretching when the edge of the inner region is fixed. The required stretching of the inner region in the constrained case is obtained by adding the displacement of the outer region at $r = a$ to the required stretching for the

case with a fixed edge of the inner region. By using Eqs. (3.37) and (3.40) we obtain the following equation:

$$\frac{a\sigma}{E}(1-\nu)=\frac{a\sigma_{fixed}}{E}(1-\nu)-\frac{a\sigma}{E}(1+\nu)$$

where σ is the radial edge stress in the cases with radially constrained edges and σ_{fixed} is the stress when the edges are fixed. By solving for the radial edge stress σ we obtain the following relation:

$$\sigma=\sigma_{fixed}(1-\nu)/2 \tag{3.41}$$

Eq. (3.41) will be used to estimate the appropriate boundary conditions for large deflection plate solutions.

3.5.3 Membrane deflection when core pressure is absent

A general solution for a point load on an initially flat membrane with prescribed edge displacement or edge stress was given by Jahsman, Field and Holmes (1962) who also performed an experimental verification. The solutions become identical in the case of a linear relation between edge stresses and edge displacements. Thus the solution given by Jahsman, Field and Holmes (1962) is generally applicable to a point load on a membrane with prescribed linear stress–displacement relations at the edge. The solution is given by the expressions:

$$\frac{F/(2\pi Eah)}{(\sigma/E)^{3/2}} = \frac{\gamma - \sin\gamma}{\sin^3(\gamma/2)} \tag{3.42}$$

$$\frac{w_{mF}/a}{(\sigma/E)^{1/2}} = \frac{\gamma}{\sin(\gamma/2)} \tag{3.43}$$

$$\frac{u/a}{\sigma/E} = \frac{\gamma - \sin\gamma}{\sin^2(\gamma/2)\tan(\gamma/2)} - (1+\nu) \tag{3.44}$$

where σ and u are the radial stress and displacement at the edge of the membrane with radius a and w_{mF} is the out-of-plane displacement due to a central point load F. The constant γ is determined from the boundary conditions. Note the typographical errors in the equations (19a,b) of Jahsman et. al. and the sign change in w_{mF} adopted here.

Combination of Eqs. (3.42) and (3.43) gives the following expression for the central deflection under a point load in terms of the load and other known quantities:

$$w_{mF} = \left[\frac{\gamma^3 F a^2}{2(\gamma - \sin\gamma)\pi E h} \right]^{1/3} \tag{3.45}$$

By using a Taylor expansion the expression containing γ can be written as follows:

$$\begin{aligned} \frac{\gamma^3}{\gamma - \sin\gamma} &= \frac{\gamma^3}{\gamma - \gamma + \gamma^3/3! - \gamma^5/5! + \ldots} \\ &= \frac{6}{1 - \gamma^2/(4\cdot 5) + \gamma^4/(4\cdot 5\cdot 6\cdot 7) - \ldots} \end{aligned} \tag{3.46}$$

When no uniform pressure p_0 is present Eq. (3.28) results in the following expression for the edge slope angle:

$$\theta = \frac{F}{2\pi a h \sigma}$$

Combination of the above equation with Eqs. (3.42) and (3.43) gives the following expression for the edge slope angle:

$$\theta = \frac{\gamma - \sin\gamma}{\gamma \sin^2(\gamma/2)} w_{mF}/a \tag{3.47}$$

We observe that the expressions in Eqs. (3.42) to (3.47) are all even with respect to the constant γ so that the solution is only dependent on the absolute value of γ. Combination of Eqs. (3.44) and (3.38) gives the following equation for γ:

$$\frac{\gamma - \sin\gamma}{\sin^2(\gamma/2)\tan(\gamma/2)} = 0$$

The above equation has solutions of the form

$$\gamma = \pm n\pi \qquad n = 1,2,3, \ldots..$$

Inspection of Eq. (3.47) shows that $\gamma = \pi$ represents the physical limit of the slope angle where $\theta = w_{mF}/a$, which corresponds to a straight cone. Larger values of γ corresponds to larger (unphysical) slope angles.

The solution when no reactive pressure is present is thus given by inserting $\gamma = \pi$ in Eq. (3.45):

$$w_{mF} = \left[\frac{\pi F a^2}{2Eh}\right]^{1/3} \tag{3.48}$$

By using the dimensionless quantities in Eq. (3.2) the above equation can be rewritten to:

$$w_{mF} = \left[\frac{F^2 \bar{a}^2}{2p_0 Eh}\right]^{1/3} \tag{3.49}$$

The solution of Eq. (3.45) when γ approaches zero can be studied by using Eq. (3.46). It is seen that $\gamma = 0$ corresponds to the solution for rigidly fixed edges and a Poisson's ratio $\nu = 1/3$, as given by Frakes and Simmonds (1985).

3.5.4 Membrane solution for combined loading

The addition of a reactive uniform pressure on the membrane loaded by a point load will result in a reduced deflection. Obviously the solution given by Eq. (3.49), which neglects the reactive pressure, represents an *upper bound* on the deflection in the combined load case. The deflection in the case of interacting loads cannot be obtained through superposition of the single load cases, due to the nonlinear nature of the membrane equations. The inclusion of a reactive pressure in the solution by Jahsman, Field and Holmes (1962) is associated with significant mathematical difficulties. In the present section an approximate solution will be derived using Ritz method, which minimizes the potential energy of an assumed deflection mode. Due to the character of Ritz approach this solution also represents a *lower bound* of the exact solution for the combined load case. The deflected shape under combined loading is shown schematically in Fig. 3.5.

In the present case we use, for simplicity, the shape of a cable under uniform vertical pressure as the assumed deflection shape. The cable is fixed at the origin, while the other end is required to match the boundary conditions of the outer region with an elastically supported face sheet. The shape is described by a second order polynomial and has been given by Leonard (1988). After considering the boundary condition of zero deflection at the membrane edge ($r = a$), the assumed deflection shape may be written:

$$w = w_m\left[1 + C(r/a) - (1+C)(r/a)^2\right] \tag{3.50}$$

where w_m is the central membrane deflection due to the combined load. Note that the assumed solution is actually of a different nature than the true membrane solution, which involves logarithmic terms. The assumed deflection shape in Eq. (3.50) can be rewritten on the following form:

$$w = \left[1 + C\left(s - s^2\right) - s^2\right] w_m \qquad (3.51)$$

where $s = r/a$

The membrane slope is given by:

$$dw/dr = \left[C(1-2s) - 2s\right] w_m / a \qquad (3.52)$$

The radial strain in a membrane element can be derived by considering Fig. 3.7.

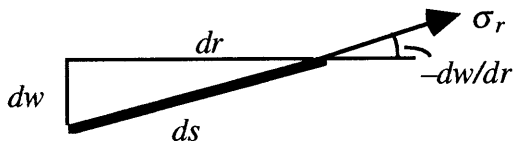

Figure 3.7 Straining of a membrane element due to deflection.

From Fig. 3.7 it can be seen that the radial strain caused by deflection of an initially unstressed membrane is given by the following expression:

$$\varepsilon_{rI} = \frac{ds - dr}{dr} = \sqrt{1 + (dw/dr)^2} - 1 \approx \tfrac{1}{2}(dw/dr)^2 \qquad (3.53.a)$$

where we have assumed small slope angles so that $(dw/dr)^2<<1$. An initial stress due to a prescribed edge displacement u causes an additional constant radial strain which is given by

$$\varepsilon_{rII} = u/a \tag{3.53.b}$$

The total radial strain for small slope angles is now given by

$$\varepsilon_r = \frac{1}{2}\left(\frac{dw}{dr}\right)^2 + \frac{u}{a} \tag{3.54}$$

Expressions for the strain energy of linearly elastic materials can be found for example in Timoshenko (1951). If linearly elastic material and plane stress is assumed the total potential energy of the membrane can be expressed as

$$\Pi = U - W = \frac{1}{2E}\int_0^{\infty}\left(\sigma_r{}^2 + \sigma_\varphi{}^2 - 2\nu\sigma_r\sigma_\varphi\right)2\pi hr\,dr - Fw_m - \int_0^a qw2\pi hr\,dr \tag{3.55}$$

where U is the internal strain energy and W the work done by external forces. Inspection of Eqs. (3.52) and (3.54) shows that the problem involves three unknown constants, u, w_m and C, which must be determined.

By use of Eq. (3.51) the work function W can be written on the following form:

$$W = Fw_m + 2\pi a^2\int_0^1 qws\,ds$$

By noting that $q=-p_0$ and by using the dimensionless relations in Eq. (3.2) we obtain the final expression for the work function:

$$W = \tfrac{1}{6} F w_m \left[6 - \bar{a}^2 (3 + C)\right] \tag{3.56}$$

For small rotations, $dw/dr<<1$, the horizontal equilibrium equation given by Jahsman, Field and Holmes (1962) can be shown to simplify to the following relation:

$$\sigma_\varphi = \sigma_r + r\, d\sigma_r / dr \tag{3.57}$$

where $\sigma_i=N_i/h$. In the following analysis we will assume that the stresses in the inner region are related as in an inextensible membrane, for which $d\sigma_r/dr=0$. The above equation then results in the following assumed stress state:

$$\sigma_\varphi = \sigma_r = \varepsilon_r E/(1-\nu) \qquad \text{for} \quad r < a \tag{3.58}$$

It can be observed that the above assumption will result in an overestimation of the strain energy in the inner region since $d\sigma_r/dr<0$. Thus, the solution will be stiffer than if the difference in radial and circumferential stresses had been included and the Ritz solution will remain a lower bound for the membrane deflection. It can also be noted from the solution by Jahsman, Field and Holmes (1962) that large gradients in the radial stress only occurs for small values of the radius r, which reduces the effect of the

last term in Eq. (3.57), especially when the strain energy is integrated over the membrane radius.

The stresses in the outer region are obtained by combining Eqs. (3.36) and (3.34):

$$-\sigma_\varphi = \sigma_r = \varepsilon_r E/(1+\nu) \qquad \text{for} \quad r \geq a \tag{3.59}$$

Note that the assumed membrane slope and stress state are discontinuous at the plastic radius. In practice there will be a transition region with a decreasing slope, resulting in a smooth change of the stress state.

By using Eqs. (3.51), (3.58) and (3.59) we may write the strain energy in Eq. (3.55) as follows

$$\begin{aligned} U &= \frac{1}{2E}\int_0^a 2(1-\nu)\sigma_r{}^2 2\pi h r\,dr + \frac{1}{2E}\int_a^\infty 2(1+\nu)\sigma_r{}^2 2\pi h r\,dr \\ &= \frac{Eh\pi a^2}{(1-\nu)}\int_0^1 \varepsilon_r{}^2 2s\,ds + \frac{Eh\pi a^2}{(1+\nu)}\int_1^\infty \varepsilon_r{}^2 2s\,ds \end{aligned}$$

The radial strain for the inner region is given by Eq. (3.54) and the strain in the outer region by differentiation of Eq. (3.37) and combination with Eq. (3.38). The total strain energy can then be written as follows:

$$U = \frac{Eh\pi a^2}{1-\nu}\int_0^1 2\left[\frac{1}{4}\left(\frac{dw}{dr}\right)^4 + \left(\frac{dw}{dr}\right)^2\frac{u}{a} + \left(\frac{u}{a}\right)^2\right] s\,ds \; + \; \frac{Eh\pi a^2}{1+\nu}\int_1^\infty 2\left(\frac{u}{a}\right)^2 \frac{ds}{s^3}$$

Rearrangement of terms and integration gives the following expression:

$$U = \frac{Eh\pi a^2}{1-\nu}\left\{\int_0^1 \left(\frac{dw}{dr}\right)^2\left[\frac{1}{2}\left(\frac{dw}{dr}\right)^4 + 2\frac{u}{a}\right] s\,ds + \frac{2}{1+\nu}\left(\frac{u}{a}\right)^2\right\} \tag{3.60}$$

The unknown constant u is obtained by differentiating the total potential energy and setting the equation to zero. Note that the work function in Eq. (3.58) is independent of u so that u is given by the following equation:

$$\frac{\partial \Pi}{\partial u} = \frac{\partial U}{\partial u} = \frac{2Eh\pi a}{1-\nu}\left[\int_0^1 \left(\frac{dw}{dr}\right)^2 s\,ds + \frac{2}{1+\nu}\frac{u}{a}\right] = 0$$

The edge displacement u is then related to the other constants by the following equation:

$$u/a = -\tfrac{1}{2}(1+\nu)\,(w_m/a)^2\left(C^2 + 4C + 6\right)/6 \tag{3.61}$$

The above expression is now inserted in Eq. (3.60). The resulting expression for the strain energy involves quartic polynomials in s and the unknown constants C and w_m. After lengthy algebraic manipulations and integrations we finally obtain the following expression for the strain energy:

$$U = \frac{Eh\pi w_m^4}{36(1-\nu)a^2} f(C) \tag{3.62}$$

where the function $f(C)$ is defined by:

$$
\begin{aligned}
&f(C) = \\
&\tfrac{1}{5}\left[C^4(9-5B)+C^3(72-40B)+C^2(252-140B)+C(384-240B)+240-180B\right] \\
&\text{where } B=(1+\nu)/2
\end{aligned}
\tag{3.63}
$$

By inserting Eqs. (3.56) and (3.62) in Eq. (3.55) we obtain the following expression for the potential energy of the membrane:

$$
\begin{aligned}
\Pi &= U - W \\
&= \frac{F}{6}\left\{\frac{\pi E h}{6(1-\nu)Fa^2} w_m^4 f(C) - \left[6-\bar{a}^2(3+C)\right]w_m\right\}
\end{aligned}
$$

Differentiation with respect to C and w_m now results in the following equation system:

$$
\begin{aligned}
\frac{6}{F}\frac{\partial \Pi}{\partial C} &= \frac{\pi E h}{6(1-\nu)Fa^2} w_m^4 f'(C) + \bar{a}^2 w_m = 0 \\
\frac{6}{F}\frac{\partial \Pi}{\partial w_m} &= \frac{\pi E h}{6(1-\nu)Fa^2} w_m^3 4f(C) - \left[6-\bar{a}^2(3+C)\right] = 0
\end{aligned}
$$

If the deflection is assumed to be nonzero, the first equation can be divided with w_m and the above equation system can be written on the following form

$$
\begin{aligned}
&\begin{bmatrix} f'(C) & \bar{a}^2 \\ 4f(C) & \bar{a}^2(3+C)-6 \end{bmatrix}\begin{Bmatrix} {W_m}^3 \\ 1 \end{Bmatrix} = 0 \\
&\text{where} \\
&{W_m}^3 = \frac{\pi E h}{6(1-\nu)Fa^2}{w_m}^3
\end{aligned}
\tag{3.64}
$$

and $f(C)$ is given by Eq. (3.63). The constant C is determined as a function of the dimensionless plastic radius by setting the determinant of Eq. (3.64) to zero:

$$\left[\bar{a}^2(3+C)-6\right]f'(C)-4\bar{a}^2 f(C)=0 \tag{3.65}$$

where $f(C)$ is given by Eq. (3.63). The central deflection w_m is then obtained from Eq. (3.64):

$$w_m=\left[\frac{6(1-\nu)\bar{a}^2}{\pi f'(C)}\frac{Fa^2}{Eh}\right]^{1/3}$$

By use of the dimensionless plastic radius defined in Eq. (3.2) the above equation can be rewritten on the following form:

$$w_m = f_w w_{mF} = f_w\left[\frac{F^2\bar{a}^2}{2p_0 Eh}\right]^{1/3}$$

where (3.66)

$$f_w=\left[\frac{12(1-\nu)\bar{a}^2}{\pi^2 f'(C)}\right]^{1/3}$$

Note that f_w is in effect a correction factor to w_{mF}, which is the solution for a membrane loaded only by a point load, given by Eq. (3.49). The function f_w ranges from 0.67 to 0.77 and has been tabulated in Appendix B.2. The edge slope angle is obtained by evaluation of Eq. (3.52) at the plastic radius (s=1):

$$\theta=-(dw/dr)\big|_{s=1}=(2+C)w_m/a \tag{3.67}$$

We note that the physical limits of θ corresponds to a value of C in the range $-2 \le C \le -1$. The function f_w and the normalized edge slope angle $\theta/(w_m/a)$ for ν=0.3 are shown in Fig. 3.8. It can be noted that the

normalized slope angle for large deflections (loads) is very close to the value 2/3 which applies to a rigidly fixed membrane under a point load when no core pressure is present, as given by Frakes and Simmonds (1985).

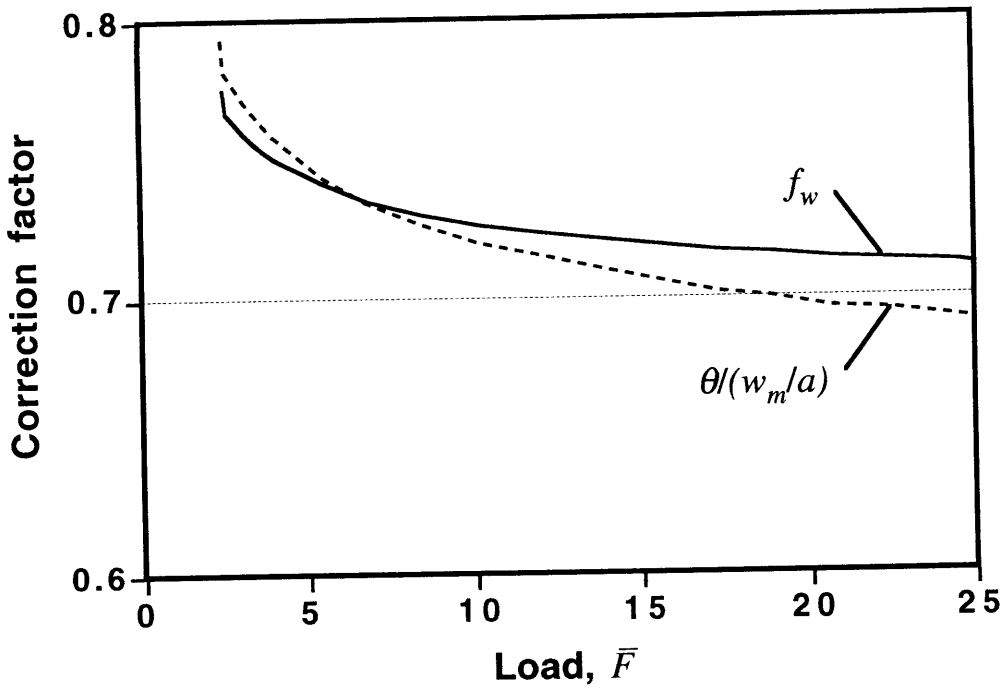

Figure 3.8 Membrane deflection and slope angle normalized by the values for a point load acting alone.

3.5.5 Cusp correction

According to the membrane theory a point load will result in a noncontinuous slope (a cusp) at r=0. In practice the load is distributed over a small area and locally the radius of curvature of a perfect membrane will be equal the to the tip radius of the indentor. The local geometry under the indentor is shown in Fig. 3.9.

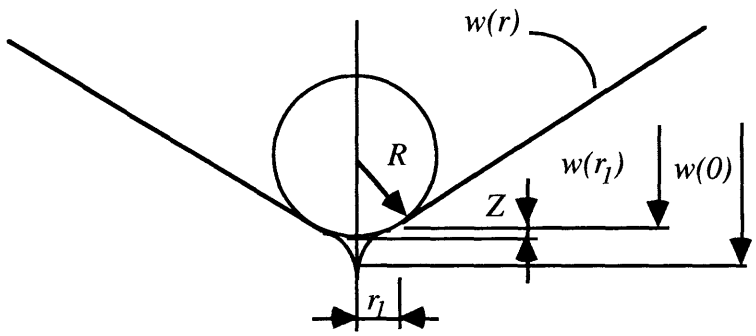

Figure 3.9 Geometry under the indentor.

The equation for the indentor surface is given by:

$$
\begin{aligned}
&(R-Z)^2 + r^2 = R^2 \qquad \text{or} \\
&Z = R\left[1-\sqrt{1-(r/R)^2}\right] \approx R\left[\tfrac{1}{2}(r/R)^2\right] \quad \text{for } (r/R)^2 << 1 \qquad (3.68)\\
&\frac{dZ}{dr} = \frac{r}{R\sqrt{1-(r/R)^2}} \approx r/R \qquad \text{for } (r/R)^2 << 1
\end{aligned}
$$

The previously derived solution is based on the assumption that the radius of contact between the indentor and the face sheet is much smaller than the plastic radius, or equivalently s<<1. From Eqs. (3.50) and (3.51) we conclude

that the deflection and slope of the membrane in this area approximately is given by:

$$w \approx w_m\left[1 + C(r/a)\right]$$
$$dw/dr \approx C w_m/a \qquad \text{for} \qquad r/a << 1 \tag{3.69}$$

The equating of slopes in Eqs. (3.68) and (3.69) gives the following expression for the radius of contact r_1, between the membrane and indentor:

$$r_1 \approx CR w_m/a \tag{3.70}$$

3.5.6 Corrected membrane deflection

After the cusp has been removed, the deflection is given by inserting Eq. (3.70) in Eqs. (3.68) and (3.69):

$$\begin{aligned} w_{mFcorr} &= w_m\left[1+C(r_1/a)\right] + Z(r_1) \\ &= w_m\left[1-RC^2\, w_m/a^2\right] + \tfrac{1}{2}RC^2(w_m/a)^2 \\ &= w_m\left[1-\tfrac{1}{2}C^2\, Rw_m/a^2\right] \end{aligned}$$

By combining the above equation with Eqs. (3.66), (3.49) and (3.2) we finally obtain the following expression for the membrane deflection after correction for the cusp:

$$w_m = f_w\left[\frac{F^2\bar{a}^2}{2p_0Eh}\right]^{1/3}\left[1-\tfrac{\pi}{2}C^2 f_w R\left(\frac{{p_0}^2}{2FEh\bar{a}^4}\right)^{1/3}\right] \tag{3.71}$$

where the last square bracket represents the cusp correction. The uncorrected expression corresponds to an indentor with zero tip radius. For small values of the plastic radius the underlying assumption of a contact radius much smaller than the plastic radius is violated, and the expression may result in an unphysical negative deflection. In such cases it is proposed to set the membrane deflection to zero.

3.6 Large deflection plate analysis

3.6.1 Introduction to large deflection analysis

The linear Kirchhoff plate theory used in section 3.6 only includes bending stresses and is based on infinitesimal deflections from the unloaded shape. It is obvious that generally membrane stresses will be present since any deflection from a flat shape to a doubly curved requires stretching of the plate midplane in addition to bending. Increasing deflections increase both the magnitude and the vertical component of the membrane stresses, resulting in a geometrically nonlinear load-deflection relation. In the following the concepts *linear* and *nonlinear solution* refer to solutions based on *small* and *large deflection theory*. The small deflection solution is based on linear theory, although the core crushing results in a nonlinear load-displacement relation.

The limit of applicability of small deflection theory depends on the type of load and the plate boundary conditions, as well as the required accuracy of the solution. Generally the deviation from linear (small deflection) theory is negligible for $w/h < 0.2$ and almost always significant for $w/h > 1$.

Equations for moderately large deflections of plates have been derived by von Karman, who assumed small strains and rotations ($\theta^2 << 1$) while allowing for large deflections ($w/h \sim 1$). Von Karman's equations in polar coordinates have been given, for example by Szilard (1974). These equations

are coupled and nonlinear, and solutions have only been found in a few cases.

Approximate solutions for large plate deflections are often based on corrections of Kirchhoff's equations for small deflections by considering the membrane stresses caused by the small deflection solution.

As discussed by Volmir (1962) first order large deflection theory neglecting shear generally results in load deflection relations of the following type:

$$\tilde{F}_{NL} = \tilde{k}_b \overline{w} + \tilde{k}_m \overline{w}^3$$
$$\text{where } \overline{w} = w_0/h \text{ and } \tilde{F} = Fa^2/\left(\pi E h^4\right) \tag{3.72}$$

and where the subscript *NL* refers to the nonlinear solution. The constants $\tilde{k}_b$ and $\tilde{k}_m$ are dimensionless stiffnesses for the particular load case associated with small deflection plate bending theory and additional membrane effects given by first order large deflection theory, respectively.

The general form of Eq. (3.72) can be understood by considering Fig. 3.7 and Eq. (3.53.a). In first order large deflection plate theory the deflection shape is assumed to remain unaltered by the membrane stresses. Thus the deflection shape is given by the small deflection solution where all slopes are proportional to the peak deflection. Assuming small rotations ($\theta << 1$) the additional vertical force component V due to large deflections is given by:

$$V = -N_r \frac{dw}{dr} \propto \varepsilon_r \frac{dw}{dr} \propto \left(\frac{dw}{dr}\right)^3 \propto \overline{w}^3 \tag{3.73}$$

The linear small deflection solution $\overline{w}<<1$ is obtained by neglecting the second term in Eq. (3.72). The ratio between the forces given by the nonlinear (*NL*) and linear (*L*) solutions for a given deflection can then be written:

$$\tilde{F}_{NL}/\tilde{F}_L = 1+\bar{k}_m\overline{w}^2 \qquad \text{where } \bar{k}_m = \tilde{k}_m/\tilde{k}_b \tag{3.74}$$

Generally the constant $\bar{k}_m$ depends on the boundary conditions and the type of load. Clearly the expression (3.74) is sensitive to the stiffness $\bar{k}_m$. The works by Dolovich et al. (1988) and Striz, Jang and Bert (1988) both indicate that simple first order variational solutions overestimate the nonlinear stiffness coefficient $\bar{k}_m$ appreciably. In addition the solution by Dolovich et al (1988) show that the ratio $\bar{k}_m$ is decreasing with increasing deflections. Large deflection plate theory is generally valid for deflections in the order of the plate thickness, but becomes increasingly inaccurate for larger deflections. We conclude that the present solution, which neglects the effects of changes in the deflection shape, is valid only for intermediate deflections, where it will give an upper estimate of the actual load.

The present problem involves the combined loading of a central point load and a uniform reactive pressure as well as rotational and radial edge constraints. No general analytical solution has been found to this problem and solutions for a combined point load and uniform pressure on a circular plate are only available for a few elementary boundary conditions. Saibel and Tadjbaksh (1960) considered von Karman's equations for an immovable clamped plate under combined loading and obtained a perturbation solution

based on the plate deflection. Schmidt and DaDeppo (1976) used nonlinear Kirchhoff plate theory to obtain a similar perturbation solution for the combined loading on a plate with sliding clamps.

3.6.2 Nonlinear stiffness under different boundary conditions

In this section solutions for a uniform pressure interacting with a point load will be given for boundary conditions in four limiting cases:

a) Edges in fixed clamps

An approximate perturbation solution to von Karman's equations for this problem was given by Saibel and Tadjbaksh (1960) who used the center deflection as perturbation parameter. The first two terms of the solution, which corresponds to a first order large deflection analysis are given by:

$$\tilde{F}=\frac{8(1+\beta)}{(1+1/\beta)}\left[\lambda_1 2\left[12\left(1-\nu^2\right)\right]^{1/2}\overline{w}+\lambda_3 8\left[12\left(1-\nu^2\right)\right]^{3/2}\overline{w}^3\right]\Big/\left[12\left(1-\nu^2\right)\right]^{3/2} \quad (3.75)$$

where

$\lambda_1=4/(1+4\beta)$

$\lambda_3=\frac{1}{64}\lambda_1^4\left[\beta^3\left(\frac{1}{8}\alpha_1-\frac{47}{81}\right)+\frac{1}{36}\beta^2\left(\alpha_2+\frac{5}{4}\alpha_1-\frac{791}{64}\right)\right.$

$\left.+\frac{1}{24}\beta\left(\frac{1}{4}\alpha_3+\frac{5}{27}\alpha_2-\frac{953}{600}\right)+\frac{1}{1728}\left(5\alpha_3-\frac{77}{10}\right)\right]$

$\alpha_1=(9-7\nu)/(1-\nu)$ $\quad$ $\alpha_2=(16-11\nu)/(1-\nu)$ $\quad$ $\alpha_3=(5-3\nu)/(1-\nu)$

$\beta=F/\left(q\pi a^2\right)$

Note: $\beta=F/\left(-p_0\pi a^2\right)=-1/\bar{a}^2$ in the present problem

The above equation can be rewritten on the following form:

$$\tilde{F}=\frac{4\beta\lambda_1\overline{w}}{3\left(1-\nu^2\right)}\left[1+\bar{k}_m\overline{w}^2\right] \quad (3.76)$$

where $\bar{k}_m=48\left(1-\nu^2\right)\lambda_3/\lambda_1$

The parameters β, λ_1 and λ_3 in Eq. (3.76) are defined in Eq. (3.75). A misprint in the original expression for α_1 has been corrected as proposed by Schmidt and DaDeppo (1976).

The radial stress at $r = a$ is given by the following expression:

$$N_r(a) = \frac{Eh^3}{3(1-\nu^2)a^2}\sum_{k=1}^{\infty}\psi_{2k}(1)W_m^{2k} \approx \frac{48Eh^3}{3a^2}\psi_2(1)\overline{w}^2$$

$$\text{where } W_m = 2\sqrt{12(1-\nu^2)}\,\overline{w} \tag{3.77}$$

$$\psi_2(1) = \tfrac{1}{32}\lambda_1^2\left[\beta^2(\alpha_1 - 7)/4 + \beta(\alpha_2 - 11)/18 + (\alpha_3 - 3)/48\right]$$

The functions used in Eq. (3.77) have been defined in Eq. (3.75). The truncation of the serial expansion of N_r after k=1 corresponds to the first order large deflection solution given in Eq. (3.75).

b) Edges in sliding clamps

An approximate solution for this problem, based on large deflection corrections to Kirchhoff's theory, was given by Schmidt and DaDeppo (1976). The first two terms, which corresponds to a first order large deflection theory are given by the following equation:

$$\tilde{F} = \frac{Fa^2}{\pi Eh^4} = \frac{\beta q a^4}{Eh^4}$$

$$= \left[\frac{4\beta\lambda_1}{3(1-\nu^2)}\overline{w} + \frac{\beta\lambda_1}{8100}\left(\tfrac{1212}{64}\beta^3\lambda_1^3 + \tfrac{4409}{16}\beta^2\lambda_1^2 - \tfrac{388}{4}\beta\lambda_1 + 2190\right)\overline{w}^3\right]$$

The above equation can be rewritten on the following form:

$$\tilde{F} = \frac{Fa^2}{\pi Eh^4} = \frac{\beta q a^4}{Eh^4} = \frac{4\beta\lambda_1 \overline{w}}{3(1-\nu^2)}\left[1 + \bar{k}_m \overline{w}^2\right] \tag{3.78}$$

where $\bar{k}_m = (1-\nu^2)\left[\frac{303}{16}\beta^3\lambda_1{}^3 + \frac{4409}{16}\beta^2\lambda_1{}^2 - 97\beta\lambda_1 + 2190\right]/10800$

The parameters β, λ_1 and λ_3 in Eq. (3.78) have been defined in Eq. (3.75).

c) Edges in fixed hinges

No solution was found for mixed loads on plates with hinged edges. We will therefore use the solutions for the clamped cases to derive an approximate solution with sufficient accuracy in the range where large deflections normally occur. For the combined point load and reactive pressure case we observe that the solutions for hinged and clamped cases will be identical when $\bar{a}^2$=2, which corresponds to $M_r(a) = 0$ in the clamped case and $\theta(a)$=0 in the hinged case. For hinged plates an additional reactive force is due to the edge slope which results in a vertical component of the edge membrane stress:

$$\delta F = 2\pi a N_r(a)\theta \tag{3.79}$$

To estimate the stiffening effect in the case of immovably hinged edges we use the expression by Saibel and Tadjbaksh (1960) for the radial edge stress in an immovably clamped plate, Eq. (3.77). For zero edge slope ($\bar{a}^2$=2) this stress will be identical to the edge stress in the immovably hinged case. To predict the edge slope θ we use the expression given by the linear solution for a hinged plate:

$$\theta = \frac{F_{Lhi}\left(2 - \bar{a}^2\right)}{8\pi D(1+\nu)} \tag{3.80}$$

where the subscript L refers to the linear solution and hi to hinged edge conditions. For large deflections of a plate with immovably hinged edges the increase in load for a given deflection is partly due to the resistance to stretching and partly due to the vertical component of the edge membrane stress. Here we will assume that the load increase due to stretching is equal to that of an immovably clamped plate, which is virtually independent of the load ratio $\bar{a}^2 = p_0 \pi a^2 / F$. With the above assumption and by use of the definition of the dimensionless force $\tilde{F}$ given in Eq. (3.72) the ratio between the nonlinear and linear solutions for a hinged plate of radius a can be written

$$\tilde{F}_{NLhi} / \tilde{F}_{Lhi} = \tilde{F}_{NLcl} / \tilde{F}_{Lcl} + 2\pi a N_{rhi} \theta / F_{Lhi}$$

where the subscripts NL and L refer to the nonlinear and linear solutions and hi and cl to hinged and clamped edge conditions. The nonlinear solutions are given by Eqs. (3.76) and (3.78) while the linear solutions are obtained by dropping the last term in these equations. For zero edge slope ($\bar{a}^2 = 2$) the assumption of an equal stiffening due to stretching in the hinged and clamped plate will be completely satisfied since the deflection shapes of the two plates are identical in this case. As the edge slope increases the stiffening due to stretching will be increasingly different for the clamped and hinged plate. A qualitative estimate of the difference can be obtained by comparing the average strains in the deflected shapes of a clamped and

hinged plate loaded only by a point load. It is seen that the average strain in the clamped plate is only a few percent higher than in the hinged plate, which indicates that the difference in stiffening due to stretching should be moderate.

An approximate solution for the case with fixed hinged edges is now obtained from the following first order Taylor expansion around θ=0 ($\bar{a}^2$=2):

$$\frac{\tilde{F}_{NLhi}}{\tilde{F}_{Lhi}} \approx \left.\frac{\tilde{F}_{NLhi}}{\tilde{F}_{Lhi}}\right|_{\theta=0} + \left.\frac{\partial}{\partial\theta}\left(\frac{\tilde{F}_{NLhi}}{\tilde{F}_{Lhi}}\right)\right|_{\theta=0} \theta \approx$$

$$\approx \left.\frac{\tilde{F}_{NLhi}}{\tilde{F}_{Lhi}}\right|_{\theta=0} + \left.\frac{2\pi a N_{rhi}}{F_{Lhi}}\right|_{\theta=0} \theta + \left.\frac{2\pi a\theta}{F_{Lhi}}\frac{\partial N_{rhi}}{\partial\theta}\right|_{\theta=0} \theta - \left.\frac{2\pi a\theta N_{rhi}}{F_{Lhi}^2}\frac{\partial F_{Lhi}}{\partial\theta}\right|_{\theta=0} \theta$$

By neglecting higher order terms in θ and by noting that the solutions for the hinged and clamped plate are identical for θ=0 ($\bar{a}^2$=2) we obtain the following approximate large deflection solution for the hinged plate:

$$\frac{\tilde{F}_{NLhi}}{\tilde{F}_{Lhi}} \approx \left.\frac{\tilde{F}_{NLcl}}{\tilde{F}_{Lcl}}\right|_{\theta=0} + \left.\frac{2\pi a N_{rcl}}{F_{Lcl}}\right|_{\theta=0} \theta$$

The use of Eqs. (3.76), (3.77) and (3.80) for ν=0.3 and $\bar{a}^2$=2 (θ=0) gives the following solution for the plate with fixed hinges:

$$\tilde{F}_{NL}/\tilde{F}_L = 1 + \left[0.466 + \frac{Eh^3\left(2-\bar{a}^2\right)}{4D(1+\nu)}0.296\right]\bar{w}^2$$

For a homogenous transversely isotropic plate $Eh^3=12(1-\nu^2)D$ and the above equation can be rewritten to:

$$\tilde{F}_{NL}/\tilde{F}_L = 1 + \bar{k}_m \bar{w}^2 \approx 1 + \left[0.466 + 3(1-\nu)\left(2-\bar{a}^2\right)0.296\right]\bar{w}^2 \tag{3.81}$$

The present approximate solution, Eq. (3.81), has been tabulated for different values of $\bar{a}^2$ in Table 3.1. The minimum value of the dimensionless plastic radius is $\bar{a}^2=0$ while an upper physical bound is $\bar{a}^2=2$, since the slope angle in Eq. (3.80) is zero or positive. We note that the deviation from known closed form solutions in Table 3.1 is 20–35% for $\bar{a}^2=0$ and 0% for $\bar{a}^2=2$, where the solutions for hinged and clamped plates coincide due to zero edge slope. Thus the proposed solution is expected to have acceptable accuracy, especially since we only consider large deflections in the plastic region which do not occur for very small values of the plastic radius.

d) Edges in sliding hinges

As for the case with fixed edges we may conclude that the solutions for edges in sliding clamps, Eq. (3.78) and sliding hinges will be identical for $\bar{a}^2=2$. The solution for vanishing plastic radius ($\bar{a}^2=0$) is given by the single load solutions for a point load, which are shown in uppermost part of Table 3.1. It is seen that the ratio is almost the same as for $\bar{a}^2=2$. No additional edge forces will occur for $\theta\neq 0$ since $N=0$ at $r = a$. We conclude that the stiffness ratio in the plate with edges in sliding hinges will be virtually constant for $0 \leq \bar{a}^2 \leq 2$ and in Table 3.1 and the following analysis it has been assumed that the stiffness ratio is equal to the value at $\bar{a}^2=2$.

The values in Table 3.1 for $\bar{a}^2=0$ and $\bar{a}^2=\infty$ correspond to single load solutions for a point load and a uniform pressure, respectively, calculated by

a variety of methods and published in the references shown in the table. Note the disagreement between many of these values. It should also be mentioned that the stiffness ratios are discontinuous in the interval $2 \leq \bar{a}^2 \leq \infty$, since there is a sign change in the deflection at a certain value of $\bar{a}^2$. Thus the stiffness ratios for a uniform pressure alone cannot be used as asymptotic values for the case of zero edge slope, which occurs at $\bar{a}^2 \geq 2$.

References for Table 3.1

1) Volmir (1962)
2) Banerjee (1983)
3) Ferriss (1991)
4) Bert and Martindale (1988), *w/h*=1
5) Way (1934), *w/h*=1
6) Schmidt (1987), *w/h*=1
7) Dolovich, Brodland and Thornton-Trump (1988), *w/h*=1
8) Striz, Jang and Bert (1988), FEM–analysis, *w/h*=1
9) Eq. (3.76), Saibel and Tadjbaksh (1960)
10) Eq. (3.78), Schmidt and DaDeppo (1976)
11) Eq. (3.81), Olsson (present work)
12) Assumed value in present analysis

References 4) to 8) are improved solutions with non–constant $\bar{k}_m$.

Table 3.1 Dimensionless stiffness for different loads and boundary conditions

$\bar{F}$	$\bar{a}^2$	$\beta = -1/\bar{a}^2$	$\bar{k}_m$ (ν=0.3)			
			fixed clamps	sliding clamps	fixed hinges	sliding hinges
∞ *	0	∞	~0.39 [8]		~0.92 [8]	
∞ *	0	∞	~0.36 [7]			
∞ *	0	∞	~0.45 [4]			0.208 [3]
∞ *	0	∞	0.430 [2]	0.110 [2]	1.260 [2]	0.160 [2]
∞ *	0	∞	0.443 [1]	0.200 [1]	1.430 [1]	0.272 [1]
2.574	0.004	−250	0.445 [9]	0.200 [10]	1.710 [11]	0.264 [12]
2.960	0.084	−11.905	0.444	0.201	1.657	|
3.802	0.262	−3.817	0.443	0.203	1.546	|
5.005	0.450	−2.222	0.441	0.206	1.399	|
7.861	0.733	−1.164	0.440	0.209	1.254	|
10.253	0.878	−1.139	0.440	0.211	1.163	|
12.057	0.959	−1.043	0.440	0.213	1.113	|
15.075	1.062	−0.942	0.439	0.216	1.088	|
17.293	1.171	−0.893	0.439	0.218	1.013	|
22.217	1.217	−0.822	0.440	0.222	0.981	|
24.240	1.248	−0.801	0.440	0.223	0.933	|
27.795	1.295	−0.772	0.441	0.225	0.904	|
~40	1.500	−0.667	0.444	0.233	0.777	|
∞	2.000	−0.500	0.466 [9]	0.264 [10]	0.466 [11]	0.264 [12]
–	1000	−0.001	0.546 [9]	0.185 [10]	–	0.264 [12]
0*	∞	0	0.544 [1]	0.146 [1]	1.852 [1]	0.262 [1]
0*	∞	0	~0.56 [4] [5]		~1.46 [8]	0.221 [3]
0*	∞	0	~0.59 [6]			
0*	∞	0	~0.53 [8]			

* Single load solutions NOTE: References given on the preceding page.

3.6.3 Ratio between large and small deflection solutions

In the present case the edges of the inner plastic region are radially and rotationally constrained rather than rigidly clamped. We will seek an approximate solution based on interpolation between the solutions for the four elementary boundary conditions given in the previous section.

From section 3.5.2 we recall that the edge stress for a radially constrained membrane under uniform stress was approximately one third of the stress for a membrane with immovably fixed edges, where the exact ratio of the stresses depends on Poisson's ratio. A comparison with the results by Jahsman, Field and Holmes (1962) shows that the addition of a point load only causes a relatively local deviation from the prestressed uniform stress state. We will assume that the membrane stress state is representative for the membrane stresses in a plate undergoing large deflections.

As shown by Pettersson (1954), for radial edge loads and axisymmetric transversal loads interacting on a circular plate of radius a, the ratio between the transversal loads required to obtain a certain deflection for the cases of radial edge load N_K and zero edge load is given by:

$$\frac{F(N=N_K)}{F(N=0)} = 1 + N_K/N_{cr} \tag{3.82}$$

where N_{cr} is the lowest critical buckling load of the plate. For the case where the edge loads are caused by large deflections, so that $F(N=N_K)$ corresponds to $F_{NL}(N=N_K)$ and $F(N=0)$ to $F_L(N=0)$ we get the following relation:

$$\frac{F_{NL}(N=N_K)/F_L(N=0)}{F_{NL}(N=0)/F_L(N=0)} - 1 = \frac{1+\bar{k}_{mK}\,\bar{w}^2}{1+\bar{k}_{mslide}\,\bar{w}^2} - 1 = N_K/N_{crK} \qquad (3.83)$$

where $\bar{k}_{mslide}$ and $\bar{k}_{mK}$ are the dimensionless membrane stiffnesses associated with stress free edges and the edge stress N_K, respectively. The quantity N_{crK} is the buckling load associated with the boundary condition which results in the edge stress N_K. The approach was checked by verifying that the stiffness ratio for plates with fixed edges could be obtained from the solutions for sliding edges (N=0) by inserting proper values of the critical buckling load and edge stresses as given by solutions for fixed edges.

By taking the ratio of Eq. (3.83) for the cases with constrained and fixed edges we obtain an expression relating the dimensionless stiffnesses to the ratio of the edge loads. By using the assumed relation between N and N_{fixed} given in Eq. (3.41) and solving for the unknown membrane stiffness in the constrained case we obtain the following expression:

$$\bar{k}_{mj} = \left[(1+\nu)\bar{k}_{mKslide} + (1-\nu)\bar{k}_{mKfixed}\right]/2 \qquad \text{where } \bar{k}_{mK} = \bar{k}_{mcl} \text{ or } \bar{k}_{mhi} \qquad (3.84)$$

where the subscript K refers to either clamped (*cl*) or hinged (*hi*) edge conditions and *slide* and *fixed* refer to radially free or fixed edges. To include the effect of rotational constraint we will use a linear interpolation between the hinged and clamped case where the dimensionless edge moment $\bar{M}(\bar{F},\nu)$ is expressed as a fraction of the corresponding moment $\bar{M}_{cl}$ for a clamped plate. By using Eq.(3.2) and equations from linear plate theory as given for example by Szilard(1974) we find that the dimensionless edge moment of a clamped plate can be written as follows:

$$\overline{M}_{cl} = \overline{a}^2 - 2 \tag{3.85}$$

The resulting nonlinearity coefficient for the present plate with radially and rotationally constrained edges will now be given by:

$$\bar{k}_m = \bar{k}_{mhi} + \left(\overline{M}/\overline{M}_{cl}\right)\left[\bar{k}_{mcl} - \bar{k}_{mhi}\right] \tag{3.86}$$

where the quantities on the right hand side are given by Eqs. (3.84), (3.85) and in the table of Appendix B.1.

The dimensionless force $\tilde{F}$ defined in Eq. (3.72) involves the plastic radius *a*. By plotting the small deflection solution for the dimensionless plastic radius versus force $\overline{F}$ in a log-log diagram it is seen that the relation can be approximated by the following relation:

$$\overline{a}^2 = C_0 \overline{F}^{\mu} \tag{3.87}$$

where the exponent μ only changes slowly with the dimensionless force, except for loads just above the load for initiation of core yielding. The value of μ has been tabulated in Table 3.2.

Two factors contribute to the increased force during large deflections of the inner region. The first is due to resistance to midplane stretching and the second is due to the vertical component of the membrane edge force, which acts a fictitious edge shear load. Only the latter contributes to an increasing plastic radius. As previously we will assume that the stiffening due to

stretching is approximately equal in the hinged and clamped plates. The effective force $\overline{F}_{NL}^{*}$ contributing to an increase in plastic radius is then obtained by subtracting the force contribution for a clamped plate. The ratio of plastic radii is now approximately given by:

$$\bar{a}_{NL}{}^2/\bar{a}_L{}^2 = \left(\overline{F}_{NL}^{*}/\overline{F}_L\right)^{\mu} = \left[1+\left(\bar{k}_m - \bar{k}_{mcl}\right)\overline{w}^2\right]^{\mu} \tag{3.88}$$

Using Eqs. (3.2), (3.72) and (3.87) we obtain the following expression for the ratio between dimensionless forces in the nonlinear and linear solutions:

$$\frac{\tilde{F}_{NL}}{\tilde{F}_L} = \frac{F_{NL}a_{NL}{}^2}{F_L a_L{}^2} = \frac{F_{NL}{}^2\bar{a}_{NL}{}^2}{F_L{}^2\bar{a}_L{}^2} = \frac{\overline{F}_{NL}{}^2}{\overline{F}_L{}^2}\left[1+\left(\bar{k}_m - \bar{k}_{mcl}\right)\overline{w}^2\right]^{\mu}$$

where $\bar{a}_{NL}$ and $\bar{a}_L$ are the plastic radii associated with the nonlinear and linear solutions, respectively. Solving for the ratio of barred forces and using Eq. (3.74) we finally obtain:

$$\overline{F}_{NL}/\overline{F}_L = \sqrt{\left(1+\bar{k}_m\overline{w}^2\right)/\left[1+\left(\bar{k}_m - \bar{k}_{mcl}\right)\overline{w}^2\right]^{\mu}} \tag{3.89}$$

where the values of $\bar{k}_m$ and μ for ν=0.3 are given in Table 3.2. Equation (3.74) gives the ratio of the forces for the nonlinear and linear plate solution for a plate with constant radius, while the solution in Eq. (3.89) in an approximate way takes into account the effect of the increase in radius caused by the increased edge load. By definition $\overline{F}_{NL}/\overline{F}_L$ is equal to, or larger than unity. For small values of the plastic radius, where this condition may not be satisfied by Eq. (3.89) it is proposed to set $\overline{F}_{NL} = \overline{F}_L$.

Table 3.2 allows for a comparison between the dimensionless edge moment $\overline{M}$ of the inner region with that of a clamped plate, $\overline{M}_{cl}$. The membrane stiffness ratio $\bar{k}_m$ for the radially constrained inner region can also be compared with the values $\bar{k}_{m\mathrm{hi}}$ and $\bar{k}_{m\mathrm{cl}}$ for a hinged and clamped plate having the same radial constraint. For practical calculations, the parameters $\overline{F}$, $\bar{a}^2$ and $8\overline{M}/\overline{F}$ are used in the linear analysis of Eq. (3.16), while the resulting deflection $\overline{w}$ and the parameters $\bar{k}_m$, $\bar{k}_{m\mathrm{cl}}$ and μ are used for the nonlinear correction in Eq. (3.89).

Table 3.2 Dimensionless nonlinear stiffness $\bar{k}_m$ versus dimensionless load $\bar{F}$, (ν=0.3)

$\bar{F}$	$\bar{a}^2$	$8\bar{M}/\bar{F}$	$8\bar{M}_{cl}/\bar{F}$ $\left(\bar{a}^2-2\right)$	clamped $\bar{k}_{m\mathrm{cl}}$	hinged $\bar{k}_{m\mathrm{hi}}$	present $\bar{k}_m$	μ
2.546	0	∞	−2				∞
2.574	0.004	+10	−1.966	0.286	0.770	3.232	~200
2.960	0.084	1.569	−1.916	0.286	0.752	1.134	6.6
3.802	0.262	0.188	−1.738	0.287	0.713	0.759	2.5
5.005	0.450	−0.345	−1.550	0.288	0.661	0.578	1.6
7.861	0.733	−0.648	−1.267	0.290	0.611	0.447	0.8
10.253	0.878	−0.689	−1.122	0.291	0.579	0.402	0.6
12.057	0.959	−0.690	−1.041	0.292	0.561	0.383	0.5
15.075	1.062	−0.673	−0.938	0.294	0.552	0.367	0.4
17.293	1.120	−0.656	−0.880	0.295	0.526	0.354	0.3
19.674	1.171	−0.637	−0.829	0.297	0.521	0.349	0.3
22.217	1.217	−0.617	−0.783	0.298	0.515	0.344	0.3
24.240	1.248	−0.603	−0.752	0.299	0.498	0.338	0.3
27.795	1.295	−0.577	−0.705	0.301	0.488	0.335	0.3
∞	2	0	0	0.335	0.335	0.335	<0.3

3.7 Contact deformation

The local compression due to the contact stresses between the indentor and the face sheet may be analyzed using a modification of Hertz's contact theory, which is based on linear elasticity of isotropic bodies. Hertz's theory relates the total contact force F, to the approach α, which is the maximum relative displacement of the bodies in contact. Here we define α as the relative displacement between the center of curvature of the indentor and the lower surface of the face sheet, Fig. 3.10.

$$\alpha = w_2 - w_1 \tag{3.90}$$

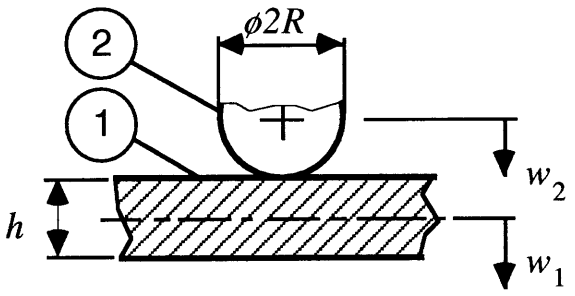

Figure 3.10 Definition of the local contact problem.

When a hemisphere is pushed into a halfspace with a contact force F, Hertz's theory states that the approach α is given by:

$$\alpha = \left(F/k_\alpha\right)^{2/3} \tag{3.91}$$

where $k_\alpha = \frac{4}{3} Q_\alpha \sqrt{R}$ (3.92)

$$\text{with} \quad Q_i = E_i/(1-\nu_i^2) \tag{3.93}$$

$$\text{and} \quad 1/Q_\alpha = 1/Q_1 + 1/Q_2 \tag{3.94}$$

where index 1 refers to the face sheet and index 2 to the indentor. For cases where the indentor is much stiffer than the face sheet Eq. (3.94) simplifies to $Q_\alpha \approx Q_1$. The contact radius is given by the following expression;

$$c = \sqrt{R\alpha} = \left(\tfrac{3}{4} FR/Q_\alpha\right)^{1/3} \tag{3.95}$$

and the contact pressure by:

$$q(r) = \frac{3F}{2\pi c^2}\sqrt{1-r^2/c^2} \qquad (r \le c) \tag{3.96}$$

The above expressions remain valid for the indentation of a transversely isotropic halfspace but Q_1 must be replaced by the expression:

$$Q_1 = 1/(\pi k_1') = 2\sqrt{G_{zr}/A_{22}}\left(A_{11}A_{22} - A_{12}^2\right)\Big/\sqrt{\left(\sqrt{A_{11}A_{22}} + G_{zr}\right)^2 - \left(A_{12} + G_{zr}\right)^2}$$

where

$$\begin{aligned} A_{11} &= E_z(1-\nu_r)\beta \\ A_{22} &= E_r\left(1-\nu_{zr}^2\delta\right)\beta/(1+\nu_r) \\ A_{12} &= E_r\nu_{zr}\beta \\ \beta &= 1/\left(1-\nu_r-2\nu_{zr}^2\delta\right) \\ \delta &= E_r/E_z \end{aligned} \tag{3.97}$$

which originally was derived by Conway (1956) and later put into the more convenient form of Eq. (3.97) by Greszczuk (1982).

In most cases the local indentation is very small in comparison to the face sheet deflection and we may use an approximate expression for the out-of-plane stiffness based on a simple generalization of Eq. (3.93):

$$Q_1 = E_z/(1 - \nu_{rz}\nu_{zr}) = E_z/(1 - \nu_{rz}^2 E_z/E_r) \tag{3.98}$$

In most laminated face sheets $\nu_{rz} \approx 1/2$ and $E_z/E_r << 1$ and the expression simplifies to

$$Q_1 \approx E_z \tag{3.99}$$

It should be noted that E_z of a laminate generally is higher than E_z of a single ply, which has been discussed by Olsson (1993).

Although the present equations were derived assuming indentation of a surface of infinite depth it has been shown by Olsson (1993) that the contact stresses are small for depths larger than c and negligible for depths larger than $2c$. Thus the assumption of a halfspace will be acceptable for $2c < h$. The cases where this condition is not fulfilled will normally correspond to load levels where the local indentation is negligible in comparison to the global face sheet deflection.

3.8 Shear deformation

The shear deformation of the face sheet in the plastic region is composed of the shear deformations due to a concentrated load and a uniform pressure. It should be noted that the size of the contact area must be taken into account since a point load yields infinite shear deformations.

Although the actual pressure distribution is parabolic, we will assume that the contact load is uniformly distributed over the contact area and use the following expression for the central shear deflection w_{sF} due to a load F uniformly distributed inside a small radius c:

$$w_{sF} = \frac{\left(1 - 4\nu_{rz}G_{zr}/E_r\right)\left(1 + \frac{3}{4}\ln[c/a]\right)}{\pi\ G_{zr}\ h} F \tag{3.100}$$

This expression was given by Shivakumar, Elber and Illg (1985) who used a model of the type shown in Fig. 3.3 to analyze large deflection impacts on circular transversely isotropic plates.

Assuming plane stress, the central shear deflection w_{sp} due to a uniform pressure on an isotropic circular plate has been given by Timoshenko and Woinowsky-Krieger (1959). An obvious generalization to transverse isotropy is obtained by replacing G related to transverse shear with G_{zr} and ν/E related to radial strain caused by transverse pressure with ν_{zr}/E_r. The shear deflection w_{sp} of a transversely isotropic plate due to a uniform pressure p_0 is then given by:

$$w_{sp} = \frac{p_0 a^2}{8h}\left[\frac{3}{G_{rz}} - \frac{4\nu_{rz}}{E_r}\right] = \frac{\bar{a}^2(3-4\nu_{rz}G_{rz}/E_r)}{8\pi\ G_{rz}h}F \tag{3.101}$$

where we have used the definition of $\bar{a}$ given in Eq. (3.2). Now the total shear deformation is given by:

$$w_s = w_{sF} - w_{sp} = \frac{(1-4\nu_{rz}G_{rz}/E_r)\left(1-\bar{a}^2/8+\frac{3}{4}\ln[a/c]\right)-\bar{a}^2/4}{\pi\ G_{rz}h}\ F$$

where (3.102)

$$\ln(a/c) = \ln\left[\bar{a}\left(\frac{4Q_c}{3\pi p_0}\right)^{1/3}\left(\frac{F}{p_0\pi R^2}\right)^{1/6}\right] = \ln\bar{a} + \tfrac{1}{3}\ln\left(\frac{4Q_c}{3\pi p_0}\right) + \tfrac{1}{6}\ln\left(\frac{F}{p_0\pi R^2}\right)$$

Here we have used Eqs. (3.2) and (3.95) to express ln (*a/c*).

3.9 Resulting load-indentation solutions

The solutions resulting from the previous analysis can now be summarized. The squared plastic radius and edge moment given by the plate and membrane solutions for ν=0.3 have been compared in Fig. 3.11 below.

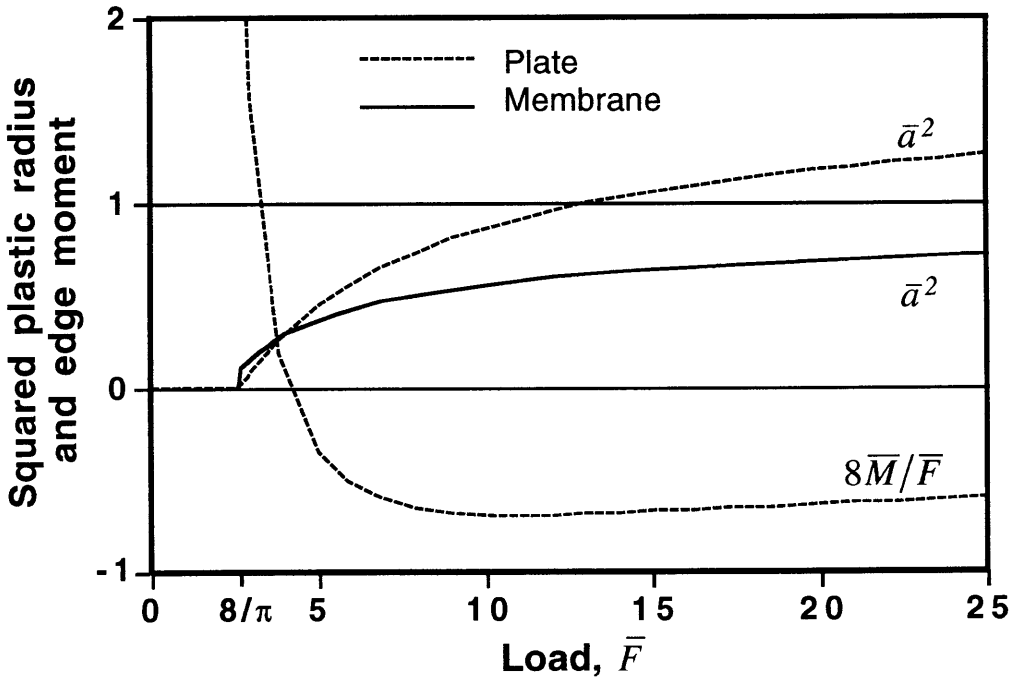

Figure 3.11 Comparison of the squared plastic radius and edge moment given by the plate and membrane solutions for ν=0.3.

When compared with the plate solution it is seen that the membrane solution results in a zero edge moment and a slightly smaller plastic radius. In Fig. 3.11 the difference between the two solutions has been enhanced by the squaring of the plastic radius. It is also seen that the plastic radius is zero for dimensionless loads equal to or smaller than 8/π. In such cases the solution for a fully elastic foundation applies.

3.9.1 Resulting small deflection plate solution

Prior to core yielding, $\overline{F} \le 8/\pi$

Neglecting shear and using Eqs. (3.91) and (3.8) we find that the deflection is given by:

$$w = \alpha + w_b = \left(F/k_\alpha\right)^{2/3} + \tfrac{1}{8} F/\sqrt{kD} \tag{3.103}$$

where k is the foundation stiffness and k_α is the contact stiffness defined in Eq. (3.92).

After core yielding, $\overline{F} > 8/\pi$

Combining Eqs. (3.91), (3.9), (3.16) and (3.102) we find the deflection to be given by:

$$w = \alpha + w_a + w_b + w_s = \left(F/k_\alpha\right)^{2/3} + \frac{p_0}{k} + \frac{F^2\overline{a}^2}{16\pi^2 p_0 D(1+\nu)}\left[(3+\nu) - \overline{a}^2(5+\nu)/4 + 8\overline{M}/\overline{F}\right] + \frac{\left(1-4\nu_{rz}G_{rz}/E_r\right)\left[4 - \overline{a}^2/2 + 3\ln\overline{a} + \ln\left(\frac{4}{3\pi}Q_\alpha/p_0\right) + \ln\left(\overline{F}\,L_0/R\right)\right] - \overline{a}^2}{4\pi\ G_{rz}h} F \tag{3.104}$$

where $\bar{a}^2$ is obtained by solving Eq. (3.27). The dimensionless edge moment $\overline{M}$ is then obtained by dividing the right hand side of Eq. (3.22) with the dimensional quantities, which can be seen from the definitions in Eq. (3.2). The solution is shown graphically for ν=0.3 in Fig. 3.11 and has been tabulated for different values of Poisson's ratio in appendix B. If contact indentation and shear deformation is neglected the solution may be written on the following dimensionless form:

$$w/w_a = (w_a + w_b)/w_a = \tag{3.105}$$

$$1 + \frac{\overline{F}^2\bar{a}^2}{16(1+\nu)}\left[(3+\nu) - \bar{a}^2(5+\nu)/4 + 8\overline{M}/\overline{F}\right]$$

3.9.2 Resulting large deflection plate solution

For large deflections, $w/h > 1$, the relation between the load obtained using large deflection analysis (NL) and small deflection analysis (L) for a given deflection is given by:

$$\overline{F}_{NL}/\overline{F}_L = \sqrt{\left(1+\bar{k}_m\overline{w}^2\right)/\left[1+\left(\bar{k}_m - \bar{k}_{mcl}\right)\overline{w}^2\right]^{\mu}} \tag{3.106}$$

where the values of $\bar{k}_m$, $\bar{k}_{mcl}$ and μ for ν=0.3 have been given in Table 3.2.

3.9.3 Resulting membrane solution

Under the assumptions of membrane theory, shear and contact deformation are not relevant. In addition, the membrane solution is only assumed to be used after core yielding has occurred. Thus, the resulting membrane solution is obtained by combining Eqs. (3.9) and (3.71):

$$w = w_a + w_m = \tag{3.107}$$

$$\frac{p_0}{k} + f_w\left[\frac{F^2\bar{a}^2}{2p_0Eh}\right]^{1/3}\left[1-\frac{\pi}{2}C^2 f_w R\left(\frac{{p_0}^2}{2FEh\bar{a}^4}\right)^{1/3}\right]$$

The function f_w, which is normally in the order of 0.7, has been tabulated in Appendix B.2. For a point load (R=0) the solution may be written in the following dimensionless form:

$$w/w_a = \left(w_a + w_{m,R=0}\right)/w_a = \tag{3.108}$$

$$= 1 + f_w\left[\frac{\pi^2\,\bar{F}^2\bar{a}^2}{24\left(1-\nu^2\right)\bar{w}_a{}^2}\right]^{1/3}$$

3.9.4 Comparison of membrane and plate solutions

The dimensionless membrane solution has been compared with the linear and nonlinear plate solutions in Fig. 3.12 below. Prior to core yielding (w/w_a=1) the load-indentation is linear. After this point the linear (small deflection) plate solution shows an increasing softening. The nonlinear (large deflection) plate solution shows a weak but monotonous stiffening and is initially stiffer than the membrane solution. At some point it is intersected by the membrane solution, which represents an approximation of the asymptotic behaviour for large indentations. The point of intersection is dependent on the ratio w/h , which is related to the magnitude of large deflection effects which are present at the initiation of core yielding.

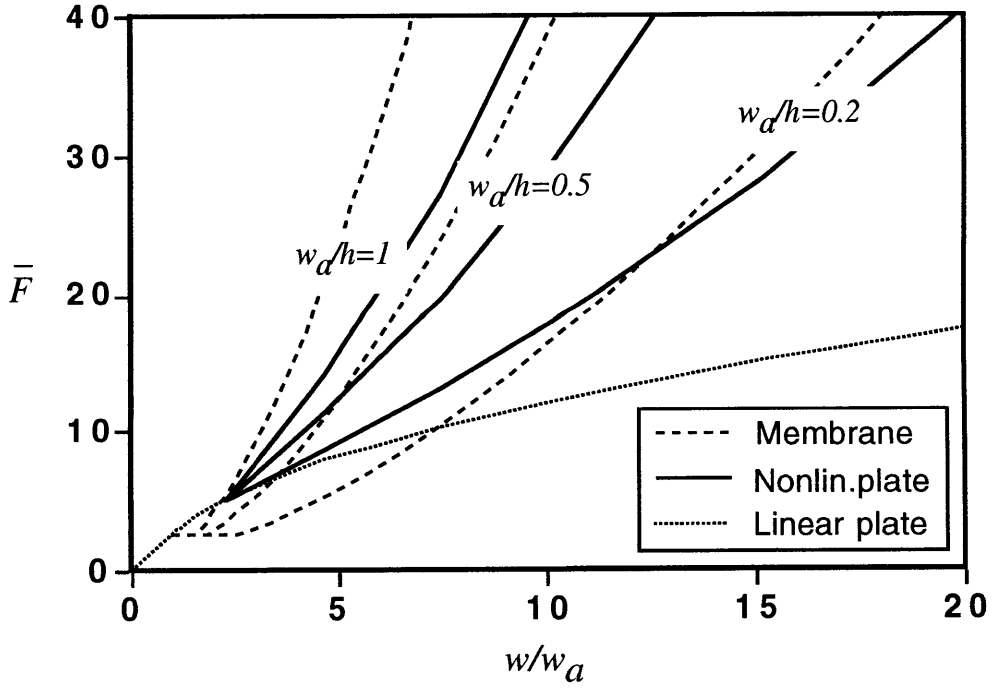

Fig. 3.12 Comparison of load-indentation solutions

The linear plate solution represents a lower limit of the true solution, since it neglects the additional stiffness due to membrane effects. The large deflection plate solution is only valid for intermediate deflections. In this range it represents an upper limit of the stiffness, since large rotations and the change in deflection shape are neglected. The approximate membrane solution represents an upper limit for large indentations, since Ritz method yields solutions which are stiffer or equal to the "true" solution. The method for removal of the membrane cusp represents an additional constraint since the relaxation of stresses caused by a distributed contact load is not taken into account.

Depending on the accuracy of the models, the "true" solution will be more or less close to the large deflection solution and membrane solution in their respective ranges of validity. At the present stage of analysis the best approximation is probably given by the upper envelope of the three solution approaches, i.e. for increasing indentation first by the linear plate solution, then by the nonlinear plate solution, and finally by the membrane solution.

4 Additional considerations

4.1 Anisotropic face sheets

4.1.1 Introductory remarks

In the previous analysis we have assumed that the core and face sheets are transversely isotropic with respect to the out-of-plane axis (z-axis), i.e. they have isotropic inplane properties. In practice foam cores generally are isotropic while honeycombs are orthotropic with a moderate difference between the inplane stiffness in the width and length ribbon directions. These differences do, however, not affect the analysis of the present work since only core out-of-plane properties are considered.

A more important factor is the anisotropy of the face sheets. In practice virtually all face sheets made of anisotropic plies are also macroscopically anisotropic. Even so called "quasi-isotropic" laminates, which possess inplane isotropy, are usually not isotropic in bending. However, many laminates used in practice can be approximated as "specially orthotropic" in bending and inplane extension. In a specially orthotropic laminate the bending–stretching coupling coefficients D_{16} and D_{26} in the plate stiffness matrix are zero, which in practice is obtained by stacking equal orthotropic plies symmetrically with respect to both the laminate midplane and an inplane coordinate axis. Here we will only consider application of the present model to specially orthotropic face sheets.

4.1.2 Effective face sheet membrane properties

The properties involved in plane stress analysis of a transversely isotropic membrane are E_r and ν_r, or in the present simplified notation E and ν. To analyze orthotropic face sheets we propose the following effective (averaged) inplane properties:

$$E^* = \frac{2}{\pi} \int_0^{\pi/2} E_r(\theta)\, d\theta \tag{4.1}$$

$$\nu^* = \frac{2}{\pi} \int_0^{\pi/2} \nu_r(\theta)\, d\theta \tag{4.2}$$

Integration over $\pi/2$ is sufficient due to the assumed symmetry with respect to the laminate x-axis. For cross-ply laminates it is sufficient to integrate over $\pi/4$. In practice the integration was performed using numerical integration by stepwise rotation of the laminate and using the output engineering quantities E_x and ν_{xy} from a standard laminate program.

4.1.3 Effective face sheet plate properties

Using classical plate theory we find that the bending of specially orthotropic plates is governed by the following single partial differential equation:

$$D_x w_{,xxxx} + 2D_{xy} w_{,xxyy} + D_y w_{,yyyy} = p_z(x,y)$$
$$\text{where} \quad D_{xy} = 2D_{12} + D_{66} \qquad D_x = D_{11} \qquad D_y = D_{22} \tag{4.3}$$

The deflection of orthotropic plates was first treated by Huber in the beginning of the century, and a thorough review of his works in this area was given by Huber (1923). For the particular case $D_{xy}^2 = D_x D_y$, as pointed out by Huber (1923), Eq. (4.3) can be transformed to an equivalent isotropic plate problem by use of the following rescaling to effective plate stiffness and lengths:

$$\tilde{D} = \sqrt{D_x D_y} \qquad \tilde{x} = x\left(\tilde{D}/D_x\right)^{1/4} \qquad \tilde{y} = y\left(\tilde{D}/D_y\right)^{1/4} \tag{4.4}$$

To derive an approximate expression for the effective plate stiffness of a generally orthotropic plate we consider Eq. (3.8) which may be rewritten as:

$$8w_0/F = L_0^{*2}/D^* \tag{4.5}$$

where L_0^* and D^* are equivalent isotropic quantities for the orthotropic plate. A point load on an isotropic plate results in a circular deformation pattern. Obviously, the corresponding deformation pattern on an orthotropic plate will be more similar to ellipses. For the orthotropic plate we consider a

rotated coordinate system x', y' and use a directional version of Eq. (3.2.a) to scale the length L_0^* to the rotated system:

$$L_0(\theta) = L_0^*[D_r(\theta)/D'(\theta)]^{1/4} \tag{4.6}$$

We now approximate the effective radius and plate stiffness in this system by the geometric average of the values in the directions x' and y':

$$L_0^2 \approx L_x' L_y' = L_0^{*2}\left[D_x' D_y'\right]^{1/4} \Big/ \sqrt{D'} \qquad\qquad D' \approx \sqrt{D_x' D_y'}$$

These two approximations can be recast into the following single expression:

$$L_0^2/D \approx L_0^{*2} \Big/ \left(D^{*2} D_x' D_y'\right)^{1/4} \tag{4.7}$$

where

$$\begin{aligned} D_x' &= D_x \cos^4\theta + 2D_{xy}\cos^2\theta\sin^2\theta + D_y \sin^4\theta \\ D_y' &= D_y \cos^4\theta + 2D_{xy}\cos^2\theta\sin^2\theta + D_x \sin^4\theta \end{aligned} \tag{4.8}$$

To get the best possible approximation of D^* we take the average of Eq. (4.7) over angles 0 to $\pi/2$ and equate it with Eq. (4.5):

$$1/\sqrt{D^*} = (2/\pi)\int_0^{\pi/2} \left(D_x' D_y'\right)^{-1/4} d\theta \qquad \text{or using Eq. (4.8)}$$

$$\frac{1}{\sqrt{D^*}} = \frac{2}{\pi}\int_0^{\pi/2} \frac{d\theta}{\left(D_x D_y\right)^{1/4}\sqrt{\left(\cos^2\theta + \sin^2\theta\right)^2 + (A-1)2\cos^2\theta\sin^2\theta}}$$

where $A = D_{xy}/\sqrt{D_x D_y}$

Using trigonometric identities this may be written

$$\frac{\left(D_x D_y\right)^{1/4}}{\sqrt{D^*}} = \frac{1}{\pi}\int_0^{\pi/2} \frac{2d\theta}{\sqrt{1+\frac{1}{2}(A-1)\sin^2 2\theta}} = \frac{2}{\pi}\int_0^{\pi/2} \frac{d\varphi}{\sqrt{1-\frac{1}{2}(1-A)\sin^2 \varphi}}$$

Observing that this is an elliptic integral we find that the effective plate stiffness may be written:

$$\begin{aligned} D^*/\sqrt{D_x D_y} &= \left\{(\pi/2)/K\left(\sqrt{(1-A)/2}\right)\right\}^2 && 0 \le A \le 1 \\ D^*/\sqrt{D_x D_y} &= \left\{(\pi/2)[(A+1)/2]/K\left(\sqrt{(A-1)/(A+1)}\right)\right\}^2 && 1 < A \end{aligned} \tag{4.9}$$

where $A = D_{xy}/\sqrt{D_x D_y}$

and $K(s) = \int_0^{\pi/2} \frac{d\theta}{\sqrt{1-s^2\sin^2\theta}}$

$K(s)$ is the complete elliptic integral of the first kind and can be found in more comprehensive mathematical tables. Results for different values of A are shown in Tab. 4.1:

Table 4.1 Effective plate stiffness for different anisotropy ratios

A	0.0	0.2	0.4	0.6	0.8	1.0	1.5	2	5	10
$D^*/\sqrt{D_x D_y}$	0.717	0.783	0.816	0.843	0.949	1.000	1.085	1.243	1.790	2.565

It is interesting to observe that, without using the above averaging assumptions, the same expression was derived independently by Frischbier (1987) and Olsson (1989,1992) when considering impact response controlled

by flexural waves in orthotropic plates. A simplified expression for the effective plate stiffness given by Olsson (1992) has been found less useful.

Note that $A=1$ $(D_{xy}^2=D_xD_y)$ corresponds to the scaling from a circle of radius L_o to an ellipse with the same area. Values of $A \neq 1$ correspond to more or less deformed ellipses, as shown in Fig. 4.1.

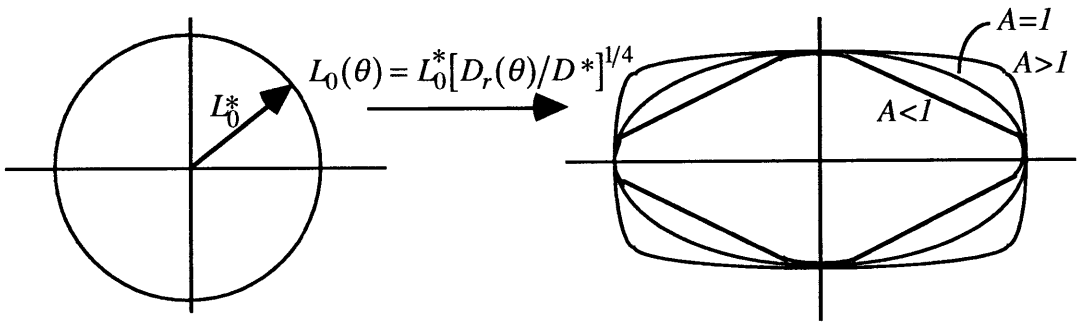

Figure 4.1 Length scaling to orthotropic plate from equivalent isotropic plate

Physically $A > 1$ corresponds to a plate with a relatively high torsional stiffness, as would be seen in an angle-ply laminate. Similarly $A < 1$ corresponds to a relatively low torsional stiffness, as would be seen in a cross-ply laminate where the fibres are aligned with the x–y-axes.

To obtain the peak deflection of an orthotropic laminate it is sufficient to use the effective plate stiffness given by Eq. (4.9). If needed, the shape of the deflected area can be obtained by the scaling indicated in Fig. 4.1.

4.2 Unloading behaviour

4.2.1 Constitutive modeling of core unloading

Estimates of the residual face sheet deflection after indentation is of interest for damage detectability and for damage tolerance analyses. A theory for the complete unloading history is of interest in impact analyses. The analysis of the unloading behaviour is complicated by the fact that the outer parts of the previously plastic region will behave elastic, but with a new neutral position. The following analysis will be limited to establishing upper and lower bounds on the residual deflection. To obtain a permanent face sheet deflection it must be assumed that the crushed part of the core is able to sustain some degree of tensile stress, σ_z, since an undamaged facesheet will otherwise return to the original undeflected position. For convenience we define the vertical pressure on the core, $p= -\sigma_z(z=h/2)$. Consider a cylinder of elastic–ideally plastic core material compressed by a face sheet deflection to $\hat{w}$ and then partially decompressed when the face sheet is displaced to a residual equilibrium position with a deflection $\breve{w}$ as shown in Fig. 4.2.

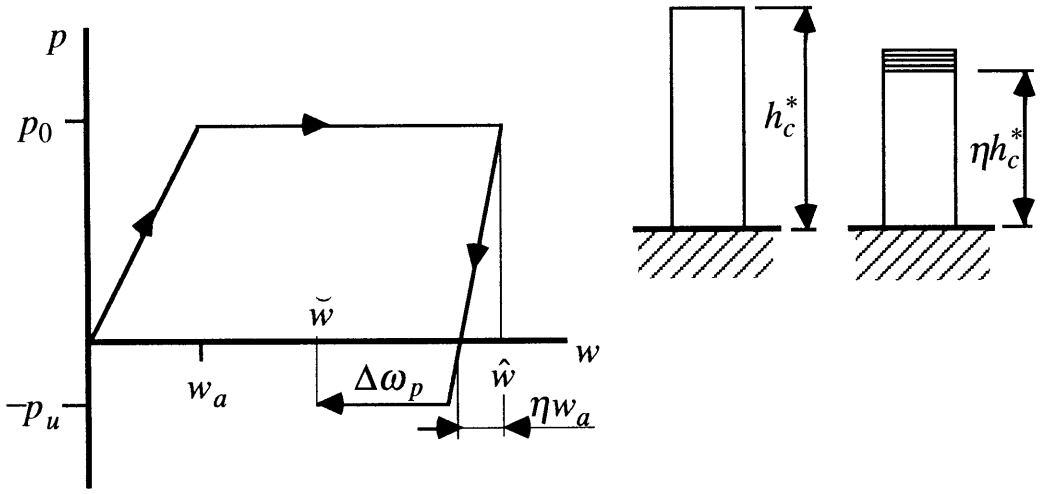

Figure 4.2 Loading–unloading cycle with core crushing

The crushing of the core reduces the effective thickness of the core that can unload elastically from h_c^* to ηh_c^*, and thus the core stiffness is proportional to $Q_c/\left(\eta h_c^*\right)$. For cases where the peak deflection is much smaller than the effective core thickness we have $\eta \approx 1$. For essentially plastically crushed cores the tensile stress p_u required to "unwrinkle" crushed cells will approach p_0 while p_u in essentially elastically crushed cores will approach zero.

Before unloading the energy stored per unit area in the plastic area is:

$$\omega_p = \int_0^{\hat{w}} p dw = p_0 w_a/2 + p_0\left(\hat{w} - w_a\right) \tag{4.10}$$

After unloading the energy per unit area is:

$$\omega_p = \int_0^{\hat{w}} p dw + \int_{\hat{w}}^{\breve{w}} p dw \tag{4.11}$$

A lower bound for the local plastic work is reached if p_u=0. From Fig. 4.2 it is seen that the local plastic work in this case is given by:

$$\omega_p \geq p_0(\hat{w} - w_a) + \tfrac{1}{2}(1-\eta)p_0 w_a$$

where the right hand side corresponds to unloading to zero residual stress. Thus, the lowest possible value of the local plastic work after unloading is obtained by assuming η=1:

$$\omega_{p\min} = p_0(\hat{w} - w_a) \tag{4.12}$$

An upper bound on the local plastic work is obtained by assuming that the crush stress p_0 corresponds to a completely plastic deformation of the core cells. If strain hardening effects are neglected the absolute value of the "unwrinkling" stress" p_u must equal the crush stress p_0 and we obtain:

$$\omega_p \leq \tfrac{1}{2} p_0 w_a + 2p_0(\hat{w} - w_a) + (1-\eta)p_0 w_a$$

where the right hand side corresponds to unloading to $\breve{w}$=0. Thus, the highest possible value of the local plastic work after unloading is obtained by assuming η=0:

$$\omega_{p\max} = 2p_0(\hat{w} - w_a) + \tfrac{3}{2} p_0 w_a \tag{4.13}$$

A more detailed description of the energy consumed in elastically deforming the core requires knowledge of the "unwrinkling stress" p_u and the remaining elastic fraction η of the core.

4.2.2 Unloading of the face sheet after core yielding

Consider the deflected face sheet after core yielding. In the plastic region the core is under constant pressure $p=p_0$, which may be modeled by equally contracted springs, i.e., the distance between the face sheet and the other end of the foundation springs is constant.

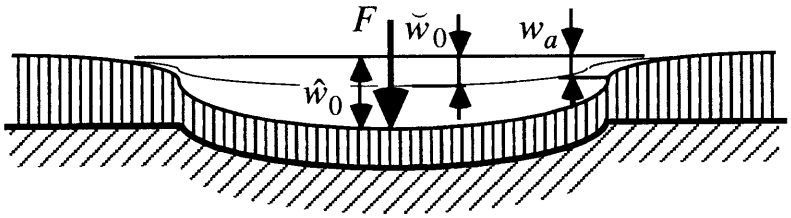

Figure 4.3 Model of plate on spring foundation after core yielding.

In the adopted "first order" large deflection analysis the face sheet deflection is assumed to be given by the linear (small deflection) solution, i.e. $w=f(F_L)$. Membrane stresses are assumed not to affect the deflection, but contribute to the total load through a magnification factor of the load F_L associated with the linear solution.

Thus, for predicting the deflection during unloading we neglect, as a first approximation, the strain energy due to membrane stresses and consider the linear solution. Since this system is linear it will unload linearly from the peak load $\hat{F}_L$. The strain energy U_L stored in the system is given by:

$$U_L = \int_0^{\hat{w}_0} F_L dw \; - W_p = W_L - W_p \tag{4.14}$$

where W_L is the work resulting from the point load as given by the linear solution and W_p is the plastic work consumed in core crushing.

Obviously, the actual unloading curve will be nonlinear due to additional membrane contributions to the load.

A lower limit for the plastic work is obtained by integrating Eq. (4.12) over the plastic radius:

$$W_{p\min} = \iint_S \omega_{p\min} dS = \iint_S p_0(\hat{w} - w_a) dS = \int_0^a p_0(\hat{w} - w_a) 2\pi r dr = \{\text{set } s = r/a\}$$
$$= 2p_0\pi a^2 \int_0^1 \delta w(s) s\, ds = 2F_L \bar{a}^2 \int_0^1 \delta w(s) s\, ds$$

Here $\delta w(s) = \hat{w}(s) - w_a$ is the deflection at $s=r/a$ of a simply supported plate of radius a under a central load F_L, a uniform pressure $-p_0$ and edge moment M. Using standard plate solutions, as given by Szilard (1974), we obtain $\delta w(s)$ from

$$\delta w(s) = \frac{F_L a^2}{16\pi D(1+\nu)}\left[(3+\nu)(1-s^2) + 2(1+\nu)s^2 \ln s\right]$$
$$- \frac{p_0\pi a^4}{64\pi D(1+\nu)}\left[2(3+\nu)(1-s^2) - (1+\nu)(1-s^4)\right] + \frac{Ma^2}{2D(1+\nu)}(1-s^2)$$

where $s = r/a$

By use of Eq. (3.2) the above equation can be rewritten as

$$\delta w(s) = \frac{F_L{}^2\bar{a}^2}{64\pi^2(1+\nu)p_0 D}\left[2(3+\nu)\left(2-\bar{a}^2\right)\left(1-s^2\right)+(1+\nu)\left[8s^2\ln s+\bar{a}^2\left(1-s^4\right)\right]+32\left(1-s^2\right)\frac{\overline{M}}{\overline{F}}\right]$$

Thus, the minimum plastic work is given by

$$W_{p\min} = 2F_L\bar{a}^2\int_0^1 \delta w(s)s\,ds = \frac{F_L{}^3\bar{a}^2}{32\pi^2(1+\nu)p_0 D}\Big[(3+\nu)\left(2-\bar{a}^2\right)\left(s^2-\tfrac{1}{2}s^4\right)$$
$$+(1+\nu)\left\{\tfrac{8}{4}s^2\ln s-\tfrac{8}{16}s^4+\bar{a}^2\left(\frac{s^2}{2}-\frac{s^4}{6}\right)\right\}+32\left(\frac{s^2}{2}-\frac{s^4}{4}\right)\overline{M}/\overline{F}\Big]_0^1$$
$$= \frac{F_L{}^3\bar{a}^2}{32\pi^2(1+\nu)p_0 D}\left[(3+\nu)\left(2-\bar{a}^2\right)/2+(1+\nu)\left(-1/2+\bar{a}^2/3\right)+8\overline{M}/\overline{F}\right]$$

The final expression for the minimum plastic work is:

$$W_{p\min} = \frac{F_L{}^3\bar{a}^2}{32\pi^2(1+\nu)p_0 D}\left[(5+\nu)/2-\bar{a}^2(7+\nu)/6+8\overline{M}/\overline{F}\right] \tag{4.15}$$

The corresponding upper limit of the plastic work is given by

$$W_{p\max} = \iint_S \omega_{p\max}dS = \iint_S\left[2\omega_{p\min}+3p_0 w_a/2\right]dS = 2W_{p\min}+\tfrac{3}{2}\iint_S p_0 w_a dS$$
$$= 2W_{p\min}+\tfrac{3}{2}p_0\pi a^2 w_a = 2W_{p\min}+\tfrac{3}{2}\hat{F}\bar{a}^2 w_a \tag{4.16}$$

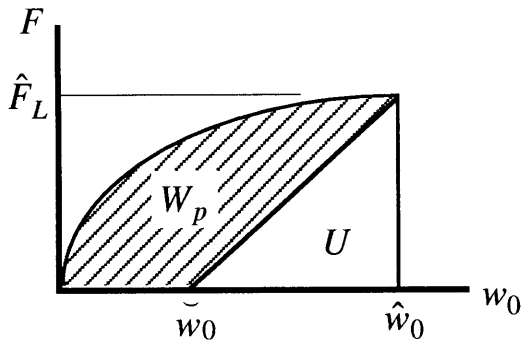

Figure 4.4 Unloading determined from elastic and plastic energies at peak load.

Assuming linear elastic unloading, we find that the residual deflection, Fig. 4.4, is obtained from the relation:

$$(\hat{w}_0 - \breve{w}_0)\hat{F}_L/2 = U = W_L - W_p$$

Solving for the residual deflection gives:

$$\breve{w}_0 = \hat{w}_0 - 2\left(W_L - W_p\right)/\hat{F}_L$$

Taking physical limits into account we obtain that the upper and lower bounds of the residual deflection are given by:

$$\begin{aligned} \breve{w}_0 &\geq \max\left\langle 0;\ \hat{w}_0 - 2\left(W_L - W_{p\min}\right)/\hat{F}_L \right\rangle \\ \breve{w}_0 &\leq \min\left\langle \hat{w}_0;\ \hat{w}_0 - 2\left(W_L - 2W_{p\min}\right)/\hat{F}_L + 3\hat{\bar{a}}^2 w_a \right\rangle \end{aligned} \tag{4.17}$$

where $W_{p\min}$ is given by Eq. (4.15) and the external work to peak load W_L in the linear solution is given by:

$$W_L = \int_0^{\hat{w}_0} F_L dw \tag{4.18}$$

The external work could theoretically be expressed in terms of the dimensionless solutions of Chapter 4. However, the deflection is a complex function of several different contributions, and it is therefore more convenient to calculate W_L by numerical integration of the load-displacement relation in a particular problem.

Any attempt to give a more accurate prediction of the unloading behaviour requires that the "unwrinkling stress" p_u is known. The calculations are complicated by the fact that the outer parts of the initial plastic region will behave elastic while the inner parts will have reached the unwrinkling stress.

4.3 Calculation of the foundation stiffness

A plate on an elastic foundation involves the interaction between a plate with a given plate stiffness D, and a foundation of a given thickness h_c and a vertical stiffness Q_c related to the elastic properties of the foundation. For a transversely isotropic foundation the out-of-plane stiffness modulus Q_c is given by:

$$Q_c = E_{zc}/\left(1 - \nu_{rzc}\nu_{zrc}\right) \tag{4.19}$$

where indices r and z refer to the vertical and radial directions and the subscript c is used to indicate a core property.

For honeycombs Gibson and Ashby (1988) have shown that $\nu_{zrc}\approx 0.3$ and $\nu_{rzc} << 1$ so that Eq. (4.19) simplifies to:

$$Q_c \approx E_{zc} \tag{4.20}$$

For foams, which are isotropic, Eq. (4.19) simplifies to:

$$Q_c = E_c/\left(1 - \nu_c^2\right) \tag{4.21}$$

For convenience the bending stiffness of the face sheet is defined as follows:

$$Q_b = 12D/h^3 \tag{4.22}$$

Before discussing the displacements of an elastic foundation under a plate it is useful to consider the maximum surface displacement of an isotropic half-space under a uniform surface pressure q_0 over a radius a given by Selvadurai (1979):

$$w_0 = 2q_0 a/Q_c = \frac{2F}{Q_c \pi a} \tag{4.23}$$

Obviously, as the radius under pressure decreases we will approach the solution for a point load, resulting in an infinite displacement. For an infinite radius under pressure, on the other hand, the half space will be in a uniform state of plane strain. We now proceed to the elastic foundation under a plate.

A uniform displacement w of the face sheet results in a uniform pressure on the core, which will then be in a state of plane strain. The foundation stiffness of an elastic transversely isotropic core is then given by:

$$k = \frac{p}{w} = \frac{Q_c \varepsilon_{zc}}{w} = \frac{Q_c w/h_c}{w} = Q_c/h_c \tag{4.24}$$

The corresponding deflection for the simple one-dimensional core model is found by insertion of Eq. (4.24) into Eq. (3.8):

$$w_{1D} = \frac{F}{8\sqrt{k_{1D} D}} = \frac{F L_{01D}^2}{8D} \qquad \text{where } L_{01D}^2 = \sqrt{D/k} = \left[D h_c/Q_c\right]^{1/2} \tag{4.25}$$

We note that the foundation stiffness based on the one-dimensional assumption of plane strain results in an infinite displacement as the core thickness h_c approaches infinity.

No solution has been found for an elastic plate on a transversely isotropic halfspace. Solutions for a plate of infinite shear stiffness on different foundations have been discussed by Sneddon, Gladwell and Coen (1975). The original solution for a plate bonded to an isotropic halfspace was given by Hogg in 1938 (as reported by Sneddon, Gladwell and Coen(1975)). The central deflection under a point load is given by

$$w_{3D} = \frac{\sqrt{3} F L_{03D}^2}{9D} \qquad where \;\; L_{03D}^2 = \left[2D/Q_c\right]^{2/3} \tag{4.26}$$

Thus, the three–dimensional solution gives a finite deflection under a point load on a plate bonded to an elastic halfspace. It is interesting to note that the same result can be obtained by assuming a plate floating without shear stresses on an elastic halfspace, as done by Timoshenko and Woinowsky-Krieger (1959, p.280). This is due to the assumption of infinite shear stiffness of the plate. The analogy between floating plates and plates on elastic foundations was discussed by Hétenyi (1966).

Now the ratio between the three- and one-dimensional solutions is given by:

$$\frac{w_{3D}}{w_{1D}} = \frac{8\sqrt{3} L_{03D}^2}{9 L_{01D}^2} = \frac{8\sqrt{3}\left[2D/Q_c\right]^{2/3}}{9\left[2Dh_c/Q_c\right]^{1/2}} = \frac{8\sqrt{3}}{9}\left[\frac{16D}{Q_c h_c^{\,3}}\right]^{1/6} \tag{4.27}$$

Using the definition in Eq. (4.22) the above equation may be rewritten as:

$$\frac{w_{3D}}{w_{1D}} = \frac{8\sqrt{3}}{9}\left[\frac{4Q_b h^3}{3Q_c h_c^3}\right]^{1/6} \tag{4.28}$$

Obviously the plane strain assumption has been violated when $w_{3D}/w_{1D}<1$ and we may in that case assume that the deflection is given by the three-dimensional solution rather than by the one-dimensional solution. The above analysis is fully applicable only for isotropic (foam) cores, but should remain relevant for most honeycomb cores. The reason is that the three–dimensional effects essentially involve interaction between transverse normal stresses and shear stresses for which the corresponding elastic modulii have a relation similar to isotropic cores.

By setting the ratio of deflections in Eqs. (4.27) or (4.28) equal to unity we may define an effective one dimensional core thickness for the three dimensional solution for a halfspace foundation:

$$h_c^{3D} = \frac{128}{27}\left[\frac{2D}{Q_c}\right]^{1/3} = h\frac{64}{27}\left[\frac{4Q_b}{3Q_c}\right]^{1/3} \tag{4.29}$$

The effective core thickness h_c^* to be used in Eqs. (4.24) and (4.25) is then given by:

$$\begin{aligned} h_c^* &= h_c \qquad \text{for} \quad h_c \le h_c^{3D} \\ h_c^* &= h_c^{3D} \qquad \text{for} \quad h_c > h_c^{3D} \end{aligned} \tag{4.30}$$

The above definition of the effective core thickness was based on matching the peak deflections for a one–dimensional and a three–dimensional core

model. Finite element analyses and analyses based on other matchings result in minor corrections of Eqs. (4.29) and (4.30) and have been discussed by Scott (1981).

The difference in Eqs. (4.25) and (4.26) clearly shows that the deflection at any point of a plate on an elastic halfspace also depends on the deflections at neighboring points. Thus the appropriate foundation stiffness and effective core stiffness of thick cores are not constants, but rather depend on the local distribution of slopes and deflections. The definition of the effective three-dimensional core thickness, Eq. (4.29), results in an accurate prediction of the central deflection in the initial phase with a completely elastic core. The prediction of the onset of core yielding and subsequent deflections in the outer (elastic) region will be less accurately described. Further studies are required to determine the most appropriate definition of the effective core thickness for predicting initiation of core yielding and face sheet deflections in the outer region. Note that a complete solution for thick cores only can be obtained by solving the corresponding three-dimensional problem. In the comparisons with experiments in chapter 5, the effective core thickness is defined using Eqs. (4.29) and (4.30), and this procedure is recommended until further studies have been done on the problem.

The interaction of shear stresses and normal stresses in cores has been modeled using two-parameter (Pasternak) foundations involving coupled shear and normal springs. However, these models are unable to describe the thickness variation of strains in the core which can only be captured in a three-dimensional analysis. Thus, the fundamental problem of determining the effective vertical foundation stiffness remains unresolved.

5 Results and correlations

5.1 Comparison with loading experiments

5.1.1 Introductory remarks

In the following section the analytical predictions have been compared with indentation experiments on a number of different sandwich panels, involving different thicknesses and materials of the face sheets and core. Predicted loading curves have been calculated from the equations in Section 3.9 and the tables in Appendix B. The effective properties of the core and face sheet have been calculated from Sections 4.3 and 4.1, respectively.

Parametric data needed for the calculations have normally been taken from the experimental references. Data not reported in the references have been taken from manufacturers data sheets, from other studies of the same material, or as a last resort estimated from the equations given by Gibson and Ashby (1988). Reported data have only been discarded when there was a significant deviation both from manufacturers data sheets and other experimental studies. Since the contact approach α is negligible except for very small face sheet deflections no attempt was made to accurately determine the contact modulus Q_α, which was assumed to be 12 GPa for all graphite/epoxy face sheets and 10 GPa for the glass/epoxy face sheet.

5.1.2 Graphite/epoxy laminate on foam core

Table 5.1 Parameters in experiment by Tsang (1989)

Reference: Tsang (1989)

Method: unsupported panel backface, displacement differentials measured

Indentor: 12.7 mm diameter steel indentor

Core material: Rohacell 71 WF

Face sheet lay-up and material: $(\pm 45/0)_s$, AS4/3501-6 tape

Face sheet ply properties:

E_1 = 142 GPa	E_2 = 9.81 GPa	E_3 = 9.81 GPa
G_{12}= 6.00 GPa	G_{13}= 6.00 GPa	G_{23}= 3.77 GPa
ν_{12} = 0.30	ν_{13} = 0.30	ν_{23} = 0.34
t_{ply}= 0.134 mm		

Core properties

E_c=105 MPa	ν_c=0.30	p_0=1.70 MPa
h_c=12.7 mm	h_c*=12.7 mm	

Face sheet properties

h=0.807 mm	D*=3.00 Nm	ν*=ν_r*=0.314
E*=51.3 GPa	G_{rz}=4.89 GPa	ν_{rz}=0.320

Contact quantities

Q_α=12.0 GPa	R=6.35 mm

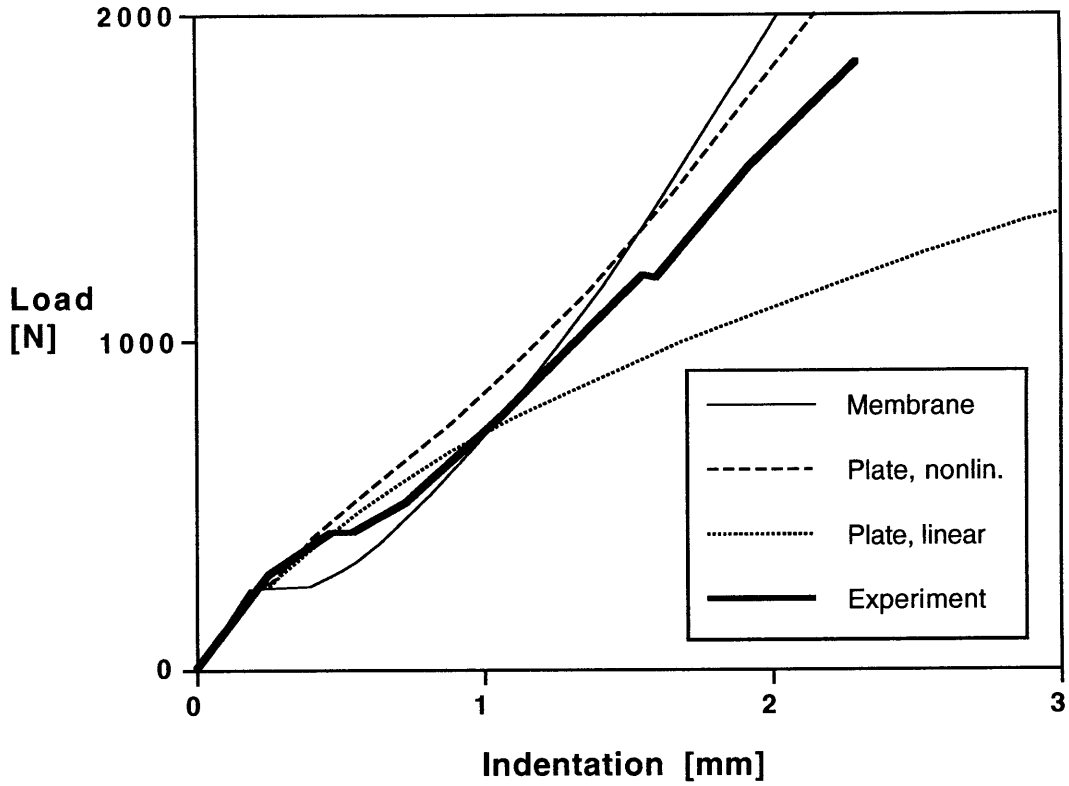

Figure 5.1 Predictions compared with experiment by Tsang (1989).

The agreement with experimental data is very satisfactory in this example. Core yielding is predicted to occur at 0.187 mm indentation. Large deflection effects are moderate and can be completely neglected before core yielding occurs. At the loads 450 N and 1200 N the experimental curve shows jags followed by a decreasing slope, which probably indicates face sheet matrix cracking or delamination. The event at the lower load may also be associated with core cracking, which has previously been reported for this brittle foam material.

Table 5.2 Parameters in experiment 1 by Sun and Wu (1991)

Reference: Sun and Wu (1991)

Method: supported panel backface, machine stroke measured

Indentor: 12.7 mm diameter steel indentor

Core material: Rohacell 200 WF

Face sheet lay-up and material: $(0_2/90)_s$, AS4/3501-6 tape

Face sheet ply properties:

E_1 = 138 GPa	E_2 = 10 GPa	E_3 = 10 GPa
G_{12}= 6.90 GPa	G_{13}= 6.90 GPa	G_{23}= 3.86 GPa
ν_{12} = 0.30	ν_{13} = 0.30	ν_{23} = 0.30
t_{ply}= 0.127 mm		

Core properties

E_c=128 MPa	ν_c=0.30	p_0=9.01 MPa
h_c=12.7 mm	h_c*=12.7 mm	

Face sheet properties

h=0.762 mm	D*=1.498 Nm	ν*=ν_r*=0.439
E*=41.8 GPa	G_{rz}=5.38 GPa	ν_{rz}=0.300

Contact quantities

Q_α=12.0 GPa	R=6.35 mm

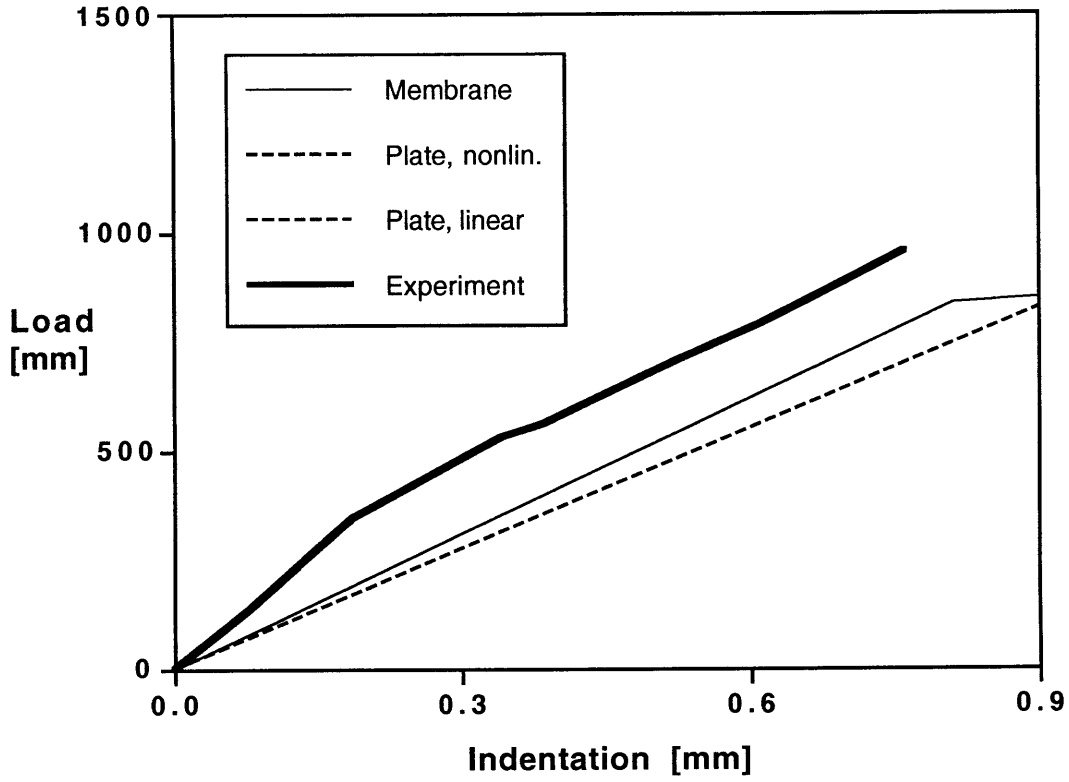

Figure 5.2 Predictions compared with experiment 1 by Sun and Wu (1991).

In this example core yielding is predicted to occur at an indentation of 0.813 mm. Thus, core yielding and residual indentation should not be observed. However, the experimental unloading curve and the residual indentation of 0.15 mm, which are not shown in the present graph, indicates a relatively significant core yielding. The membrane solution is initially stiffer than the plate solution, since it does not include the approach due to Hertzian contact. Both solutions are more compliant than observed experimentally which can be partly explained by the fact that the theory does not include large deflection effects prior to core yielding. A slightly improved agreement with experimental data can also be obtained by using E_c=206 MPa, which is the core modulus given by the material producer.

5.1.3 Graphite/epoxy laminate on aluminium honeycomb core

Table 5.3 Parameters in experiment 2 by Sun and Wu (1991)

Reference: Sun and Wu (1991)

Method: supported panel backface, machine stroke measured

Indentor: 12.7 mm diameter steel indentor

Core material: 5052 Aluminium honeycomb, 1/8"–0.001", density =4.5 lb/ft^3

Face sheet lay-up and material: $(0_2/90)_s$, AS4/3501-6 tape

Face sheet ply properties:

E_1 = 138 GPa	E_2 = 10 GPa	E_3 = 10 GPa
G_{12}= 6.90 GPa	G_{13}= 6.90 GPa	G_{23}= 3.86 GPa
ν_{12} = 0.30	ν_{13} = 0.30	ν_{23} = 0.30
t_{ply}= 0.127 mm		

Core properties

E_{zc}=887 MPa	p_0=1.70 MPa
h_c=12.7 mm	h_c*=7.11 mm

Face sheet properties

h=0.762 mm	D*=1.498 Nm	ν*=ν_r*=0.439
E*=41.8 GPa	G_{rz}=5.38 GPa	ν_{rz}=0.300

Contact quantities

Q_α=12.0 GPa	R=6.35 mm

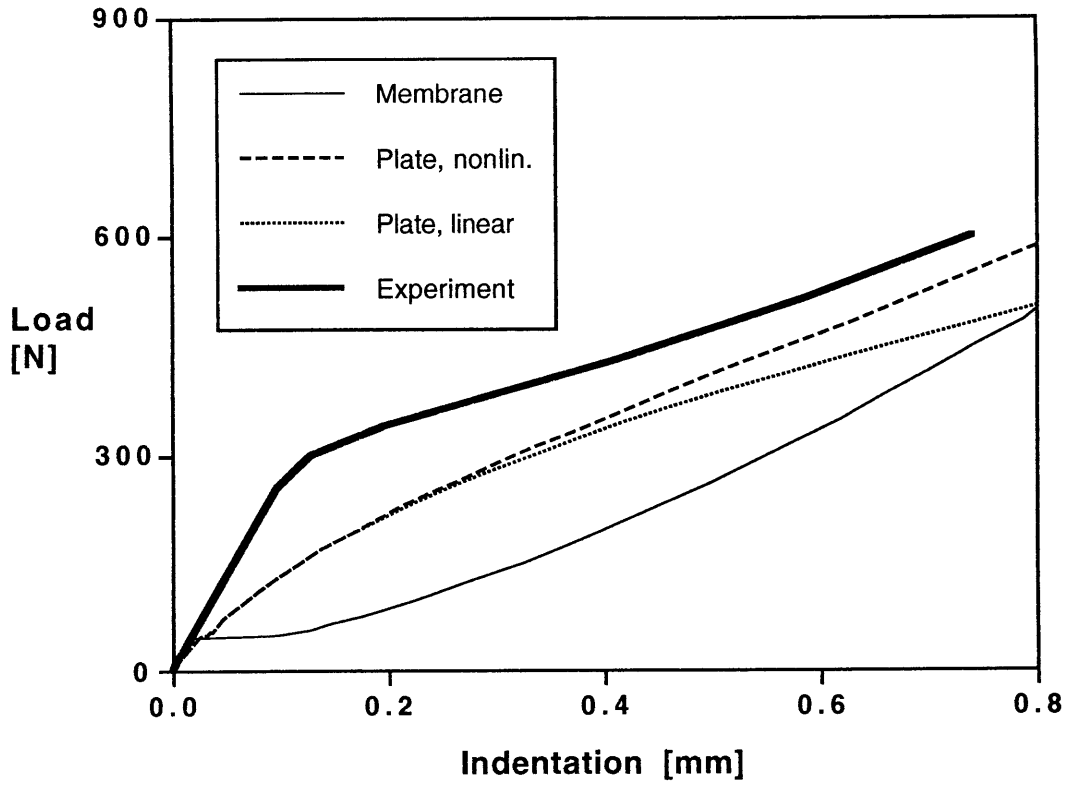

Figure 5.3 Predictions compared with experiment 2 by Sun and Wu (1991).

In this example core yielding is predicted to occur at an indentation of 0.014 mm. The predicted load is lower than the experimentally observed, which is probably due to the fact that the initial compressive strength σ_{cu} (Fig. 2.1) in common aluminium honeycombs is significantly higher than the following crush stress p_0. This conclusion is also supported by the fact that the experimental and predicted values are approaching each other at larger values of the indentation, where errors in the assumed stresses in the elastic region are less influential.

5.1.4 Graphite/epoxy laminate on paper honeycomb core

Table 5.4 Parameters in experiment by Williamson (1989)

Reference: Williamson(1989)

Method: supported panel backface, machine stroke measured

Indentor: 25.4 mm diameter steel indentor

Core material: Nomex honeycomb, cell size =3.2 mm, density =48 kg/m^3

Face sheet lay-up and material: (0/90) , AW193/3501-6 (AS4/Epoxy fabric)

Face sheet ply properties:

E_1 = 64 GPa	E_2 = 64 GPa	E_3 = 9.81 GPa
G_{12}= 6.27 GPa	G_{13}= 5.00 GPa [a)]	G_{23}= 5.00 GPa [a)]
ν_{12} = 0.15	ν_{13} = 0.45 [a)]	ν_{23} = 0.45 [a)]
t_{ply}= 0.175 mm	a) = assumed properties	

Core properties

E_{zc}=150 MPa	p_0=1.41 MPa
h_c=25.4 mm	h_c*=6.47 mm

Face sheet properties

h=0.350 mm	D*=0.191 Nm	ν*=ν_r*=0.503
E*=37.5 GPa	G_{rz}=5.00 GPa	ν_{rz}=0.450

Contact quantities

Q_α=12.0 GPa	R=12.7 mm

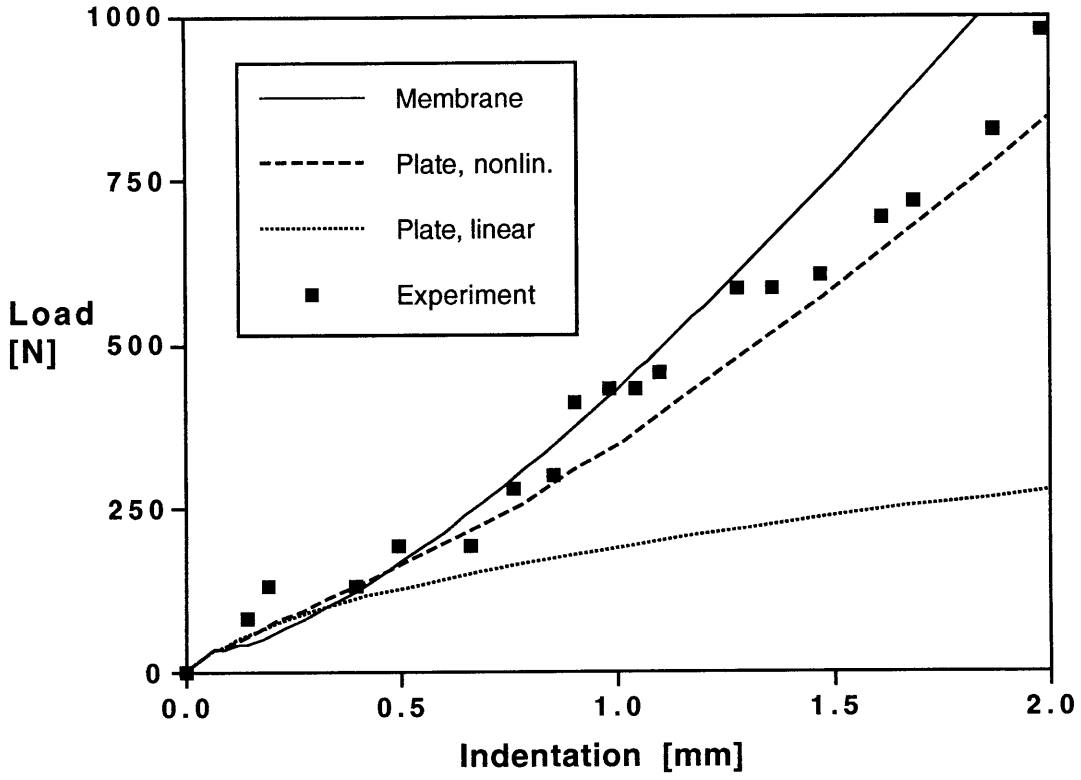

Figure 5.4 Predictions compared with experiment by Williamson (1989).

The agreement between predicted and experimental values in this example is very good, although the experimental data are rather scattered. Large deflection effects are significant, but can be neglected before core yielding, which is predicted to occur at an indentation of 0.061 mm. At a load of 600 N there appears to be an increased compliance, which is probably due to face sheet matrix cracking or delamination.

5.1.5 Glass/epoxy laminate on aluminium honeycomb core

Table 5.5 Parameters in experiment by Mines, Worrall and Gibson(1990)

Reference: Mines, Worrall and Gibson(1990)

Method: supported panel backface, machine stroke measured

Indentor: 50 mm diameter steel indentor

Core material: 3003 aluminium honeycomb, 1/4" cell size, density =5.2 lb/ft^3

Face sheet lay-up and material: $(0/90)_s$, glass/epoxy fabric

Face sheet ply properties:

E_1 = 18.0 GPa	E_2 = 18.0 GPa	E_3 = 9.00 GPa
G_{12}= 4.60 GPa	G_{13}= 4.60 GPa [a)]	G_{23}= 4.60 GPa [a)]
ν_{12} = 0.09	ν_{13} = 0.45 [a)]	ν_{23} = 0.45 [a)]
t_{ply}= 0.187 mm	a) = assumed properties	

Core properties

E_{zc}=1200 MPa	p_0=1.60 MPa
h_c=25.4 mm	h_c*=2.34 mm

Face sheet properties

h=0.375 mm	D*=0.0719 Nm	ν*=ν_r*=0.261
E*=15.0 GPa	G_{rz}=4.60 GPa	ν_{rz}=0.300

Contact quantities

Q_α=10.0 GPa	R=25 mm

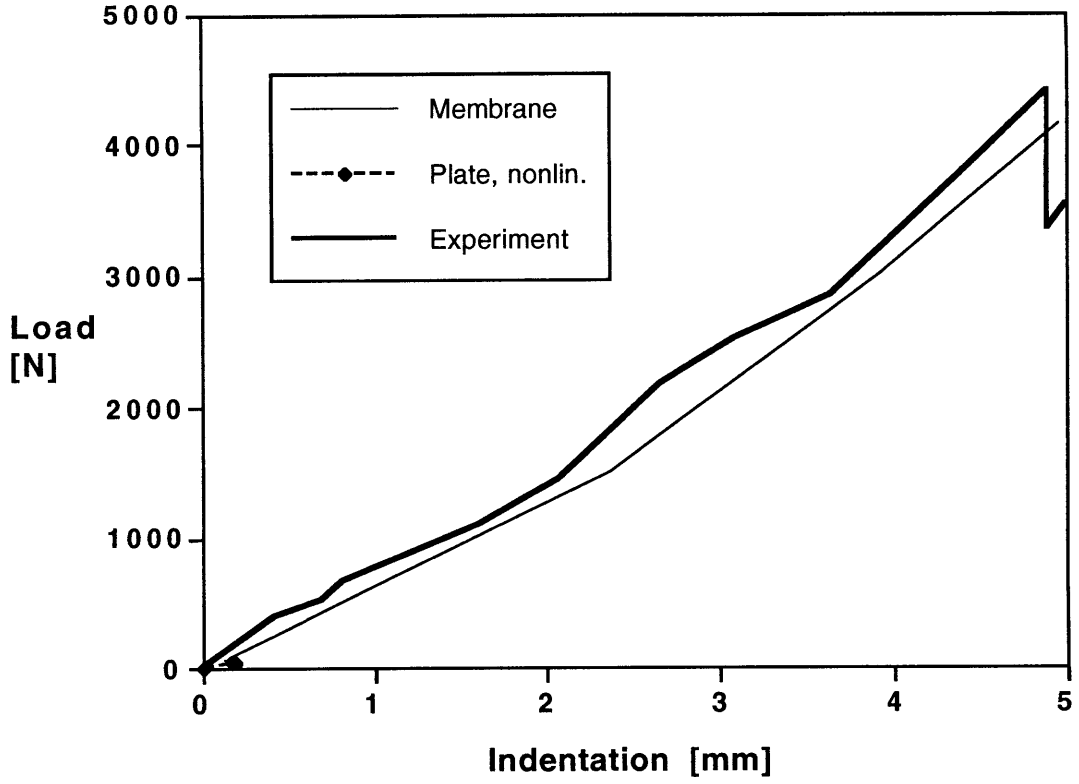

Figure 5.5 Predictions compared with experiment by Mines et al. (1990).

In this example the response is completely dominated by membrane effects since the maximum deflection is more than ten times larger than the face sheet thickness. Core yielding is predicted to occur at 0.003 mm indentation and the tabulated solutions in Appendix B cover only a fraction of the entire load–deflection curve. The membrane solution in Appendix B has been extrapolated to a dimensionless load of 2200 and is in good agreement with the experimental results. The load drop at 4400 N is associated with fibre failure in the face sheet.

5.2 Comparison with unloading experiments

5.2.1 Introductory remarks

Experimentally observed unloading behaviour has only been reported in a few references. In this section the predicted upper and lower limits for the residual indentation, derived in section 4.2, have been compared with the unloading behavior in two experiments. For clarity the unloading has been shown as a straight line from the peak load although it is recognized that the real behaviour will be nonlinear.

5.2.2 Graphite/epoxy laminate on aluminium honeycomb core

This experiment was performed by Sun and Wu (1991) and is identical to the experiment described in Table 5.3. The comparison between predicted and experimentally observed behaviour is shown in Fig. 5.6.

In this case the experimentally observed residual indentation is approximately in the middle of the predicted interval.

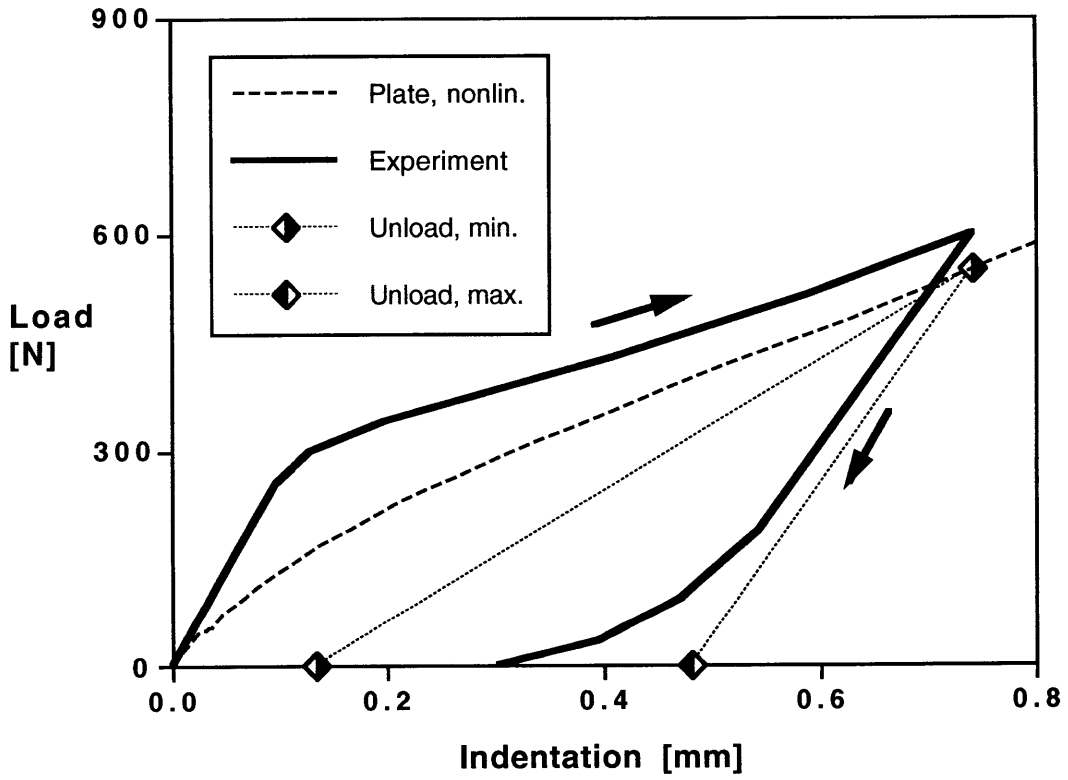

Figure 5.6 Comparison between predicted and observed unloading behaviour in experiment by Sun and Wu (1991).

5.2.3 Graphite/epoxy laminate on paper honeycomb core

This experiment was performed by Williamson (1989), and differs from the experiment described in Table 5.4 on two points. In the present case the indentor radius was 19 mm and the indented panel had two clamped edges instead of a supported backface. In the experiment the indentation was measured as the difference in displacement of the upper and lower face of the panel. A comparison between the predicted and experimentally observed load versus indentation is shown in Fig. 5.7.

The experimentally observed residual indentation is again found to be close to the average of the predicted lower and upper bounds. It should also be noted that virtually identical load-indentation relations were obtained by Williamson (1989) during experiments on panels with supported backface. This observation indicates a negligible coupling between the global bending and local indentation, and hence the applicability of the present model which is based on the assumption of a supported panel backface.

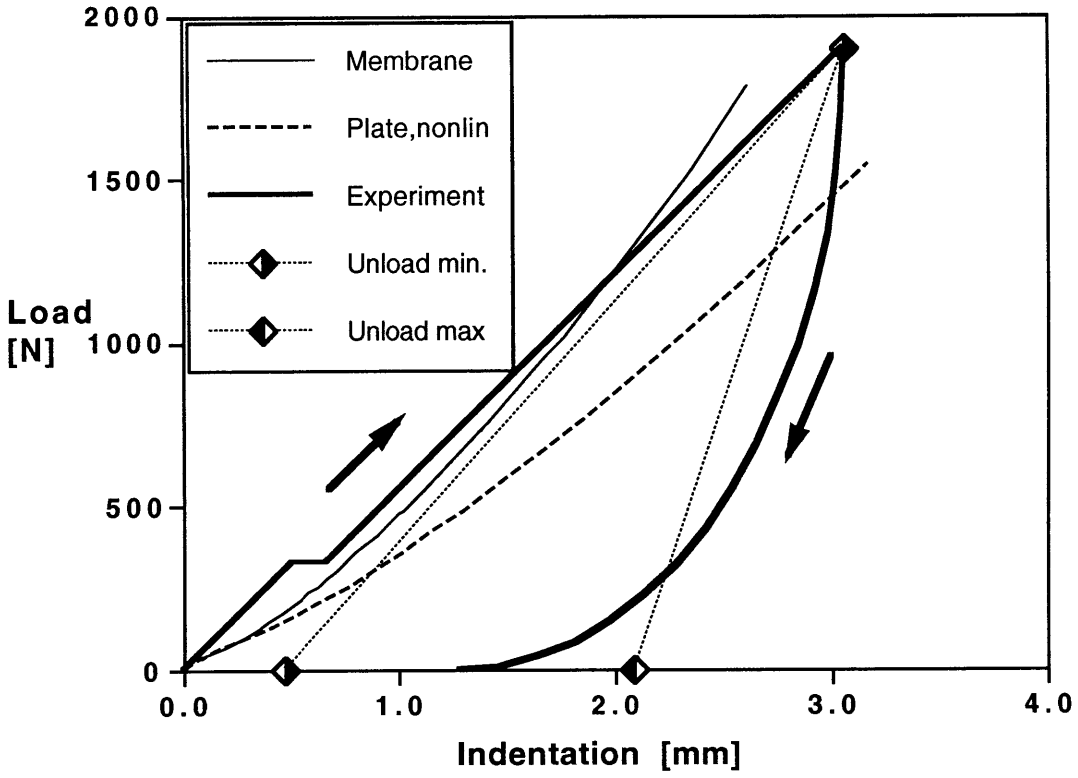

Figure 5.7 Comparison between predicted and observed unloading behaviour in experiment by Williamson (1989).

5.3 Parametric studies

5.3.1 Model parameters and their relative importance

The membrane and plate models involve a total of eleven parameters and a presentation of the effect of all parameters could easily distract the attention from the parameters of importance. The dimensional quantities can be combined to dimensionless groups in several different ways, but any presentation will still involve several different dimensionless parameters, which may not be easily related to physical quantities. Thus, the parametric study will be presented using dimensional quantities.

In order to make the presentation tractable, Tsang's (1989) experiment with a 0.807 mm thick carbon/epoxy face sheet on a 12.7 mm rigid foam core was chosen as a reference case. The material data have been given in Table 5.1. The predicted relative magnitude of the contributions due to bending, shear and Hertzian approach in this experiment are compared in Fig. 5.8. It is seen that shear and Hertzian approach is of minor importance except for relatively small values of the indentation. Thus, the quantities related to shear (G_{rz} and ν_{rz}) and contact stiffness (Q_α and R) can be considered as secondary parameters in the present case. The Young's modulus and Poisson's ratio can be treated as a single stiffness quantity so that five major parameters remain. These are the face sheet bending and inplane stiffness (Q_b), the core vertical stiffness (Q_c), the face sheet thickness (h), the core thickness (h_c) and the core crush stress (p_0).

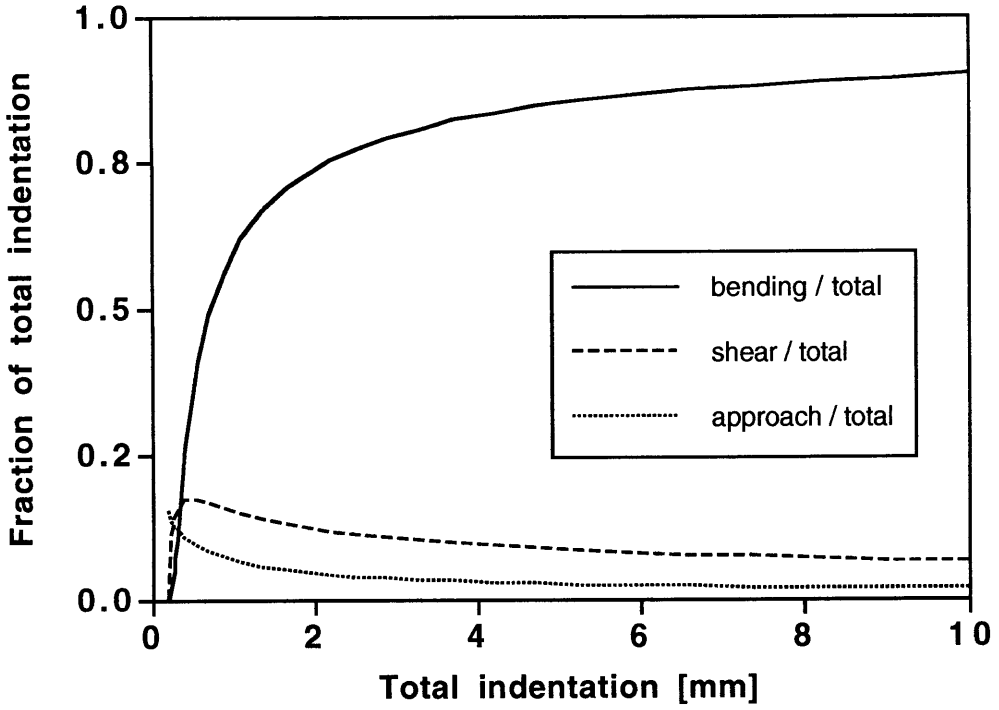

Figure 5.8 Comparison of contributions due to bending, shear and Hertzian approach for the example in Fig. 5.1.

In most design cases the stiffness range of the face sheet material is relatively limited and the choice is governed by overall strength or stiffness requirements. Thus, the parametric study was limited to four parameters:

1) Core crush stress (p_0)
2) Face sheet thickness (h)
3) Core thickness (h_c)
4) Vertical core stiffness (Q_c)

The parametric studies were done by varying one parameter at the time in the case described in Table 5.1. The results are presented in the following sections. In each case results have been shown for moderate indentations (up to 1 mm) using the nonlinear plate solution and for significant indentations (up to 5 mm) using the membrane solution.

5.3.2 Effect of core crush stress

The effect of the core crush stress, Figs. 5.9 and 5.10 is substantial, and affects both the yield point and loads in the subsequent region of partially crushed core.

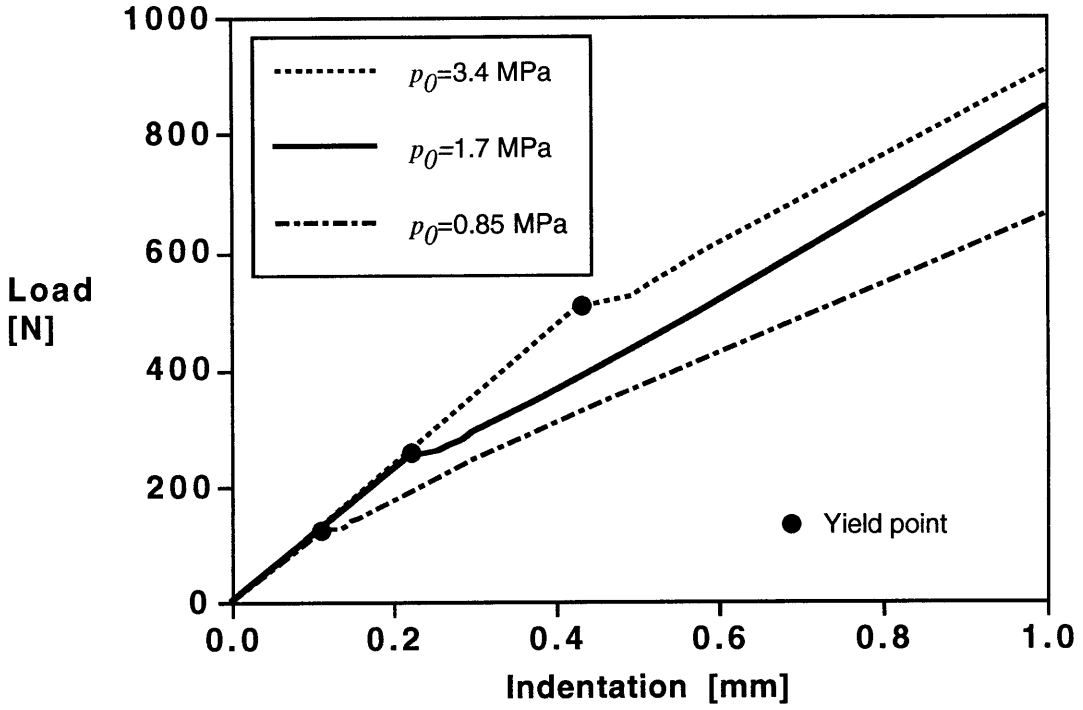

Figure 5.9 Effect of the crush stress on the nonlinear plate solution.

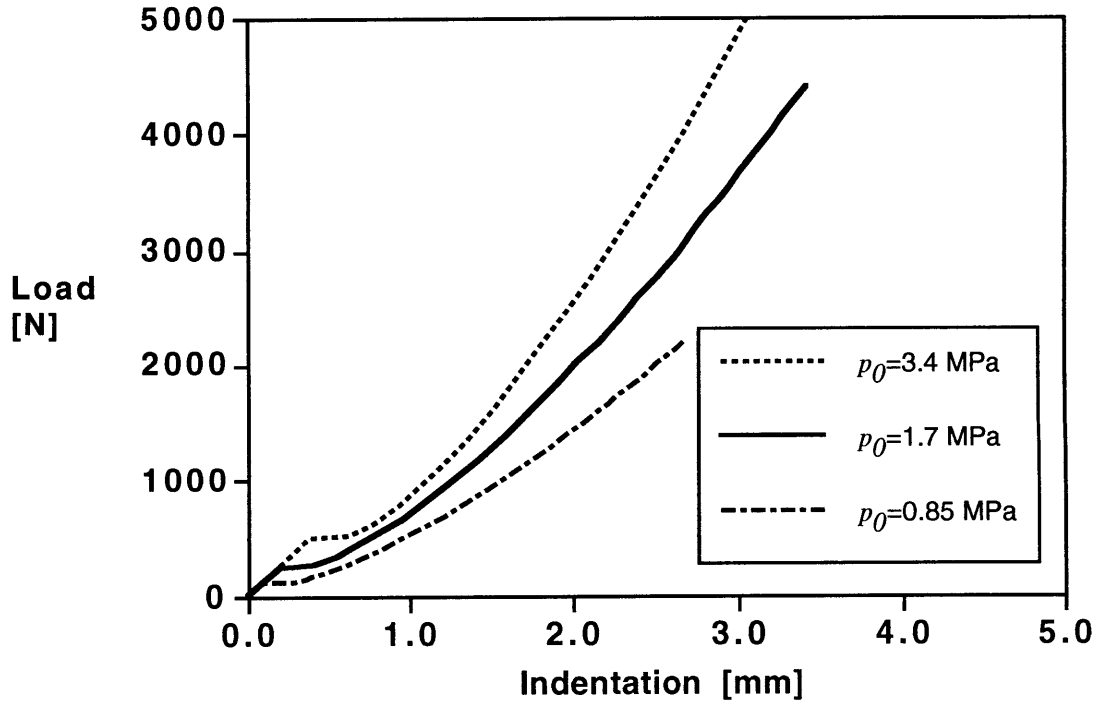

Figure 5.10 Effect of the crush stress on the membrane solution.

5.3.3 Effect of the face sheet thickness

The effect of an increased face sheet thickness, Figs. 5.11 and 5.12, is even stronger than the influence of the core crush stress. Effects are seen both prior to, and after core yielding. After core yielding an increased face sheet thickness increases the load both in the initial region where the behaviour can be described by the plate solution, and in the region where the membrane solution is becoming increasingly valid. The effect on the plate solution, however, is larger than on the membrane solution, which is to be expected since the plate stiffness is proportional to the cube of the face sheet thickness while a linear relation applies for the membrane stiffness.

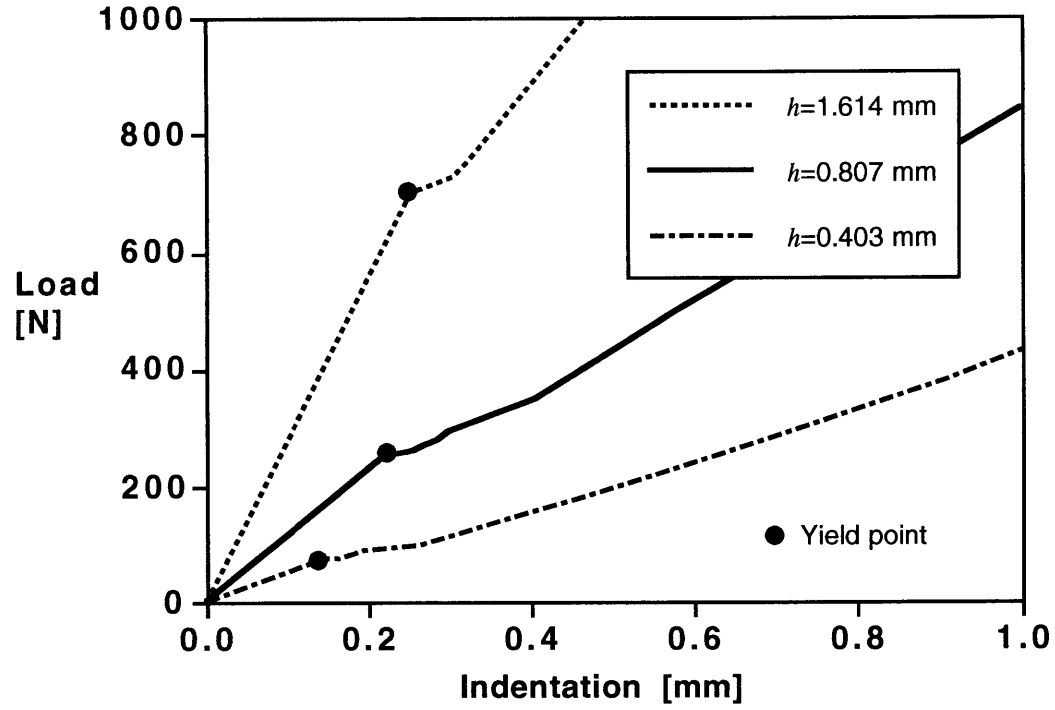

Figure 5.11 Effect of the face sheet thickness on the nonlinear plate solution

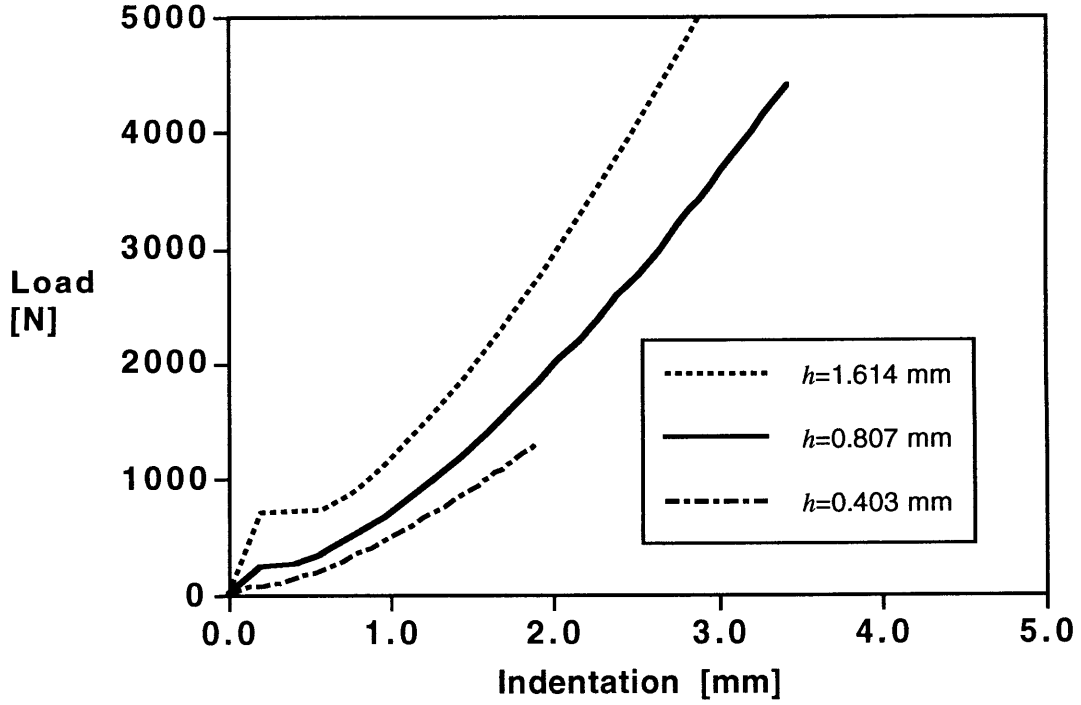

Figure 5.12 Effect of the face sheet thickness on the membrane solution.

5.3.4 Effect of the core thickness

The effect of the core thickness, shown in Figs. 5.13 and 5.14, is small and primarily affects the core yield point and the preceding elastic region. It may be concluded that the elastic properties of the core, which only affect the outer elastic region, have a small effect on the behaviour when significant core crushing is present. The fraction of the contact load which is balanced by the pressure in the plastic region is directly related to the dimensionless plastic radius. The contact load is completely balanced by the reactive plastic pressure when the dimensionless plastic radius is equal to one, which from Figure 3.11 occurs at a load less than three times the load for initiation of core yielding. Furthermore, in the present case there is no influence of the core thickness for core thicknesses exceeding 17 mm since the behaviour in the outer region will then be governed by the three-dimensional solution for a plate on an elastic half-space. The influence of the elastic region is also diminished by the increasing influence membrane stresses due to large deflection effects.

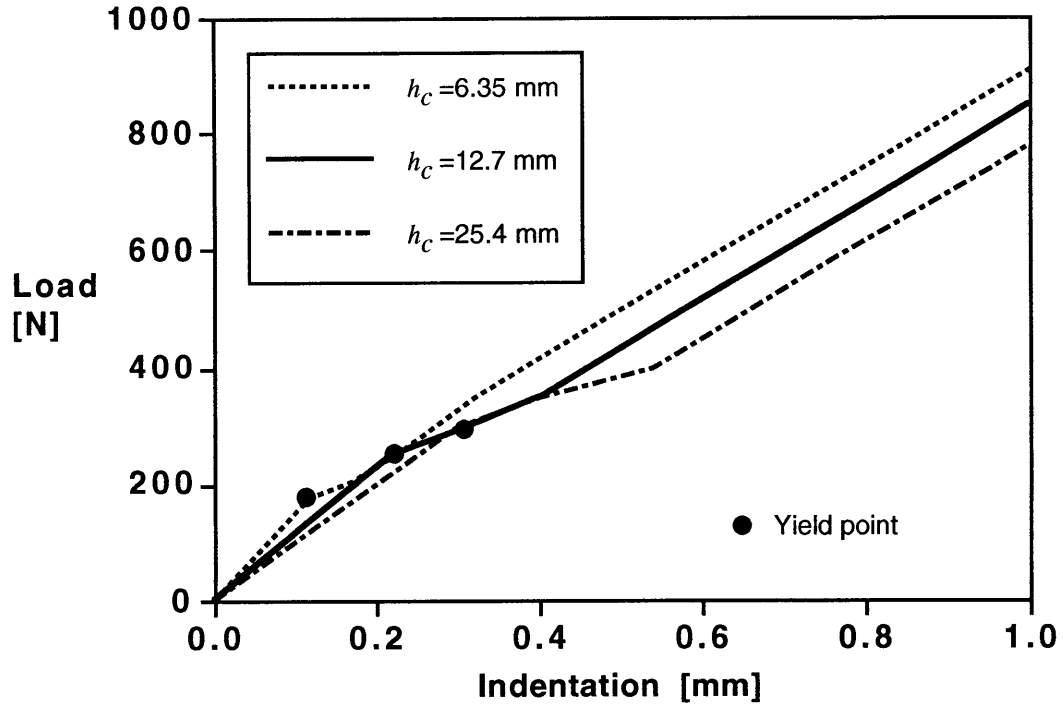

Figure 5.13 Effect of core thickness on the nonlinear plate solution

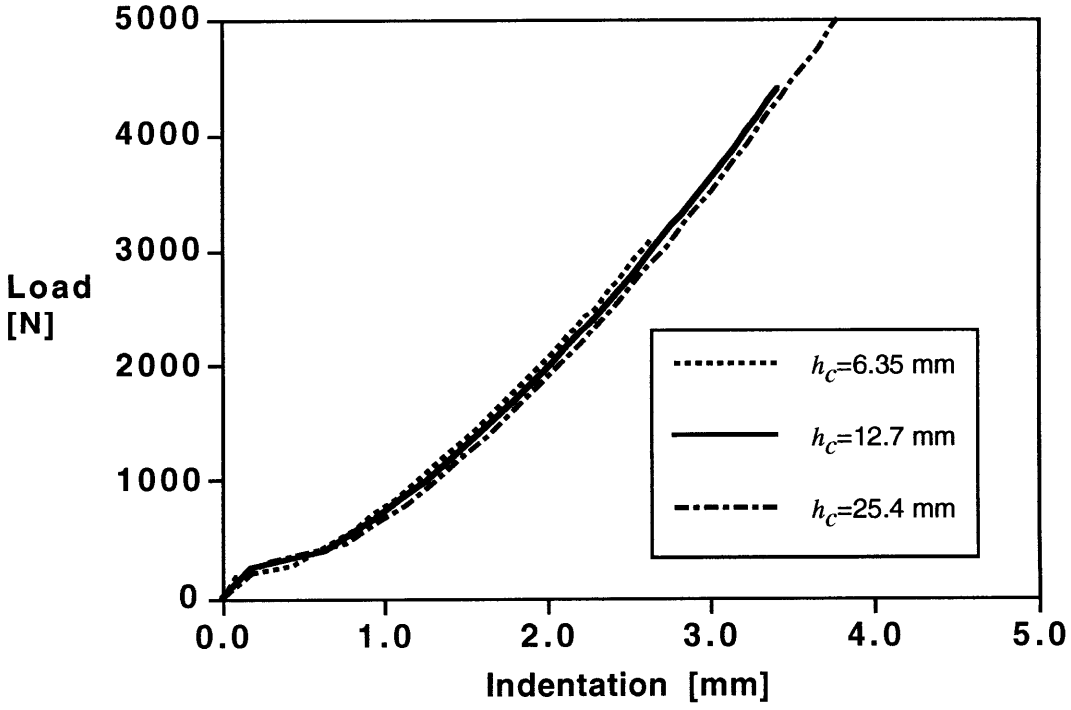

Figure 5.14 Effect of core thickness on the membrane solution.

5.3.5 Effect of core stiffness

No results are presented for the influence of the core stiffness modulus Q_c, since the effects were very small and similar to the effect of the core thickness shown in Figs. 5.13 and 5.14. Obviously the elastic properties of the core, which are related to the core modulus and thickness, are of small importance when the core crush load has been exceeded and the core is partially yielded.

6 Discussion and recommendations

6.1 Main features of the model

By the inclusion of core yielding (crushing) and large deflection effects, the present theory has been able to explain the load–indentation behaviour observed for sandwich panels. Upper and lower bounds have been given for the residual indentation, which is of interest for damage detectability and damage tolerance. Approximate expressions for the average transversally isotropic properties of orthotropic face sheets have been developed. The predictions have been compared with indentation experiments on a number of different sandwich panels, involving cores and face sheets of different materials and thicknesses. The face sheets were all orthotropic and both honeycomb and foam cores have been considered. The agreement between predictions and experiments is surprisingly good, in spite of the large uncertainty in several material parameters, in particular for the out-of-plane properties. We may also conclude that the expressions for average properties of orthotropic face sheets appear satisfactory for use in the present theory.

The predicted behaviour involves an initial phase where the core is elastic and a secondary phase where the core is locally yielded. For typical sandwich panels indented to final face sheet failure it is seen that the initial phase in most cases is of small importance in comparison to the secondary phase.

The vertical displacement in the plastic region has been obtained by modeling the face sheet either as a plate or as a membrane. For small deflections a solution based on linear plate theory is applicable. For intermediate deflections, corrections based on large deflection plate theory have been proposed. An approximate solution based on pure membrane theory represents the asymptotic behaviour for deflections significantly larger than the face sheet thickness. Initially, the nonlinear plate solution is stiffer than the membrane solution. For larger deflections the two solutions intersect and the large deflection plate solution becomes increasingly inaccurate.

In the plate model the total indentation has been modeled as the superposition of an approach of the indentor and face sheet due to contact stresses, and local face sheet deflection due to shear and bending. The superposition method is based on the assumption that the different deformation modes are uncoupled, which is valid only for small deflections.

The load–indentation relation in the initial elastic phase is virtually linear. The only sources of nonlinearity in this phase are the contributions from approach due to Hertzian contact, which is included in the model, and large deflection effects of the face sheet, which are not included for the initial phase.

The load–indentation relation in the partially plastic phase is nonlinear. The softening caused by increasing core yielding is gradually resisted by an increasing stiffening due to membrane stresses caused by large face sheet deflections. For loads significantly larger than the load at initiation of core

crushing, the resulting overall load–indentation is approximately linear, as observed in experiments.

The predicted asymptotic load–indentation relation for large plastic radii is approximately of the form $F \sim w^{3/2}$. This applies both for the large deflection plate solution in Eq. (3.89) where μ approaches 1/3, and for the membrane solution, Eq. (3.71), where the squared plastic radius for large loads is virtually independent of the load as can be seen in Fig. 3.6. Surprisingly, the load–indentation relation for *large* face sheet deflections has the same mathematical form as in Hertzian elastic contact, Eq. (3.91). It is interesting to note that Lie (1987) postulated a load–indentation relation of Hertzian form, based on assumed *elastic core* behaviour and *small* deflections. In fact it is seen that neither of the assumptions was satisfied, and that if they were the relation would be linear, as long as the contact approach is small in comparison to the local face sheet deflection.

6.2 Parameter bounds in the solution

Physically, the partially plastic phase consists of an increasing face sheet deflection under gradually increasing load and plastic radius. Vertical equilibrium for the face sheet in the plastic region shows that the contact load is balanced by a uniform core pressure and the edge load at the plastic radius. The increasing load from the uniform pressure results in a decreasing slope at the plastic radius. A lower physical bound on the slope angle is obviously zero, since the core pressure changes sign for negative deflections, which would result from a negative slope angle.

A lower bound on the edge moment $\overline{M}$ is obtained by requiring a positive slope angle in Eq. (3.17). Eq. (3.18) shows that the shear force Q is positive for $\bar{a}^2>1$. Inspection of Fig. 3.2 shows that for positive shear forces Q a positive slope angle θ can only be realized if the edge moment M is negative. From Eq. (3.17) we conclude that the moment is negative for $\bar{a}^2>1$. The bounds on the edge moment are now given by:

$$\begin{aligned} 8\overline{M}/\overline{F} &\geq \bar{a}^2 - 2 \qquad \text{for } 0 \leq \bar{a}^2 \leq 2 \\ 8\overline{M}/\overline{F} &< 0 \qquad\quad \text{for } 1 \leq \bar{a}^2 \leq 2 \end{aligned} \tag{6.1}$$

From Eq. (3.17) and the condition that the slope angle at the plastic radius must be positive we obtain the following upper bound on the plastic radius in the plate solution:

$$\bar{a}^2 \leq 2 \qquad \text{for a plate} \tag{6.2}$$

A similar upper bound for the plastic radius in the membrane solution is obtained by considering vertical equilibrium in Eq. (3.28) under the assumption that the slope angle is positive. The upper bound in the membrane solution is then given by:

$$\bar{a}^2 \leq 1 \qquad \text{for a membrane} \tag{6.3}$$

It should be noted that the difference in plastic radius for the plate and membrane solutions at a given load is exaggerated in Figs. 3.5 and 3.6, since these graphs show the square of the plastic radius.

No attempt has been made to examine the asymptotic behaviour of the equations for the plastic radius, Eqs. (3.27) and (3.32), and it should be recognized that the asymptotic values given by these equations could be smaller than the physical bounds given by Eqs.(6.2) and (6.3).

6.3 Conclusions and recommendations

Comparisons with previous attempts, which were all based on elastic core behaviour and small deflection theory, shows that the present model represents an important step towards a more realistic description of the sandwich indentation problem. However, several issues remain for further study. These include the initiation and size of damages resulting from indentation, a complete description of the unloading behaviour, the effect of including shear and analysis of the effect of the core thickness. Other issues include dynamic effects and improved experimental data for the out-of-plane properties of the materials. A more rigorous treatment of the membrane problem is also of interest.

The present model can provide all the information needed to predict flexural and membrane strains in the face sheet. Future studies must examine the quantitative ability of the model to predict initiation of face sheet damage. In its present form the model gives an exact value of the plastic radius and upper and lower bounds on the residual deflection. The above quantities are identical to the core crush radius and dent depth, which are both important parameters in residual strength predictions, exemplified in the study by Tsang (1994).

For most cases of interest, the flexural strains in the outer region are likely to be comparatively small, resulting in face sheet damages confined to the plastic region, so that the damage area is approximately proportional to the square of the plastic radius. For linear load–displacement relations a simple energy balance equation, as given for example by Olsson (1993), shows that the peak impact force in quasi-static impacts is proportional to the square root of the kinetic energy. For loads significantly exceeding the load at initiation of core yielding, the overall load–indentation relation for sandwich panels with undamaged face sheets is approximately linear. The squared plastic radius is then approximately proportional to the square root of the peak force, as can be seen from Figs. 3.5 and 3.6.

It has been shown that face sheet membrane action is dominating in most cases of interest. Furthermore, the face sheet inplane modulus is relatively insensitive to face sheet matrix cracks and delaminations. It may be concluded that the squared plastic radius, and thus the delamination area, should be approximately proportional to the fourth root of the impact energy. This relation gives a sharp initial increase in delamination area versus impact energy followed by very moderate increases for larger energies, which is in agreement with the experimental observations by Tsang and Dugundji (1992) and with the numerous experimental studies referenced by Tsang (1994). Thus, it seems possible that the present model can be used for at least qualitative predictions of the face sheet damage size. Further studies are needed to determine the quantitative value of such predictions.

A limited parametric study indicates that the load-indentation behaviour is primarily governed by the core crush stress and face sheet thickness (and modulus). The influence of core modulus and thickness, which are of some importance prior to core yielding, diminishes quickly after initiation of core yielding.

The comparison with experiments in Ch. 5 indicates that the residual indentation is fairly accurately bounded by the expressions given in Sect. 4.2, at least when significant crushing is present. The comparison with the experiment in Fig. 5.2 indicates that the predictions may be less useful for peak loads close to the initiation load for core yielding. This could be due to an inaccurate prediction of the yield point, caused by the simplifications of the one-dimensional core model, which were discussed in Sect. 4.3. Further work is required to obtain closer bounds for the residual indentation and the entire unloading curve, which may be needed in global impact analyses.

Effects of face sheet and core shear in the outer elastic region were not included in the present analysis, but can easily be taken into account by using the expressions in Appendix A, which should improve the results quantitatively.

A more important fundamental issue, however, is to study the relation between the simplified one-dimensional core model used in the analysis and a three-dimensional core analysis for cores of different thicknesses. The results should be used to improve the one-dimensional model, rather than to replace it. A general use of a three-dimensional description is likely to make

the problem intractable for analytical solution, which has clear advantages in spite of the fact that the three-dimensional problem cannot be completely described in a one-dimensional core model.

In Ch. 4 the solution for a point load on a plate resting on an elastic halfspace was compared with the solution for a one-dimensional foundation of finite thickness. The effective stiffness (thickness) for thick cores was then obtained by matching the deflections under the point load. However, as shown by Scott (1981), different values are obtained by matching the deflections at other points. An important issue is to find a matching which is relevant in the elastic region close to the plastic radius. It should also be noted that the matching of core pressures requires a different effective stiffness, which will affect load for initiation of core yielding.

Dynamical effects should be considered before the present solution is used in impact analyses. In most cases, inertial effects are likely to be of minor importance, since the masses in motion are small due to the local character of the face sheet deflection. However, material rate effects, and dynamic buckling of the core cells, could have a significant effect on the response at larger strain rates.

Finally, there is a need for more reliable data on material out-of-plane properties, particularly for the core materials. Ideally, such properties should be determined in situ in complete sandwich panels, since the face sheet–core adhesive seems to have a significant effect on the core behaviour.

7 Summary

Numerous experiments show that contact indentation of sandwich panels normally is associated with crushing of the core cells and large deflections of the face sheets. In the present work, these two effects have been incorporated in a simplified model of sandwich contact indentation. The model is based on the assumptions of an infinite face sheet resting on a core bonded to a rigid foundation, where both the core and face sheet are transversely isotropic with respect to the load axis. The face sheet is assumed to be completely elastic while the core is elastic in tension and elastic–ideally plastic in compression.

For contact loads where core yielding occurs, the problem is separated into an inner plastic region, where the face sheet is supported by a constant pressure, and an outer elastic region, where the face sheet is supported by an elastic foundation. The unknown plastic radius is found by matching boundary conditions for the inner and outer regions.

In order to obtain solutions for the whole range of face sheet deflections, three different approaches for describing the inner region have been proposed. For small deflections, a classical plate theory with shear corrections is proposed. For intermediate deflections, an upper limit of the contact force is given by a first order large deflection plate theory, while a lower limit is given by the small deflection plate theory. The asymptotic solution for large deflections is represented by the pure membrane solution. The resulting solutions are obtained after iteration to obtain the plastic

radius. They have been put in dimensionless form and tabulated so that no further calculations are required to use the equations. To allow analysis of orthotropic face sheets, approximate expressions have been developed for their effective average plate and membrane properties.

At the initiation load for core crushing all three solutions are obtained from the small deflection solution for a point load on a plate on an elastic foundation. Initially, the large deflection solution is stiffer than the membrane solution. For larger deflections the latter solutions intersect, and the asymptotic behaviour for large deflections is given by the approximate membrane solution.

Qualitatively, it is shown that the approximately linear load–indentation relation observed in experiments is in fact the combined effect of softening due to core crushing and stiffening due to membrane effects in the face sheets.

The predictions of the model have also been compared quantitatively with results from indentation experiments on several sandwich panels having different face sheets and honeycomb or foam cores of different thickness and materials. Good agreement with experiments is found well beyond the point where core yielding is initiated. At significantly higher loads, an additional softening is observed, apparently due to matrix cracking in the laminated face sheets, which results in an increasing deviation from the predicted behaviour.

A limited parametric study indicates that the load-indentation behaviour is primarily governed by the core crush stress and face sheet thickness (and modulus). The influence of core modulus and thickness, which are of some importance prior to core yielding, diminish quickly after initiation of core yielding.

When comparing with previous attempts, which were based on small deflection theory and an assumed elastic core behaviour, it may be concluded that the present model gives a much better description of the local face sheet deflection and the controlling parameters during contact indentation of sandwich panels.

The local indentation model may be used in a global impact model to predict impact response of sandwich panels, or as a starting point for more detailed stress analyses for prediction of damage due to impact and contact loads. A natural continuation of the work is to determine the ability of the present simplified model to predict initiation and extent of face sheet damage.

Future workers may want to include face sheet and core shear, which should improve the results quantitatively. A more important fundamental issue, however, is to determine the most appropriate expressions for the foundation stiffness in the outer elastically supported region for different finite core thicknesses.

8 Acknowledgements

The present research project was sponsored by the Swedish Defence Materials Administration. My studies at M.I.T were sponsored by my employer, The Aeronautical Research Institute of Sweden, and would not have been possible without the support by the Head of the Structures Department, Dr. Martin Svenzon and the former Head of the Composites Section, Dr. Pavel Sindelar.

I am also obliged to my thesis advisors, Prof. Hugh McManus and Prof. Mårten Landahl, who both contributed with valuable advice and suggestions during the course of this work.

Finally, I want to thank my former fellow student Dr. Wilson Tsang for important background information and generous access to his large collection of references on sandwich impact and indentation.

9 References

Abramowitz, M. and Stegun, I.A. (1970), "Handbook of mathematical functions", 9th printing, U.S. Department of Commerce, National Bureau of Standards, Washington.

Abrate, S. (1991), "Impact on laminated composite materials", Appl. Mech. Rev., **44** (4) 155-190.

Banerjee, B. (1983), "Large deflection of a circular plate under a concentrated load – a new approach", Industrial Mathematics, **33** (1) 57–61.

Bert, C.W. and Martindale, J.L. (1988), "An accurate, simplified method for analyzing thin plates undergoing large deflections", AIAA J., **26** (2) 235–241.

Brodland, G.W. (1988), "Highly non-linear deformation of uniformly-loaded circular plates", Int. J. Solids and Structures, **24** (4) 351–362.

Chen, C.-F. and Gürdal, Z. (1990), "Stress analysis of orthotropic plate on elastic foundation with transverse point load", J. Aerospace Engng., **3** (1) 64-77.

Cheng, C.-J. (1989), "Nonlinear bending of polar orthotropic circular plates", Solid Mech. Archives, **13** (4) 17–36.

Chia, C.Y. (1980), "Nonlinear analysis of plates", McGraw-Hill, New York.

Conway, H.D. (1956), "The pressure distribution between two elastic bodies in contact", Zeitschrift für Angewandte Mathematik und Physik, **7**, 460-465.

Datta, S. (1975), "Large deflection of a circular plate on elastic foundation under a concentrated load at the center", J. Appl. Mech., **42** (2) 503-505.

Dillard, D.A. (1989), "Bending of plates on thin elastomeric foundations", J. Appl. Mech., **56** (2) 382-386.

Dolovich, A.T, Brodland, G.W. and Thornton-Trump, A.B. (1988), "An approximate solution of the axisymmetric von Karman equations for a point-loaded circular plate", J. Appl. Mech., **55** (1) 241–243.

Ericsson, A. and Sankar, B.V. (1992), "Contact stiffness of sandwich plates and application to impact problems", 2nd Int. Conf. on Sandwich Constr., Gainesville, FL.

Ferris, D.H. (1991), "Approximate large deflection analysis of circular plates loaded symmetrically", NPL Report DMM (A)25, National Phys. Lab., Teddington, UK.

Flügge, W. (1966), "Concentrated forces on shells", Applied Mechanics – Proc. 11th Int. Cong. of Appl. Mech., Munich, Springer Verlag, Berlin, 270–276.

Frakes, J.P. and Simmonds, J.G. (1985), "Asymptotic solutions of the von Karman equations for a circular plate under a concentrated load", J. Appl. Mech., **52** (2) 326–330.

Frischbier, J. (1987), "Theorie der Stossbelastung orthotroper Platten und ihre experimentelle Überprüfung", Mitteilung Nr.51, Institut für Mechanik, Rühr-Universität, Bochum, Germany.

Gibson, L.J. and Ashby, M.F. (1988), "Cellular solids", Pergamon Press, Oxford.

Gladwell, G.M.L. (1980), "Contact problems in the classical theory of elasticity", Sijthoff & Noordhoff, Alpen aan den Rijn, Netherlands.

Goldsmith, W. and Sackman, J.L. (1992), "An experimental study of energy absorption in impact on sandwich plates", Int.J. Impact Engng.,**12** (2) 241–262.

Greszczuk, L.B. (1982), "Damage in composite materials due to low velocity impact", in Impact dynamics, ed. Zukas, J.A., John Wiley & Sons, New York, 55–94.

Hall, R. (1991), "Effective moduli of cellular materials", Proc. Am. Soc. for Composites, 6th Techn. Conf., Albany, NY, 1080–1089.

Hamada, M. and Seguchi, Y. (1965), "On the accuracy of the v. Kármán equations for axisymmetric non-linear bending of circular plates", Trans. Japan Soc. Aeron. and Space Sciences, **8** (12) 6–14.

Hétenyi, M. (1966), "Beams and plates on elastic foundations and related problems", Appl. Mech. Reviews, **19** (2) 95–102.

Huang, H.A. and Hahn, H.T. (1990), "Compressive failure Mechanics of composite honeycomb cores", Ed. Kobyashi, A., 5th Japan–US Conf. on Comp. Matls., Tokyo, 153–160.

Huber, M.T. (1923), "Die Theorie der kreuzweise bewehrten Eisenbetonplatten nebst Anwendungen auf mehrere bautechnisch wichtige Aufgaben über rechteckige Platten", Der Bauingenieur, **12**, 353-360 and **13**, 392-395.

Jackson, W.C. and Poe, C.C.Jr. (1993), "The use of impact force as a scale parameter for the impact response of composite laminates", J. Comp. Tech. & Res., **15** (4)282-289.

Jahsman, W.E., Field, F.A. and Holmes, A.M.C. (1962), "Finite deformations in a prestressed, centrally loaded, circular elastic membrane.", Proc. 4th U.S. National Cong. of Applied Mechanics, Am. Soc. Mech. Engineers, Berkeley, California, 585–594.

Koller, M.G. (1986), "Elastic impact of spheres on sandwich plates", J. Appl. Math. and Phys. (ZAMP), **37**, 256–269.

Lagace, P.A. et al. (1993), "A preliminary proposition for a test method to measure (impact) damage resistance", J. Reinf. Plastics and Composites, **12** (5) 584-601.

Lee, L.J., Huang. K.Y. and Fann, Y.J. (1993), "Dynamic responses of composite sandwich plate impacted by a rigid ball", J. Comp. Mat., **27** (13) 1238–1256.

Lewandowski, R. and Switka, R (1991), "Unilateral plate contact with the elastic-plastic Winkler-type foundation", Computers and Structures, **39** (6) 641-651.

Leonard, J.W(1988), "Tension structures – behavior and analysis", McGraw-Hill, New York.

Lie, S.C. (1989), "Damage resistance and damage tolerance of thin composite facesheet honeycomb panels", S.M. Thesis, Dept. of Aero. and Astro., MIT, Cambridge.

Mines, R.A.W., Worrall, C.M. and Gibson, A.G. (1990), "The response of GRP sandwich panels to dropped object impact loading", FRC'90 Fibre Reinforced Composites, Proc. of the Institution of Mech. Eng.s., Fourth Int. Conf., Liverpool, 149–155.

Nemes, J.A. and Simmonds, K.E. (1992), "Low-velocity impact response of foam-core sandwich composites", J. Comp. Mat., **26** (4) 500–519.

Nowinski, J.L. and Ismail, I.A. (1964), "Application of a multi-parameter perturbation method to elastostatics", Developments in Theor. & Appl. Mech., Proc. 2nd Southeastern Conf. on Theor. and Appl. Mech., Atlanta, Georgia, Vol.2, 35–45.

Oda, J. and Kubota, T. (1992), "Approximate solution on the elastic contact problems between two–layered bodies", AIAA/ASME/ASCE/AHS/ASC 33rd Structures, Structural Dynamics and Materials Conference, Dallas, Texas, 965–969, (AIAA–92–2531–CP).

Olsson, R. (1989), "Impact response of orthotropic composite laminates predicted by a one-parameter differential equation", FFA TN 1989–07, The Aeronautical Research Institute of Sweden, Bromma.

Olsson, R. (1992), "Impact response of orthotropic composite laminates predicted from a one-parameter differential equation", AIAA J., **30** (6) 1587-1596.

Olsson, R. (1993), "Impact response of composite laminates – a guide to closed form solutions", FFA TN 1992–33, The Aeronautical Research Institute of Sweden, Bromma.

Oplinger, D.W. and Slepetz, J.M. (1975), "Impact damage tolerance of graphite/epoxy sandwich panels", in Foreign object impact damage to composites, ASTM STP 568, Am. Soc. for Testing and Matls., Philadelphia, 30-48.

Panc, V. (1975), "Theories of elastic plates", Noordhoff Int. Publ., Leyden.

Pettersson, O. (1954), "Circular plates subjected to radially symmetrical transverse load combined with uniform compression or tension in the plane of the plate", Acta Polytechnica, Mech. Eng. Ser., **3** (1) 1–31.

Riis, R.J. (1992), "Nondimensional models for low-velocity impact of rectangular sandwich and composite plates", (Presented as M.Sc. Thesis to the Royal Inst. of Technology, Stockholm, Sweden), Dept. of Aerospace Engn. Mechs. and Eng. Sci., Univ. of Florida, Gainesville FL.

Saibel, E. and Tadjbakhsh, I. (1960), "Large deflections of circular plates under uniform and concentrated loads", Zeitschr. für Angew. Mathematik und Physik, **11** (6) 496–503.

Schleicher, F. (1926), "Kreisplatten auf elasticher Unterlage", Springer, Berlin.

Schmidt, R. (1987), "Nonlinear flexure of a uniformly loaded plate with an immovably clamped edge", Industrial Mathematics, **37** (1) 17–27.

Schmidt, R. and DaDeppo, D.A. (1976), "Large axisymmetric deflections of a loosely clamped circular plate subjected to a system of two interacting loads", Industrial Mathematics, **26** (1) 11–16.

Schwerin, E. (1929), "Über Spannungen und Formänderungen kreisringförmiger Membranen", Zeitschrift für technische Physik, (12) 651–659.

Scott, R.F. (1981), "Foundation analysis", Prentice-Hall, Englewood Cliffs.

Selvadurai, A.P.S. (1979), "Elastic analysis of soil–foundation interaction", Elsevier, Amsterdam.

Shivakumar, K.N., Elber, W. and Illg, W. (1985), "Prediction of impact force and duration due to low-velocity impact on circular composite laminates", J. Applied Mechanics, **52** (3) 674–680.

Slepetz, J.M. et al. (1974), "Impact damage tolerance of graphite/epoxy sandwich panels", AMMRC TR 74-20, US Air Force Matls. and Mechs. Res. Center, Watertown, MA.

Sneddon, I.N., Gladwell, G.M.L. and Coen, S. (1975), "Bonded contact of an infinite plate and an elastic foundation", Letters in Appl. Engn. Sciences, **3** (1) 1-13.

Striz, A.G., Jang, S.K. and Bert, C.W. (1988), "Nonlinear bending analysis of thin circular plates by differential quadrature", Thin-walled Structures, **6**,51-62.

Sun, C.T. and Wu, C.L. (1991), "Low velocity impact of composite sandwich panels", AIAA paper 91-1077-CP, 32nd AIAA/ASME/ASCE/AHS/ASC Structures, Structural Dynamics and Materials Conference, Baltimore, Maryland , 1123–1129.

Szilard, R., (1974), "Theory and analysis of plates", Prentice-Hall, Englewood Cliffs, NJ.

Timoshenko, S. and Goodier, J.N., (1951), "Theory of elasticity", 2nd edition, McGraw-Hill, New York.

Timoshenko, S. and Woinowsky–Krieger, S, (1959), "Theory of plates and shells", 2nd edition, McGraw-Hill, New York.

Tsang, P.H.W. (1989), "Impact resistance of graphite/epoxy sandwich panels", S.M. Thesis, Dept. of Aero. and Astro., Massachusetts Inst. of Techn., Cambridge, MA.

Tsang, P.H.W. (1994), "Impact resistance and damage tolerance of composite sandwich panels", Ph.D. Thesis, Dept. of Aero. and Astro., Massachusetts Inst. of Techn., Cambridge, MA.

Tsang, P.H.W. and Dugundji, J. (1992), "Damage resistance of graphite/epoxy sandwich panels under low speed impacts", J. Am. Helicopter Soc., **37** (1), 75–81.

Vlasov, V.Z. and Leont'ev, U.N. (1966), "Beams, plates and shells on elastic foundations", Israel Program for Scientific Translations, Jerusalem (English translation of 1960 Russian edition).

Volmir (Wolmir), A.S. (1962), "Biegsame Platten und Schalen", Verlag für Bauwesen, Berlin (Corrected German edition of 1961 Russian edition).

Way, S. (1934), "Bending of circular plates with large deflection", (Trans. of the ASME), J. Appl. Mech., **56** (12) 627–636.

Williamson, J.E. (1991), "Response Mechanisms in the impact of graphite/epoxy honeycomb sandwich panels", S.M. Thesis, Dept. of Aero. and Astro., MIT, Cambridge.

Williamson, J.E. and Lagace, P.A. (1993), "Response Mechanisms in the impact of graphite/epoxy honeycomb sandwich panels", 8th Technical Conf. on Comp. Matls. , Cleveland, OH.

Yu, H.U., Sanday, S.C. and Rath, B.B. (1990), "The effect of substrate on the elastic properties of films determined by the indentation test – axisymmetric Boussinesq problem", J. Mech. Phys. Solids, **38** (6) 745–764.

Zhang, J. and Ashby, M.F.(1992), "The out-of-plane properties of honeycombs", Int. J. Mech. Sci., **34** (6) 475-489.

Zhou, Y.-H. and Zheng, X.-J. (1989), "On the range of applicability of von Karman plate equations", J. Appl. Mech., **56** (3) 724–725.

Appendix A Solution for plate on elastic foundation

For axisymmetric deformation of a transversely isotropic plate on an elastic foundation we may define the quantities:

$$L_0^4 = D/k \qquad \rho = r/L_0 \qquad \Delta_\rho = d^2/d\rho^2 + \rho^{-1} d/d\rho \tag{A.1}$$

The equilibrium equation for a Kirchhoff plate on a shear deformable foundation is given by Vlasov and Leont'ev (1966) as follows:

$$\Delta_\rho^2 w - 2\lambda\Delta_\rho w + w = p/k \tag{A.2}$$

$$\text{where} \quad \lambda = \frac{G_c}{2\sqrt{Dk}} \int_0^{h_c} \psi^2(z)dz$$

Here $\psi(z)$ is a suitable shape function for the vertical displacements in the foundation.

The corresponding equilibrium equation for a shear deformable plate on a Winkler foundation is given by Panc (1975):

$$\Delta_\rho^2 w - 2\lambda\Delta_\rho w + w = (1 - 2\lambda\Delta_\rho) p/k \tag{A.3}$$

$$\text{where} \quad \lambda = \frac{3\sqrt{Dk}}{5Gh}$$

Panc (1975) also showed that the analysis could be extended to a two-parameter foundation with the same homogenous equation if λ and L_0 were defined as follows:

$$L_0 = \left[\frac{D}{k_1} + \frac{h^2 k_2}{5(1-\nu)k_1}\right]^{1/4} \qquad \lambda = \frac{1}{2L_0^2}\left[\frac{k_2}{k_1} + \frac{h^2}{5(1-\nu)}\right] \tag{A.4}$$

For λ smaller than one, which is the case encountered in practice, the general solution of the homogenous Eqs. (A.2) and (A.3) is given by:

$$
\begin{aligned}
w(\rho) &= C_1 u_0(\rho) + C_2 v_0(\rho) + C_3 f_0(\rho) + C_4 g_0(\rho) \\
\frac{dw}{dr} &= -\frac{1}{L_0}\sum_{i=1}^{4} C_i \theta_i(\rho) \\
\omega_r &= \frac{1}{L_0}\sum_{i=1}^{4} C_i \omega_i(\rho) \\
M_r &= \frac{D}{L_0^{\,2}}\sum_{i=1}^{4} C_i \left[M_i(\rho) - (1-\nu)\overline{M_i}(\rho) \right] \\
Q_r &= -\frac{D}{L_0^{\,3}}\sum_{i=1}^{4} C_i Q_i(\rho)
\end{aligned}
\qquad \text{(A.5)}
$$

where $u_n(\rho) + i v_n(\rho) = J_n(\rho e^{i\psi})$ $\qquad$ $f_n(\rho) + i g_n(\rho) = H_n^{(1)}(\rho e^{i\psi})$ *

and $\psi = \frac{1}{2}\left[\pi - \arctan\sqrt{\lambda^{-2} - 1} \right]$ $\qquad$ $\pi/4 \le \psi \le \pi/2$

* Note the incorrect sign of g_0 in Vlasov and Leont'ev (1966) since $g_n(\rho) = \mathrm{Im}\, H_n^{(1)}(\rho e^{i\psi}) = -\mathrm{Im}\, H_n^{(2)}(\rho e^{-i\psi})$.

Here ω_r is the rotation of the plate midplane normal, the functions u_0, v_0, f_0 and g_0 are real and the function θ is given by:

$$
\begin{aligned}
\theta_1(\rho) &= u_1(\rho)\cos\psi - v_1(\rho)\sin\psi \\
\theta_2(\rho) &= u_1(\rho)\sin\psi + v_1(\rho)\cos\psi \\
\theta_3(\rho) &= f_1(\rho)\cos\psi - g_1(\rho)\sin\psi \\
\theta_4(\rho) &= f_1(\rho)\sin\psi + g_1(\rho)\cos\psi
\end{aligned}
\qquad \text{(A.6)}
$$

For an infinite plate C_1 and C_2 must be set to zero since $u_0, v_0 \to \infty$ as $\rho \to \infty$. At the origin $f_0 = 1/2$ and g_0 is infinite.

For a plate with infinite shear stiffness on a shear deformable foundation Vlasov and Leont'ev (1966) give the following expressions for the midplane rotation and sectional forces:

$$\omega_i(\rho) = \theta_i(\rho)$$

$$M_1(\rho) = u_0(\rho)\cos 2\psi - v_0(\rho)\sin 2\psi$$
$$M_2(\rho) = u_0(\rho)\sin 2\psi + v_0(\rho)\cos 2\psi$$
$$M_3(\rho) = f_0(\rho)\cos 2\psi - g_0(\rho)\sin 2\psi$$
$$M_4(\rho) = f_0(\rho)\sin 2\psi + g_0(\rho)\cos 2\psi$$

$$\overline{M}_i = \theta_i/\rho$$

$$Q_1(\rho) = u_1(\rho)\cos 3\psi - v_1(\rho)\sin 3\psi \qquad \text{(A.7.a)}$$
$$Q_2(\rho) = u_1(\rho)\sin 3\psi + v_1(\rho)\cos 3\psi$$
$$Q_3(\rho) = f_1(\rho)\cos 3\psi - g_1(\rho)\sin 3\psi$$
$$Q_4(\rho) = f_1(\rho)\sin 3\psi + g_1(\rho)\cos 3\psi$$

For a shear deformable plate Panc (1975) give the following expressions:

$$\omega_1(\rho) = -u_1(\rho)\cos 3\psi - v_1(\rho)\sin 3\psi$$
$$\omega_2(\rho) = u_1(\rho)\sin 3\psi - v_1(\rho)\cos 3\psi$$
$$\omega_3(\rho) = -f_1(\rho)\cos 3\psi - g_1(\rho)\sin 3\psi$$
$$\omega_4(\rho) = f_1(\rho)\sin 3\psi - g_1(\rho)\cos 3\psi$$

$$M_1(\rho) = -u_0(\rho)\cos 2\psi - v_0(\rho)\sin 2\psi$$
$$M_2(\rho) = u_0(\rho)\sin 2\psi - v_0(\rho)\cos 2\psi$$
$$M_3(\rho) = -f_0(\rho)\cos 2\psi - g_0(\rho)\sin 2\psi$$
$$M_4(\rho) = f_0(\rho)\sin 2\psi - g_0(\rho)\cos 2\psi$$

$$\overline{M}_i = \omega_i/\rho$$

$$Q_1(\rho) = -u_1(\rho)\cos\psi - v_1(\rho)\sin\psi \qquad \text{(A.7.b)}$$
$$Q_2(\rho) = u_1(\rho)\sin\psi - v_1(\rho)\cos\psi$$
$$Q_3(\rho) = -f_1(\rho)\cos\psi - g_1(\rho)\sin\psi$$
$$Q_4(\rho) = f_1(\rho)\sin\psi - g_1(\rho)\cos\psi$$

From Vlasov and Leont'ev (1966) the deflections due to a point load on an infinite plate are given by:

$$w(\rho) = \frac{FL_0^2 f_0(\rho)}{4D\sin 2\psi} \tag{A.8}$$

The corresponding expression from Panc (1975) is:

$$w(\rho) = \frac{FL_0^2\left[-f_0(\rho)\cos 4\psi + g_0(\rho)\sin 4\psi\right]}{4D\sin 2\psi} \tag{A.9}$$

Obviously, since g_0 is infinite at the origin, a finite deflection cannot be realized for a point load on a shear deformable plate. Rather, the load must be assumed to be distributed over a finite area, as given by a contact stress analysis.

Appendix B Plastic radius and moment versus load

B.1 Plate solution

Table B.1 Dimensionless plastic radius and edge moment versus load for plate

$\overline{F}$	$\overline{a}^2$	$8\overline{M}/\overline{F}$		
		ν=0.0	ν=0.3	ν=0.5
2.546	0.000	∞	∞	∞
2.637	0.015	2.475	3.813	4.705
2.725	0.033	1.694	2.792	3.524
2.834	0.056	1.160	2.091	2.711
2.960	0.084	0.764	1.569	2.105
3.802	0.262	-0.256	0.188	0.484
5.005	0.450	-0.623	-0.345	-0.160
5.857	0.553	-0.720	-0.502	-0.356
6.810	0.648	-0.770	-0.595	-0.478
7.861	0.733	-0.791	-0.648	-0.553
9.009	0.809	-0.795	-0.677	-0.597
10.253	0.878	-0.789	-0.689	-0.622
12.057	0.959	-0.771	-0.690	-0.636
13.022	0.995	-0.760	-0.686	-0.637
14.028	1.029	-0.747	-0.681	-0.636
15.075	1.061	-0.735	-0.673	-0.633
16.163	1.091	-0.721	-0.665	-0.628
17.293	1.120	-0.708	-0.656	-0.622
18.463	1.146	-0.695	-0.647	-0.615
19.674	1.171	-0.681	-0.637	-0.608
20.925	1.195	-0.668	-0.627	-0.600
22.217	1.217	-0.655	-0.617	-0.592
23.550	1.238	-0.643	-0.607	-0.583
24.975	1.256	-0.634	-0.597	-0.575
26.338	1.277	-0.618	-0.587	-0.566
27.795	1.295	-0.607	-0.577	-0.558

Note: $\overline{a}^2$ was obtained by solving Eq. (3.27) and $8\overline{M}/\overline{F}$ from Eqs. (3.22) and (3.2).

B.2 Membrane solution

Table B.2a Dimensionless plastic radius versus load for membrane, ν=0.0

$\overline{F}$	$\overline{a}^2$	C	f_w
2.546	0.000	-1.271	0.788
2.635	0.060	-1.279	0.783
3.183	0.154	-1.293	0.776
3.422	o.187	-1.298	0.773
3.985	0.251	-1.308	0.768
5.799	0.388	-1.331	0.756
7.159	0.453	-1.344	0.750
8.711	0.506	-1.354	0.745
10.452	0.551	-1.364	0.741
12.379	0.589	-1.372	0.737
14.490	0.621	-1.380	0.734
17.591	0.657	-1.388	0.731
19.263	0.673	-1.392	0.729
21.016	0.687	-1.396	0.727
22.850	0.700	-1.399	0.726
24.765	0.712	-1.402	0.725
26.761	0.723	-1.405	0.724
28.836	0.734	-1.408	0.722
30.993	0.743	-1.411	0.721
33.229	0.752	-1.413	0.720
34.378	0.757	-1.415	0.720
35.546	0.761	-1.416	0.719
36.736	0.765	-1.417	0.719
37.944	0.769	-1.418	0.718
39.174	0.772	-1.419	0.718
40.326	0.778	-1.421	0.717
41.695	0.779	-1.421	0.717
42.980	0.783	-1.422	0.717
44.290	0.786	-1.423	0.717
45.623	0.789	-1.424	0.716

Note: $\overline{a}^2$ and C were obtained from Eqs. (3.32) and (3.65), f_w from Eq.(3.66).

Table B.2b Dimensionless plastic radius versus load for membrane, ν=0.3

$\overline{F}$	$\overline{a}^2$	C	f_w
2.546	0.000	-1.206	0.776
2.600	0.112	-1.218	0.767
3.137	0.204	-1.229	0.760
3.397	0.238	-1.233	0.757
3.998	0.303	-1.241	0.751
5.492	0.410	-1.256	0.742
6.850	0.473	-1.265	0.736
8.401	0.525	-1.273	0.731
10.141	0.568	-1.280	0.727
12.068	0.604	-1.285	0.724
14.179	0.635	-1.291	0.721
17.281	0.669	-1.298	0.717
18.953	0.684	-1.300	0.716
20.706	0.697	-1.304	0.714
22.540	0.710	-1.305	0.713
24.455	0.721	-1.308	0.712
26.451	0.732	-1.310	0.711
28.527	0.742	-1.312	0.709
30.684	0.751	-1.314	0.709
32.920	0.759	-1.315	0.708
34.069	0.763	-1.316	0.707
35.237	0.767	-1.317	0.707
36.428	0.771	-1.318	0.707
37.635	0.775	-1.319	0.706
38.866	0.778	-1.319	0.706
40.028	0.783	-1.320	0.706
41.387	0.785	-1.321	0.705
42.672	0.788	-1.321	0.705
43.982	0.791	-1.322	0.704
45.315	0.794	-1.323	0.704

Note: $\overline{a}^2$ and C were obtained from Eqs. (3.32) and (3.65), f_w from Eq.(3.66).

Table B.2c Dimensionless plastic radius versus load for membrane, ν=0.5

$\overline{F}$	$\overline{a}^2$	C	f_w
2.546	0.000	-1.157	0.767
2.657	0.184	-1.172	0.752
3.147	0.257	-1.179	0.746
3.442	0.291	-1.182	0.743
4.088	0.352	-1.188	0.738
5.248	0.429	-1.196	0.731
6.609	0.490	-1.203	0.725
8.164	0.540	-1.209	0.721
9.907	0.581	-1.214	0.717
11.836	0.616	-1.219	0.713
13.950	0.645	-1.222	0.710
17.054	0.678	-1.227	0.707
18.728	0.692	-1.229	0.706
20.482	0.705	-1.231	0.704
22.317	0.717	-1.233	0.703
24.233	0.728	-1.234	0.702
26.230	0.738	-1.236	0.701
28.306	0.748	-1.237	0.700
30.464	0.756	-1.238	0.699
32.701	0.764	-1.240	0.698
33.850	0.768	-1.240	0.698
35.019	0.772	-1.241	0.697
36.209	0.776	-1.241	0.697
37.417	0.779	-1.242	0.697
38.648	0.783	-1.242	0.696
39.818	0.788	-1.243	0.696
41.169	0.789	-1.243	0.696
42.455	0.792	-1.244	0.695
43.765	0.795	-1.244	0.695
45.098	0.798	-1.245	0.695

Note: $\overline{a}^2$ and C were obtained from Eqs. (3.32) and (3.65), f_w from Eq.(3.66).